Selected Constitutive Models for Simulating the Hygromechanical Response of Wood

Frandsen, Henrik Lund

Publication date:
2007

Document Version
Publisher's PDF, also known as Version of record

Selected Constitutive Models for Simulating the Hygromechanical Response of Wood

Henrik Lund Frandsen

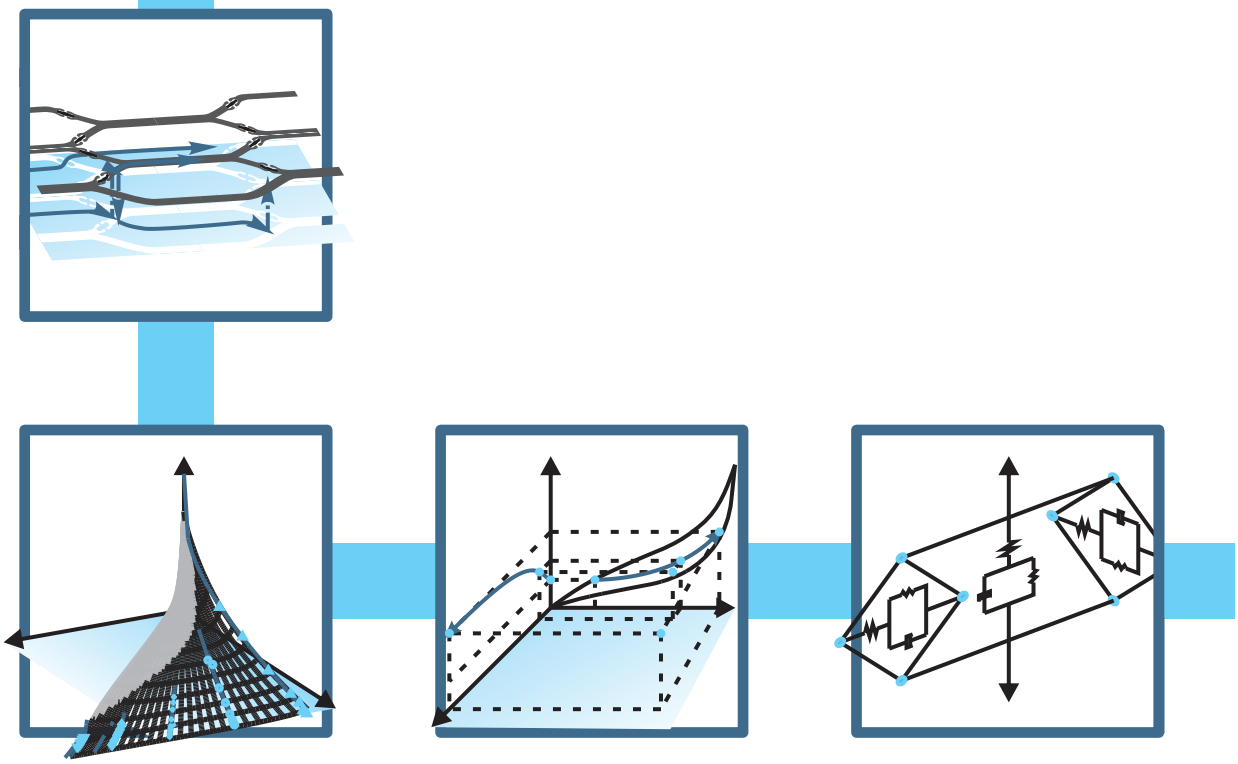

PhD Thesis
Department of Civil Engineering
Aalborg University 2007

Selected Constitutive Models for Simulating the Hygromechanical Response of Wood

Henrik Lund Frandsen

PhD Thesis
Department of Civil Engineering
Aalborg University
Aalborg 2007

Selected Constitutive Models for Simulating the Hygromechanical Response of Wood
Department of Civil Engineering
Aalborg University
ISSN 1901-7294 DCE Thesis no. 10

Preface

Present PhD dissertation "Selected Constitutive Models for Simulating the Hygromechanical Response of Wood" has been prepared in connection with my PhD study carried out from November 2003 to April 2007 at the Department of Civil Engineering, Aalborg University, Denmark. The work has been financed by the Danish Forest and Nature Agency. The financial supported is gratefully acknowledged.

First of all, I wish to thank my supervisor, associate professor Dr. Staffan Svensson, for sharing his pool of ideas and broad overview of research on wood, and for his enthusiastic guidance throughout my study.

Likewise I would like to thank assistant professor Dr. Lech Muszynski for his surprising ideas and inspiring co-operation during my 5 months study at Oregon State University. Also thanks to Milo Clauson and the guys at OSU for great company during that period.

I am also grateful to professor Dr. Lars Damkilde and professor Dr. Techn. Henrik Myhre Jensen for their support and guidance during the final phase of my PhD study.

For great patience and the many suggestions for improvements of my English I wish to thank technical translator Kirsten Aakjær. For his help with typesetting and the fruitful occasional discussions I also wish to thank postdoc Dr. Johan Clausen.

Furthermore, I wish to thank my family, friends and colleagues, especially those in the "bunker", for being the great social distraction from my PhD work and hereby forming the adherence of this past period's composite living. Finally, special thanks goes to my girlfriend Maria for her support, encouragements, great patience and for being the wonderful person she is.

Summary

The present thesis is a compilation of papers. Three of the papers, I, VI and VII, are published in this thesis only, i.e., an introductory paper and two so-called discussion papers. The papers II, III and V have been published in the international journal, Holzforschung. Paper IV is a conference paper presented at 19th Nordic Seminar on Computational Mechanics, Lund, Sweden, 2006.

Paper I The theories for the phenomena leading to hygromechanical response of wood relate to the orthotropic cellular structure and the hydrophilic and hydrophobic polymers constituting the cells. This introductory paper presents these theories for the hygromechanical response and hereby also provides the frame of reference and the connecting thread of of the present thesis.

Paper II Multiple paths for moisture transport and slow sorption yield non-Fickian effects. This calls for a new type of multi-phase transport model. In this paper a so-called multi-Fickian model is revised with respect to the incorporated essential sorption rate model. Based on existing experimental results the sorption rate model is studied. A desorption rate model analogous to the adsorption rate model is proposed. Furthermore, the boundary conditions are discussed based on discrepancies found for similar research on moisture transport in paper stacks.

Paper III In this paper a new sorption hysteresis model suitable for implementation into a numerical method is developed. The prevailing so-called scanning curves are modeled by closed-form expressions, which only depend on the current relative humidity of the air and current moisture content of the wood. Furthermore, the expressions for the scanning curves are formulated independent of the temperature and species-dependent boundary curves.

Paper IV In this paper the sorption hysteresis model developed in Paper III is applied to two different wood species and to bleach-kraft paperboard.

Paper V In this paper the sorption hysteresis model is implemented into the multi-Fickian model allowing simultaneous simulation of non-Fickian effects and hysteresis. A key point for this implementation is definition of the condition of wood as a state in the sorption hysteresis space, which is independent of the condition of water vapor in the lumens. Two approaches are developed and tested by implementation into a commercial software.

Paper VI In this paper the temperature dependencies of the hysteretic multi-Fickian moisture transport model are discussed. The constitutive moisture transport models are coupled with a heat transport model yielding terms that describe the so-called Dufour and Sorret effects, however, with multiple phases and hysteresis included.

Paper VII In this paper the modeling of transverse couplings in creep of wood are discussed based on experimental observation of time dependent Poisson ratios and new theoretical findings on the Poisson ratio. A new orthotropic creep model, which provides directionally independent creep rates, is proposed. Furthermore, the procedure for an ongoing experimental study of the phenomenon is presented.

Sammenfatning

Denne afhandling er en samling af artikler. Tre af artiklerne, I, VI og VII, er kun publiceret i denne afhandling, det være sig en introduktionsartikel og to såkaldte diskussionsartikler. Artikelerne II, III og V er publiceret eller godkendt til publicering i det internationale tidsskrift Holzforschung. Artikel IV er en konferenceartikel præsenteret på 19th Nordic Seminar on Computational Mechanics, Lund, Sverige, 2006.

Artikel I Teorierne for fænomenerne, der leder til det hygromekaniske respons af træ, relaterer sig til dets ortotrope cellulære struktur og de hydrofile og hydrofobe polymerer, som udgør trævævet. Denne introduktionsartikel formidler disse teorier for den hygromekaniske respons og tilvejebringer hermed også en referenceramme og den røde tråd i nærværende afhandling.

Artikel II Flere fugttransportveje og langsom sorption medfører (såkaldte) ikke-Fickske effekter. Dette fordrer en ny type multifaset transportmodel. I denne artikel bliver den essentielle sorptionshastighedsmodel indeholdt i den såkaldte multi-Fickske model revideret. Sorptionshastighedsmodellen bliver undersøgt på basis af eksisterende eksperimentielle resultater. En model for desorptionshastighed svarende til modellen for adsorptionshastighed bliver foreslået. Derudover bliver randbetingelserne diskuteret på basis af afvigelser, som er fundet i lignende forskning på fugttransport i papirstakke.

Artikel III I denne artikel bliver en ny sorptionshysterese-model, som er egnet til implementering i en numerisk metode, udviklet. Den forudgående såkaldte *scanning*-kurve bliver modelleret med et udtryk på lukket form, som kun afhænger af den nuværende relative fugtighed i luften og det nuværende fugtindhold i træet. Derudover er udtrykkene for scanning-kurverne formuleret uafhængigt af de temperatur- og træsortsafhængige randkurver.

Artikel IV Sorptionshysterese-modellen udviklet i Artikel III bliver anvendt på to forskellige træsorter og på afbleget kraft-karton.

Artikel V I denne artikel bliver sorptionshysterese-modellen implementeret i den multi-Fickske model, hvormed både ikke-Fickske effekter og hysteresis kan simuleres samtidig. Et nøglepunkt for denne implementering er definitionen af træets tilstand som et punkt i hysterese-rummet, der er uafhængig af tilstanden af vanddampen i cellehulrummene. To metoder bliver udviklet og testet ved implementering i en kommerciel software.

Artikel VI I denne artikel bliver temperaturafhængigheden af den multi-Fickske model med hysterese diskuteret. De konstitutive fugttransport-modeller bliver koblet med en varmetransportmodel, hvilket frembringer led, som beskriver de såkaldte Dofour- og Sorret-effekter, hvor der dog her er taget højde for flere faser og hysterese.

Artikel VII I denne artikel bliver modelleringen af de transversale koblinger i krybning af træ diskuteret på basis af eksperimentelle observationer og nye teoretiske fund omkring tidsafhængige Poissonforhold. En ny ortotrop krybningsmodel, som giver retningsuafhængige krybningshastigheder, bliver foreslået. Derudover bliver forsøgsopstilling for et igangværende eksperimentielt studium af fænomenet præsenteret.

Contents

Paper I

On the shape stability of wooden structural members

An introductory paper

Paper I

On the shape stability of wooden structural members

- An introductory paper -

Henrik Lund Frandsen
Department of Civil Engineering, Aalborg University, Denmark

Abstract

The general design criteria and serviceability design criteria of the European code for design of timber structures involves assessment of the stress and moisture dependent deformations of wood over time due to climatic changes. The mechanical response of a wooden structural component exposed to moisture variations combined with a stress field can lead to quite significant deformations. Theories for the phenomena causing this hygromechanical response relate to the orthotropic cellular structure of wood and the hydrophilic and hydrophobic polymers constituting the cells. Analysis tools, which apply these theories to predict the hygromechanical response, can facilitate the design process. This introductory paper presents the theories along with existing constitutive models and hereby also provides the frame of reference for the constitutive models presented in the present thesis. Through a short description of the structure and composition of wood, moisture transport in wood and the mechanical response to that are addressed. With the overview of the work of the present thesis, perspectives on further research on the subjects attended are given conclusively.

1 Introduction

The design of timber structures involves analysis of the mechanical resistance, serviceability, durability and fire resistance. According to the European code for design of timber structures, Eurocode 5, 2.2.1:(1)P, the design models for the different limit states shall generally, as appropriate, take into account the following:

- different material properties (e.g. strength and stiffness)
- different time-dependent behavior of the materials (duration of load, creep)
- different climatic conditions (temperature, moisture variations)
- different design situations (stages of construction, change of support conditions)

And furthermore in the code it is stated about the serviceability limit states in 2.2.3:(1)P that:

> "The deformation of a structure which results from the effects of actions (such as axial and shear forces, bending moments and joint slip) and from moisture shall remain within appropriate limits, having regard to the possibility of damage to sur-

facing materials, ceilings, floors, partitions and finishes, and to the functional needs as well as any appearance requirements."

This thesis presents a selection of constitutive models for simulating the hygromechanical response of wood. The hygromechanical response of wood is its mechanical response to simultaneous exposure of moisture and stress over time. Although the object is to contribute to general knowledge on this topic, the work of the present thesis is highly motivated by these design criteria for timber structures. Hence, the constitutive models presented here are also contributions to a model set, which can be applied to assess the stress and moisture dependent deformations of wood over time due to climatic changes.

Where the hygromechanical response of wood is of interest for different applications such as wood drying and duration of load problems, the application of it is here limited to assessment of shape stability of wooden structural members. Roughly spoken, the shape instability of wooden structural members owes to the response to variations of the moisture content of wood combined with the mechanical loading and support of the members.

The variation of the moisture content in wood depends on the external exposure. An example of this is illustrated in Figure 1, which shows the measurements of moisture content in the frame of a wood sheathing. The measured moisture content variations are caused by the varying climate. For reference, the indoor climate is kept as constant as possible. The measurements are performed on the side facing the interior, and have thus the highest inertness to variations. Still, variations with high frequency are observed, which means that even though the entire structure does not experience the daily variation of humidity in the air, a relatively fast adaptation to the external climate still occurs.

These moisture content variations results in swelling and changes of the shape of the structure. In a good design the support of the structural component allows it to expand unconstrained, and in many situations the generated deformations are reversible.

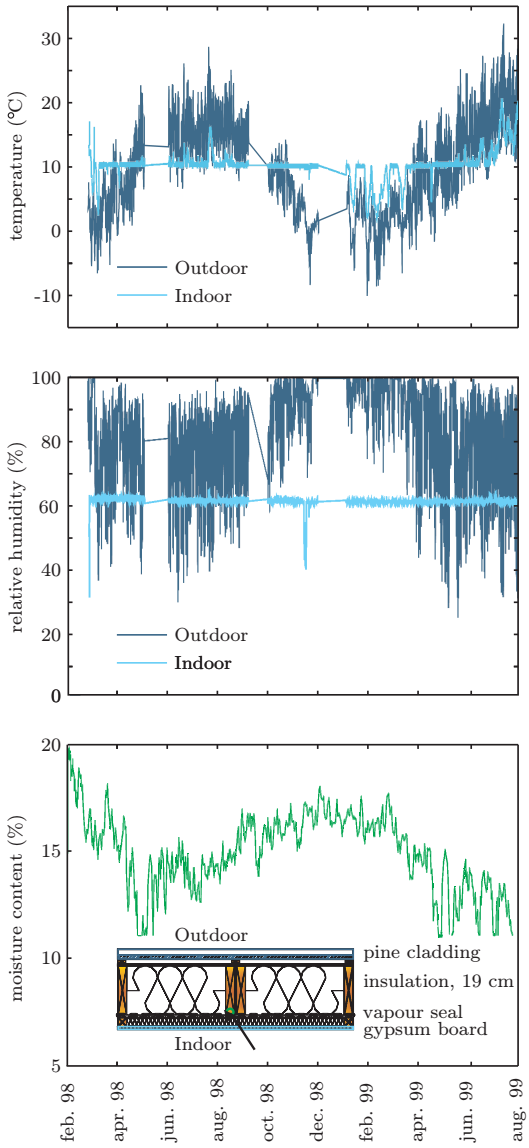

Figure 1 Moisture content in the frame of a wood sheathing caused by the outdoor varying climate and a constant reference indoor climate (Andersen et al., 2002).

In other cases the function of the structure does not allow this type of design, and the

swelling is accompanied by stresses. This type of combined exposure of moisture and stress can also be found in a load-carrying component exposed to a varying climate. Dependent on the magnitude of the stress and moisture variations the so-called hygromechanical response of wood can cause significant deformations, so that the requirements for serviceability cannot be fulfilled.

The classical experiment by Hearmon and Paton (1964) shown in Figure 2 illustrates the magnitude and significance of the hygromechanical response of a combined exposure of moisture and stress of wood. Three matching beams in a three-point bending test are exposed to following conditions:

1 Constant high relative humidity of 93% and a load corresponding to 3/8 of maximum load in a short-term experiment.

2 Varying relative humidity between 0% and a load corresponding to 93% and 1/8 of maximum load in a short-term experiment.

3 Varying relative humidity between 0% and a load corresponding to 93% and 3/8 of maximum load in a short-term experiment.

The deformations shown in Figure 2 are normalized with respect to the immediate elastic deformation. The deformations for the beams simultaneously exposed to relative humidity variations are seen to be significantly larger than for the one in a constant climate - even for one third of the load. The deformations of the beam in a varying climate with a load of 3/8 of the maximum load are up to 25 times greater than the elastic deformations, and the beam fails within the period of observation.

The deformations of a structural component of wood exposed to a stress field and a varying climate can be assessed to some degree by physical principles and material models. Especially with the introduction of numerical methods in the analysis of timber structures, a strong tool to asses various responses is at hand.

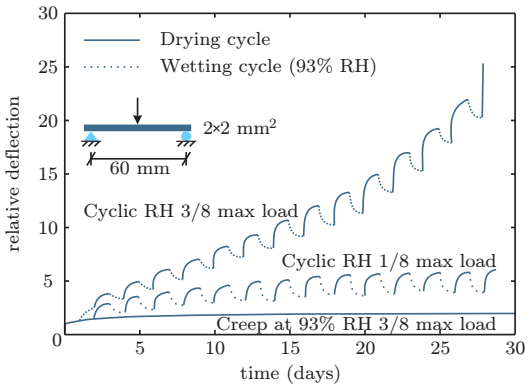

Figure 2 Deformations over time of three beams in three-point bending exposed to different load levels and ambient climates (Hearmon and Paton, 1964).

Calculating the response of wood is, however, not trivial, which is due to many factors. To mention a few: stochastic variations, irregularities (knots, etc.), ageing, orthotropic structure and a large number of non-linear coupling effects between different types of phenomena.

The localized effects such as knots and other irregularities mainly influence the load-carrying capacity, whereas the global deformation is mainly governed by the majority of the wood tissue. Although the localized effects might have some influence, this study is limited to clear wood without knots and defects.

The hygroscopic response of the structural member can be obtained by:

1 Prediction of external exposure of the structural member, i.e., the ambient climate and loads.

2 Modeling of moisture transport and sorption in the orthotropic cellular material to obtain the distribution of adsorbed water.

3 Modeling of deformations in a hygroscopic orthotropic material prone to swelling and creep.

In this study, 1 is not addressed, whereas 2 is treated thoroughly. For 3, the mathematical

framework for multi-dimensional creep in an orthotropic material is addressed, whereas no material model for a specific species is treated. Hereby it is also implied that this work is not a guideline for engineers to design shape-stable structures. However, the models in this work have been developed with the aim to be suitable for implementation into numerical methods and thus also for practical application. The same holds for the level of complexity of the models, which has been chosen to suit the specific task of modeling shape stability of wooden structural components. The models presented in this work can of course be modified to other applications, e.g. wood drying, impregnation.

The object of this introductory paper is primarily to set the work of this thesis into a frame of reference, but also to introduce the reader to the concepts used in following papers.

The theories for the phenomena leading to shape instability relate to the orthotropic cellular structure of wood and the hydrophilic and hydrophobic polymers constituting the cells. Therefore the structure and composition of wood will be described in section 2 as a way of introduction to moisture transport in wood in section 3 and the mechanical response to that in section 4. With this overview of the work of this thesis, perspectives on further research relating to present work are given in section 6.

2 Structure and composition of wood

In this section the structure of wood is described through a four level division, to which the various theories for shape stability can be related, i.e.: macrostructure, microstructure, ultrastructure and molecular structure. The majority of wood used for structural purposes in northern hemisphere are softwoods, and therefore the description is limited to treatment of these.

2.1 Macrostructure

The macroscopic features can be identified with the naked eye. Considering a log, wood is the tissue inside the bark, which consists of a number of characteristic growth rings stemming from the annual incremental growth. Each increment consists of a sub-increment of lighter earlywood produced at the beginning of the growth season and darker sub-increment of latewood at the end of it (Figure 3). The layer of living cells in the cambium layer found between the bark and wood is responsible for this production. A zone of growth rings closest to the center, the heartwood, has taken a darker color (more distinct for some species than others). The darker color is due to extractives, which protect the heartwood against insects and fungal attacks. The outer lighter zone, the sapwood, is in the living tree used for conduction of water and minerals.

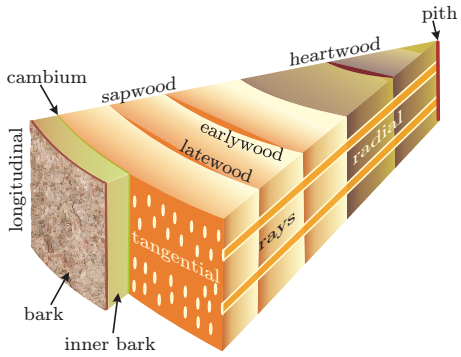

Figure 3 Macroscopic features of a softwood and material directions.

2.2 Microstructure

Each growth ring consists of a number of adjacent longitudinal tracheid cells, which are organized in a honeycomb pattern in the tangential-radial plane (Figure 4). The honeycomb pattern tends to be organized in radial rows. This organization gives space to radial channels of parenchyma and tracheid cells, rays, which are used for storage of food materials. The cells are

cemented by a middle lamella layer (Figure 7).

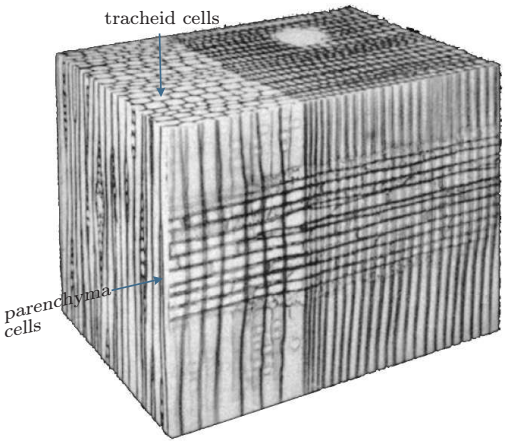

Figure 4 Orientation of tracheid and parenchyma cells (Dinwoodie, 2000).

The tracheid cells constitute the major part of the tissue, and the functions of the cells are structural support of the tree and conduction of water and nutrients. The cell is a tapered oblong tube with a length to width ratio of about 1:100. The longitudinal direction of the cell is oriented in left-hand spiral closest to the pit. The angle of the spiralling incline is highest at the pit and decreases with the distance from the pit and can become negative, i.e., oriented in a right-hand spiral (Figure 5).

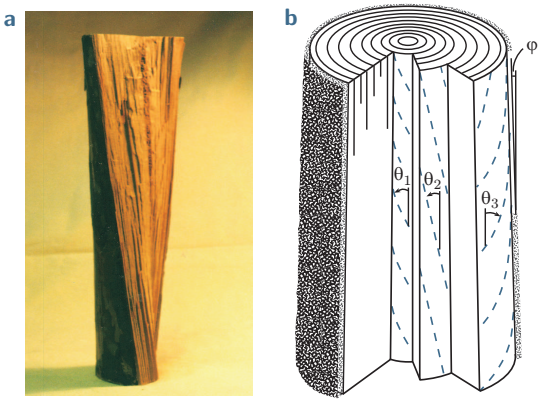

Figure 5 Spiral orientation of the tracheid fibers growth direction (Ormarsson, 1999).

To facilitate a high growth rate in the beginning of the season the cells in the earlywood have a larger diameter for conduction of nutricients, and the cell walls are thinner compared to those of the latewood (Figure 6).

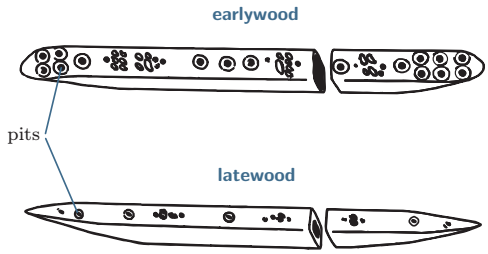

Figure 6 Earlywood and latewood tracheid cells (Siau, 1995).

Besides, the number and size of the intercellular connections, the pits, is larger in the earlywood tracheid cells. A membrane placed in the pits will aspire if a pressure difference on each side of the pit occurs e.g. during drying. Aspiration is a irreversible process where the pit membrane seals the pit (?). A major part of the wood tissue is constituted by that type of cells, and thus the mechanical response of wood inherits from the behavior of this type of cell.

2.3 Ultrastructure

The cell wall is constituted by a primary and a secondary wall. The latter consists of three distinguishable layers, i.e., S1, S2 and S3 (Figure 7). Each layer can be considered to be a composite material with reinforcing 'fibers', i.e., microfibrils, and a 'matrix' material. Their molecular composition will be described in the next section.

In the primary wall the microfibrils are loosely packed and interweave at random, whereas in the secondary wall the microfibrils are parallel to each other and densely packed.

In the secondary wall the middle layer S2 is by far the thickest. The microfibrils in this layer are closely packed and oriented in a right-hand spiral with a low inclination to the longitudinal

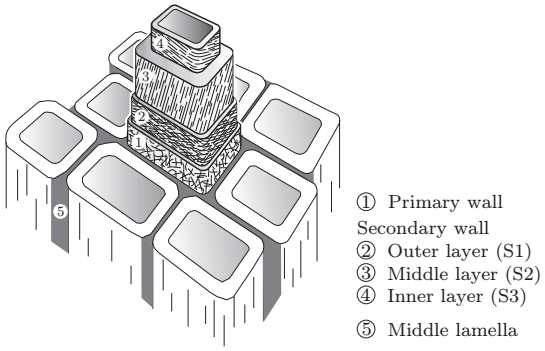

Figure 7 Ultrastructure of a tracheid cell (Ormarsson, 1999).

axis of the fiber, i.e., the so-called microfibrillar angle (Figure 7). Due to this orientation the microfibrils will provide some shearing stiffness, but mainly contribute to the bending and tensile properties of the cell. Bending and axial tensile or compressive loading in this composite structure couples to a torsional component (Figure 8).

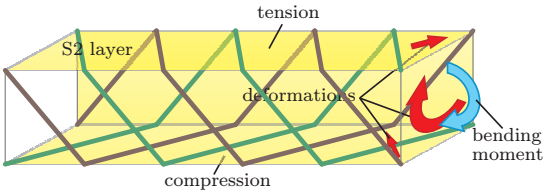

Figure 8 Torsional deformations by bending of the microfibrillar "reinforced" S2 layer of the secondary cell wall.

The high microfibrillar angle and concentric orientation of the microfibrils in the S1 and S3 layer provide torsional stiffness in these layers (Figure 7). This might be a mean to counteract the torsion of the S2 layer.

2.4 Molecular structure

The molecular constituents of wood are cellulose, hemicellulose and lignin. The rigid part of the microfibrils is constituted by hydrogen bonded glucane chains of cellulose. The glucane chains are incrusted in hemicelluloses and lignin. The matrix material is constituted by hemicelluloses and lignin.

The hydrogen bonds linking the glucane chains together consists of a hydroxyl group and a hydrogen atom on an adjacent cellulose chain. The unbounded hydroxyl groups are called sorption sites. Each sorption site can bind several layers of water molecules as the closest molecule displays a ghost of the sorption site (Avramidis, 1997). Between the crystalline regions of parallel cellulose chains, extra hygroscopic amorphous and paracrystalline regions with a high number of available sorption sites occur (Siau, 1984).

The most hygroscopic constituent is, however, the hemicelluloses, which are chemically composed as the cellulose (Dinwoodie, 2000). A detailed description of various hemicelluloses is found in (Siau, 1984). Lignin also has available sorption sites, but is the least hygroscopic of the three components. It can be regarded as a protective adhesive encrusting the cellulose chains, which softens and weakens mechanically in a wet state. The middle lamella consists of lignin only.

3 Moisture transport in wood

Moisture transport in wood below the fiber saturation point is a process governed by three phenomena: bound-water and water-vapor diffusion (Stamm, 1959, 1960a; Stamm and Nelson, 1961) and the coupling between the two phases of water.

A change of vapor pressure in the ambient air results in diffusion of water vapor, J_v, in wood, sorption of bound-water and consequential bound-water diffusion, J_b. In Figure 9 the time-dependent processes of the phenomenon, i.e., diffusion in wood in the two phases and the sorption coupling, are schematically illustrated. It is important to recognize that the time-dependent sorption plays a significant role in the phenomenon.

At low relative humidities, bound-water diffusion is a relatively slow process, and the mois-

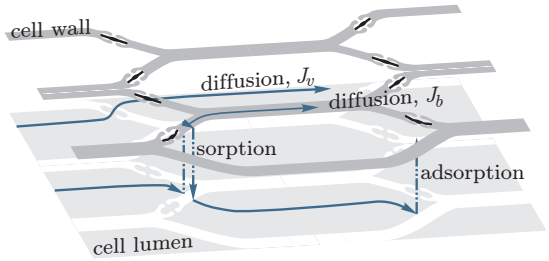

Figure 9 Various time-dependent processes responsible for moisture transport in the cellular structure of wood.

ture transport in wood is governed by water-vapor diffusion, which can be seen from the ratio between the diffusion coefficients $D_v : D_b \simeq 1 : 4 \cdot 10^{-6}$ (Schirmer, 1938; Siau, 1995). Subsequently, a relatively fast sorption of bound water commences. Hence, the process governing the combined process is water-vapor diffusion, and moisture transport is traditionally modeled by a single Fickian diffusion equation.

At higher relative humidities, bound-water diffusion becomes more significant ($D_v : D_b \simeq 1 : 2 \cdot 10^{-5}$) and the sorption slows down (Christensen, 1965). This combined two-phase diffusion and sorption phenomenon has characteristics that cannot be described by a single diffusion equation (Krabbenhøft and Damkilde, 2004). Therefore, it has been referred to as anomalous behavior and non-Fickian effects (Crank and Park, 1951; Wadsö, 1994a).

For a single diffusion equation to model a one-dimensional diffusion, the fractional weight increase, E $((w(t) - w_0)/(w_\infty - w_0))$, as a function of time, t, for different specimen thicknesses, a, is identical when time is normalized by $t^{1/2}/a$ (Crank, 1967), where w_0, w_∞ are the initial and final weight, respectively, and $w(t)$ is the weight at the time t. This is under the assumption that the surface resistance can be neglected due to sufficient convection at the surface. An effort to ensure this condition has been attempted in the experiments mentioned in the following.

The first researchers to report the non-Fickian effects were Crank and Park (1951) for long polymers and Mandelkern and Long (1951) for cellulose acetate.

Wadsö (1994b; 1994a) measured the bound-water uptake in pine (*Pinus silvestris*) specimens of various widths, a, and different material directions at the relative humidity steps: 54-75% and 75-84%. The specimens were exposed on two symmetrically oriented surfaces in a ventilated climate chamber humidified by salt solutions. The air velocity was about 3 ms^{-1}, so that effects from the boundary layer can be assumed to be very small (Rosen, 1978).

In Figure 10 the fractional weight increases for diffusion in the tangential direction in some of these measurements are shown. The $\sqrt{t}/a$ normalization of the time-axis should result in identical curves for different specimen lengths, even for moisture dependent diffusion coefficients (Crank, 1967).

At the first relative humidity step (54-75%) the thick specimen shows a slightly faster increase of fractional weight increase. At the second relative humidity step (75-84%) the thick specimen gains weight significantly faster. Besides, these fractional weight increase curves do not have the Fickian characteristic of an initial almost linear increase succeeded by an abrupt bend into a horizontal asymptote, but are smoother.

Thus, it can be concluded that the observed phenomenon cannot be modeled by a single Fickian diffusion equation. In this section, the development of a moisture transport model, which captures this behavior, is presented.

3.1 Moisture transport modeled by a multi-Fickian model

Already in the sixties, a detailed model to take several moisture transport routes into consideration was suggested by Stamm (1960b), and Siau (1984) presented a simpler, but similar model. In these models, the resistances to diffusion from cell walls and lumens are parallel and serially connected. The underlying assumption connecting these resistances is instantaneous sorption or immediate equilibrium be-

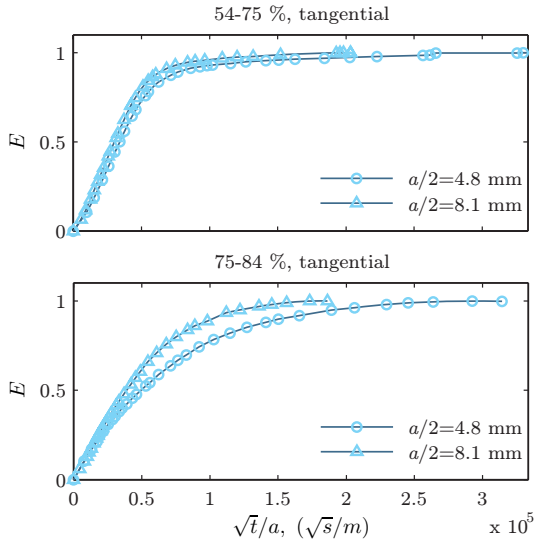

Figure 10 Fractional weight increase, E, in pine specimens over time normalized with respect to specimen thickness a from measurements by Wadsö (1994b).

tween the water vapor and bound water. Thus, the time dependency of sorption, i.e., the vertical process in Figure 9, is neglected. This kind of model is therefore unable to describe the non-Fickian behavior caused partly by slow sorption.

Consequently, the transport of water vapor and bound water must be modeled in separate phases connected through a phase change, i.e., time-dependent sorption. This type of model is here referred to as a multi-Fickian model, since bound-water and water-vapor transport are described by two coupled Fickian diffusion equations, i.e., one for each phase.

The earliest researcher to follow up on Wadsö's experiments with this type of mathematical model was Cunningham (1994). The posed differential equations were solved analytically, so that a number of simplifications on the physics were made, i.e., bound-water diffusion (J_b in Figure 10) was neglected and the sorption isotherm was assumed to be linear. However, with the equation solving tool available, this approach gave quite good results when comparing to *one* of Wadsö's experiments.

Salin (1996) included the bound-water diffusion and solved the problem analytically, so the isotherm was again assumed to be linear. Again, relatively good results were obtained using an analytical solution. Salin correctly indicated the applied sorption function to be the reason why his model deviates from Wadsö's measurements at higher relative humidities. Salin assumed a sorption rate, which is independent of the moisture content.

Absetz and Koponen (1997) modeled multi-Fickian moisture transport in laminated veneer lumber (LVL) parallel to grain in specimens of different thicknesses. Since all experiments were performed at the same relative humidity step, a moisture independent sorption rate was sufficient to obtain good results. Further, Absetz and Koponen provided an important discussion of the magnitude of different parameters involved in their model, but without identifying them.

Krabbenhøft and Damkilde (2004) discussed and identified some of these physical constants, introduced an expression for moisture-dependent sorption rate and applied a non-linear isotherm. Furthermore, the two diffusion equations were formulated in terms of concentration of bound water and water-vapor pressure in preference to concentrations only (Cunningham, 1994; Salin, 1996) or pressures only (Absetz and Koponen, 1997). An overview of the model development is provided in Table 1. Parallel to this line of research, the type of models has also been applied to moisture transport in paper stacks; see e.g. (Bandyopadhyay et al., 2000; Foss et al., 2003; Massoquete et al., 2005; Nyman et al., 2006).

In Paper II (Frandsen et al., 2007a) the following revisions and contributions to the multi-Fickian model for moisture transport in wood is presented:

- The adsorption rate is studied based on measurements of weight gain of thin wood specimens in absence of air by Christensen (1965).

	Cunningham (1994)	Salin (1996)	Absetz and Koponen (1997)	Krabbenhøft and Damkilde (2004)
Water-vapor diff., J_v	√	√	√	√
Bound-water diff., J_b		√	√	√
Non-linear isotherm				√
Moist. dep. sorp. rate				√
Pressure and conc.				√

Table 1 Progress of the multi-Fickian model refinement.

In these experiments no stagnant air to form a boundary layer is present, and the small extent of the specimens allowed diffusion to be neglected. Thus, the sorption rate could be studied independently of other phenomena. The result of this investigation is a revised sorption rate model, which has a continuous variation with vapor pressure.

- The desorption rate has been observed to be slower at higher relative humidities in experiments by Håkansson (1994) as well. Based on this observation, an expression for the desorption rate analogous to the adsorption rate model is proposed.
- The boundary conditions for the problem is presented and discussed based on differences in similar models for moisture transport in paper stacks.
- A minor revision of the governing equations is given.

The results from the revised model were compared with the measurements by Wadsö (1994b), and a good agreement was found.

3.2 Sorption hysteresis

Variation of the relative humidity in ambient air causes variations in the moisture content of wood. However, a given relative humidity does not uniquely define the equilibrium moisture content. The history of the variations must also be taken into account. Figure 11 illustrates the dependence of moisture content, m, due to a sequence of relative humidity, h, variations.

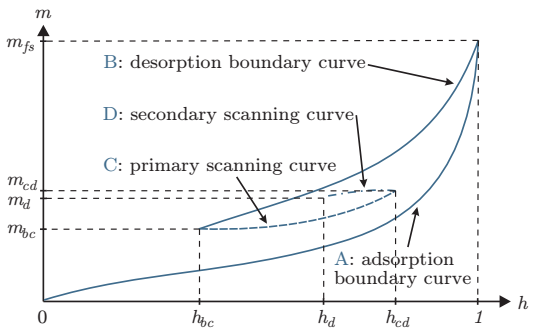

Figure 11 Various boundary and scanning curves..

The explanation for the sorption hysteresis phenomenon is found in the chemical behavior and complex structure of wood, which is described in section 2.

Adsorption of water leads to swelling of the cell wall and breaking of hydrogen bonds, and thus more available sorption sites become unbound. The hydrogen bonds are re-established during desorption, but this process is delayed, since water molecules now occupy the sorption sites. Hence, wood contains more water at a given relative humidity during desorption than during adsorption. For an arbitrary variation in the relative humidity, conditions between pure adsorption and pure desorption dependent on the availability of sorption sites can be obtained.

The terminology is presented in Figure 11. Using initial conditions of the dry state with a moisture content and relative humidity equal to zero and increasing the relative humidity to 100% provide the so-called adsorption boundary curve, A. Decreasing the relative humidity also decreases the moisture content along the desorption boundary curve, B. An increase in relative humidity before reaching the dry

state again results in movement along a so-called scanning curve, C, which gradually approaches the adsorption boundary curve. This type of scanning curve is called a primary scanning curve, and a scanning curve taking origin in this is called a secondary scanning curve, D, etc. The points at which a shift from a desorption curve to an adsorption curve occurs $\{h_{bc}, m_{bc}\}$, or the reverse $\{h_{cd}, m_{cd}\}$, are called reversal points.

Modeling of hysteresis

A classical approach for modeling sorption hysteresis is the independent domain model developed by Everett and co-workers (Everett and Whitton, 1952; Everett and Smith, 1954; Everett, 1954, 1955). A discretization of the model was applied to measurements of sorption hysteresis in yellow poplar (*Liriodendron tulipifera* L.) by Peralta (1995b,a). However, the discretization only allowed steps between the relative humidity values 0%, 11%, 32%, 53%, 75%, 92% and 100%, so Peralta (1996) refined the model to take smaller relative humidity steps into account. However, this refinement violates the original method of Everett, and in the general case the method will lead to loss of water in the accounting (explained in detail in Paper III (Frandsen et al., 2007c)). To generalize the measurements from a given isotherm for a given species, and thus avoid extensive experimental work, Peralta and Bangi (1998a,b) presented two models based on the work of Mualem (1973, 1974).

All of the models involve accounting for an independent domain or entire history of relative humidity variations to obtain the moisture content. In addition to the accounting complications, the independent domain model has another major numerical drawback for isotherms with a slope different from zero at the dry condition (e.g. for wood, paper, unsaturated soil, concrete). Thus, here it implicitly involves singularities in a function used to obtain the moisture content, see Paper III (Frandsen et al., 2007c).

Pedersen (1990) presented a formulation, which involves differential equations that must be solved numerically in the $h - m$ domain for each step in time to obtain the prevailing scanning curves. This model has been generalized and calibrated to the measurements performed by Peralta (1995b) on yellow poplar (*Liriodendron tulipifera* L.) at 30°C and to measurements on Norway spruce (*Picea abies*) at 20°C performed by Ahlgren (1972) in (Frandsen, 2005).

Besides these two models, models for describing sorption hysteresis in unsaturated soil have been proposed (Scott et al., 1983; Kool and Parker, 1987; Huang et al., 2005). The physics is different from sorption hysteresis in wood, since the driving forces of sorption in wood are primarily of a chemical nature compared to the capillary force-driven sorption in porous materials (Avramidis, 1997). Mathematically, however, the models are more similar. The model by Huang et al. (2005) has the advantage of describing the scanning curves using closed-form expressions, with the two previous reversal points as input. A drawback is that the model for the scanning curves is not naturally bounded by the boundary curves.

The independent domain models and Pedersen's model are both cumbersome to implement into a numerical method such as the finite element method, since the prevailing scanning curve must be evaluated by numerical integration for each step forward in time.

In Paper III (Frandsen et al., 2007c) a new sorption hysteresis model is presented. The model is suitable for implementation into a numerical method due to the following features:

- The prevailing scanning curves are provided as closed-form expressions, which only depend on the current moisture content and relative humidity. Hence, no history of relative humidity variations or other storage parameters are necessary.
- By a normalization, the scanning curves are modeled independently of the boundary

curves. This makes the model applicable to different species and materials. Furthermore, this independency allows temperature variations of the boundary curves to be taken into account.

The normalized scanning curves are known to vary slightly from species to species, but from the experimental data available it is not possible draw conclusions on their temperature dependency.

As mentioned, hysteresis is a phenomenon occurring in various materials. To illustrate the applicability of the model, it is also applied to bleached-kraft paperboard in the short conference paper, Paper IV (Frandsen and Damkilde, 2006).

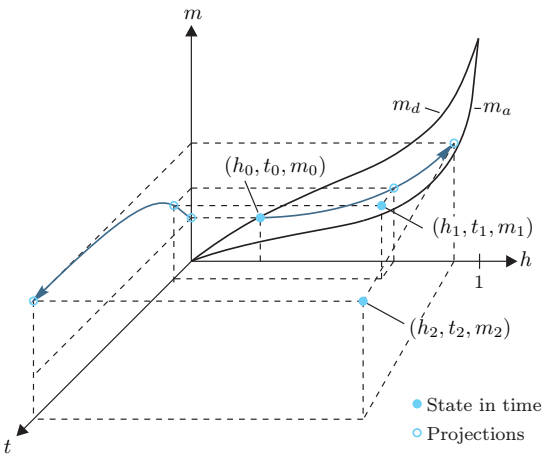

Figure 12 The increase of moisture content, m, over time, t, along an adsorption scanning curve, due to an increase in relative humidity, h.

3.3 Sorption hysteresis in a multi-Fickian model

Both sorption hysteresis and multi-Fickian moisture transport influence the moisture content of wood. The multi-Fickian moisture transport influences it in time and space, and hysteresis controls the equilibrium moisture content by the preceding relative humidity variations. The sorption takes place inside the wood specimen between air in the lumens and the cell wall. For a point in a cell wall, the increase of moisture content along an adsorption scanning curve in time can be illustrated as in Figure 12.

Exposed to an increase in relative humidity from h_0 to h_2, the moisture content will over time trace along the adsorption scanning curve to the equilibrium point (h_2,t_2,m_2). Hence, the equilibrium moisture content, which influences the sorption rate, is governed by hysteresis.

The sorption rate, diffusion of vapor and bound water to the point determine the rate, by which the state traces along the scanning curve.

In Paper V (Frandsen and Svensson, 2007) these relations are formulated in a mathematical and physical model. An essential part of the model is definition of the moisture condition in wood as a state in preference to moisture content alone. This consideration allows a simple accounting for hysteresis effect at the individual points of the material. Furthermore, together with a similar state for the condition of the air in the lumens, it is used to describe sorption rate and hysteresis.

The sorption rate can be formulated in terms of pressure or concentration. Both approaches allow implementation of sorption hysteresis into a multi-Fickian moisture transport model. The implementation of a hysteresis model for both approaches is presented and tested in a finite element program. To illustrate the combined effect of the sorption hysteresis and multi-phase moisture transport, simulations from one of these implementations are presented conclusively, where the model also is compared to experimental results.

3.4 Influence of temperature on a hysteretic multi-Fickian moisture transport model

The influence of a spatially varying temperature field on moisture transport has among others been investigated experimentally by Choong (1963); Siau et al. (1986); Avramidis et al.

(1987); Avramidis and Siau (1987). The experiments showed the so-called Soret effect, i.e., the moisture diffused from dryer to moister climates if a sufficiently large temperature gradient occurred as well.

The reason for this phenomenon can be explained by the following theory. The positioning or bonding of a water molecule to a sorption site is because the molecule experiences a minimum of potential energy at that position, i.e., a stable state. The molecule oscillates around this stable state. By continually occurring collisions, kinetic energy is transferred between the water molecules. If a molecule gains sufficient kinetic energy to exceed the potential energy of the bond, the molecule will diffuse from the site and is said to be activated. Thus, the kinetic energy required to exceed the this potential barrier is called the activation energy e_b (Figure 13).

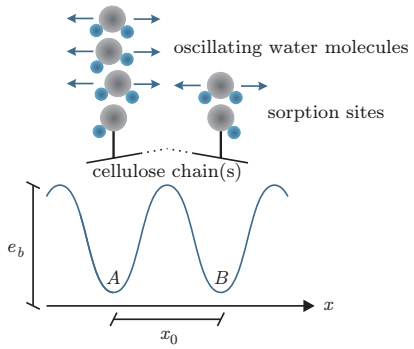

Figure 13 Oscillating water molecules bound at sorption sites A and B.

Different models to describe this phenomenon have been proposed by Briggs (1967); Skaar and Siau (1981); Siau (1982); Nelson (1986, 1991), and the various models have been reviewed in (Siau and Avramidis, 1993; Siau, 1995). The models are based on either activated bound water or free energy, but without regards to the vapor diffusion and internal sorption. Numerical considerations for implementation of the model by Skaar and Siau (1981) in FEM are described by Eriksson et al. (2006), and most recently also by a neural network in (Avramidis and Wu, 2007).

The temperature influences the moisture transport, but on the other hand the diffusion of molecules with a given enthalpy also results in transport of energy. The moisture transport will therefore influence the temperature field as well, and a fully coupled equation system must be invoked.

Whitaker (1977, 1998) proposed a theory for coupled heat, mass, and momentum transfer in porous media under the assumption of a rigid indeformable matrix. This formulation was earlier applied to model drying of wood by Perré et al. (1990; 1996; 1999). Besides, from the heat conduction by diffusion also known as the Dufour effect, Whitaker's heat transfer model also includes terms from the phase changes. The phase change in this case is sorption.

The temperature dependency of sorption relates to heat of sorption Δh_{bv}, i.e., the amount of heat consumed per mole of water desorbed from water vapor to bound water (Figure 15). Note that the location of the abscissa in Figure 15 corresponds to liquid water, but any axis could have been chosen, since only the differences between the enthalpy levels are meaningful.

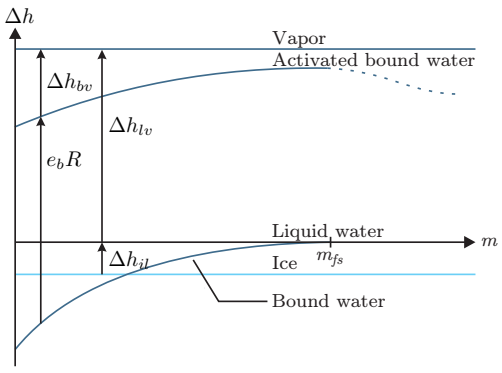

Figure 15 Various heats Δh required at a phase change as a function of moisture content (Skaar and Siau, 1981). Δh_{bv} is heat of sorption, Δh_{lv} heat of evaporation, Δh_{il} heat of fusion, e_b the activation energy, and R the universal gas constant.

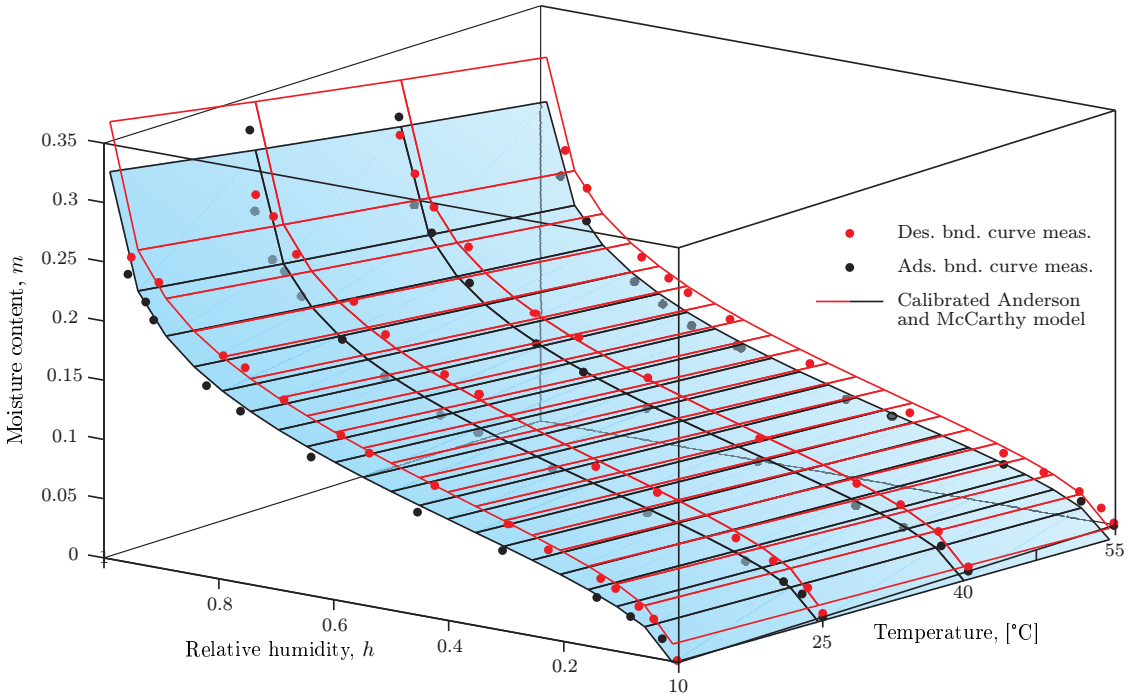

Figure 14 Measurements of the sorption boundary curves at different temperatures by Kelsey (1956) and calibrations of the Anderson and McCarthy model to them.

Thus, adsorption is a time dependent exothermic reaction, i.e., heat is produced during the reaction. Hence, the reaction is according to Le Chatelier's principle promoted by lowering the temperature, i.e., more water can be bound in the cell wall. This is seen in Figure 14 as a negative slope of the sorption boundary "surfaces" with temperature.

To the authors knowledge, the temperature dependency of hysteresis has never been explicitly experimentally investigated, but the the temperature dependency of the boundary curves has been investigated by a number of authors. The desorption boundary curve of sitka spruce (*Picea sitchensis*) was measured at several temperatures by Hawley (1931) here cited from (Kollmann and Côté, 1968). Babiak (1990) calibrated the Anderson-McCarthy model to data from an unknown species at 21.1°C, 35.0°C, 43.3°C, 51.6°C and 71.1°C from data in the USDA Wood Handbook (1974). Choong (1963) measured both boundary curves of Western fir (*Abies nobilis*) at 25°C, 32.2°C, 40°C and 50°C. Kelsey (1956) measured adsorption and desorption boundary curves of klinki pine (*Araucaria hunsteinii*) at 10°C, 25°C, 40°C and 55°C (Figure 1).

Remaining is the question regarding the temperature dependency of the scanning curves. In (Frandsen et al., 2007c) it was observed that the normalized shape of the scanning curves of yellow poplar (*Liriodendron tulipifera* L.) at 30°C and Norway spruce (*Picea abies*) at 20°C were quite similar.

In the discussion Paper VI "Influence of temperature on hysteretic multi-Fickian moisture transport in wood" (Frandsen, 2007) the theory by Whitaker (1977, 1998) is modified to put forth a model for moisture transport in a

wood structure. The model is modified to describe the conditions in a wood structure, where liquid water is absent and convection can be neglected. Furthermore, the model is modified to describe transport of bound water and sorption hysteresis. In the paper the following steps towards a temperature-dependent hysteretic multi-Fickian moisture transport model have been taken:

- Moisture transport depends on temperature gradients, i.e., the so-called Soret effect, but conversely, mass transport involves transport of heat as well. Therefore, a fully coupled mass and heat transport model, which includes the reaction during phase changes between water vapor and bound water, was formulated.
- A constitutive model for temperature dependent bound-water diffusion based on diffusion kinetics has been derived.
- A constitutive model for temperature dependent diffusion of water vapor has been proposed based on the empirical model by Schirmer (1938). This model has not been verified and should be used with caution.
- In formulation of the temperature dependent sorption hysteresis model, temperature dependence of the boundary curves has been taken into account. This was possible due to decoupling of the scanning curves from the boundary curves in the applied hysteresis model described in Paper III (Frandsen et al., 2007c). The temperature dependency of the boundary curves was described with the Anderson and McCarthy model calibrated to data by Kelsey (1956).
- The shape of the normalized scanning curves are assumed to be independent of temperature, since in the few available measurements the shape does not vary significantly. A designated experimental investigation of the temperature dependency of the normalized scanning curves remains.

4 Influence of moisture on mechanical behavior

As bound water is adsorbed to sorption sites in the molecular structure of wood, a number of mechanical responses occur. Especially, if the considered structural wooden member is loaded simultaneously the response can be very complex.

A number of theories for the combined response have been proposed, but no definite and proved theory has been stated. In (Hanhijärvi, 1995) an excellent review of the most common theories is given.

To the author's believe the reasons for the combined response is found on different levels of the structure of wood, and a combination of the theories described in (Hanhijärvi, 1995) yields the complex response. Especially studies on recovery reveal the nature of the time, moisture, load and temperature dependent deformations.

The different contributions due to sustained load and moisture changes are classically divided up into four contributions, i.e., hygroexpansion, elastic, creep, and mechano-sorptive creep. In this section, the description of the complex response will be explained through this classical division.

4.1 Hygroexpansion

As water adsorbs on the sorption sites in the amorphous regions of the glucane chains, the chains are forced apart and more sorption sites become available. This and adsorption on the hydrophilic hemicelluloses result in the swelling of wood.

The major part of the cellulose chains are located in microfibrils in the S2 layer. Since cellulose chains are forced apart the microfibrils mainly expand transversely to their longitudinal direction. As the microfibrils are normally orientated with a low microfibrillar angle in the S2 layer, the fiber mainly expands transversely to the fiber direction. In wood cells, which has been grown in a continuous compressive environment, the microfibrillar angle of the S2 layer

tends to be larger. Consequently, the hygroexpansion is more pronounced in the longitudinal direction for this type of wood.

A number of theories for hygroexpansion have been proposed. The classical theory by Barber (1968) considers the microfibrils as reinforcing fibrils and the matrix material, constituted by lignin and hemicelluloses, as hygroscopic and expanding. Some of the more recent models are based on the theory by Barber (1968) and are generalized by application of the classical laminate theory (Yamamoto, 1999; Pang, 2002) to take different properties of the layers in the micro- or ultrastructure into consideration.

For structural wood continuum models at the macrostructure level are typically applied, see e.g. (Ormarsson, 1999). In this type of model the hygroexpansion in the different material directions is approximated to be linear with the moisture content as found in (Meylan, 1972). This type of model captures the distortions caused by the hygroexpansion and the helix orientation of the fibers (Figure 16).

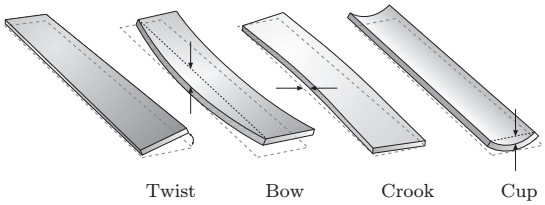

Figure 16 Different modes of deformation due to helix orientation of the fibers in the boards (Ormarsson, 1999).

In figure 17 variants of distortions of the cross-section dependent on the location to the pit are shown.

4.2 Creep and Elastic response

The elastic deformation is defined as the immediate deformation at loading or removal of load. But since wood even at very high frequency excitation exposes time dependent behavior ((Launay, 1987) here cited from (Hanhijärvi, 1995)) it leads to the conclusion that

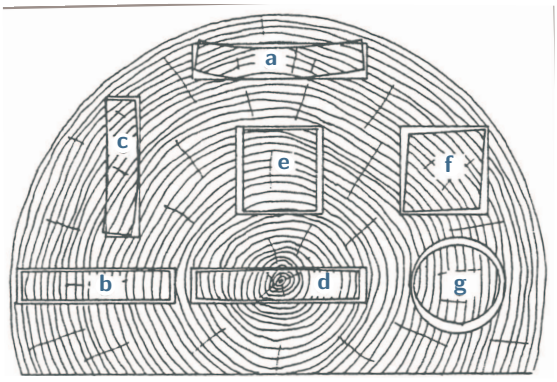

Figure 17 Distortions for different cross-sections dependent on location in the log (USDA, 1974).

elastic response can be considered to be a fast creep component. For most purposes modeling of the initial response as being elastic is sufficient, since the time scale of interest allows neglecting of this short transient response.

Creep is the gradually increasing deformation over time occurring under a sustained load. During this increase of deformation wood is modified at different levels of its structure. For loads below 30-50% of the ultimate load the behavior is linear and almost recoverable when the load is removed (discussed further below). Hence, little damage has been applied to the "bearing" structure.

The microfibrils are here considered to be the stiff bearing structure, which is stretched elastically by uncurling of the polymer chains and changing the angle of some of the covalent bonds. Simultaneous molding of the adhesive matrix materials, hemicelluloses and lignin, provides the viscose response. The deformation in the matrix material is occurring by slippage of hydrogen bonds. The comparatively weak bonds are broken and reestablished continuously until a steady state, the creep limit, has been reached.

The creep limit depends on temperature and moisture content. An example of this is shown in Figure 18, where the relative creep is the

creep response normalized with respect to the elastic deformation. Since water will occupy sorption sites in the amorphous regions of the cellulose chains during adsorption, the stiffness of the bearing structure decreases with moisture content. This is seen for the immediate "elastic" response, but as seen in Figure 18 also for creep. According to the kinetic theory (see section 3.4), breaking of hydrogen bonds are promoted by a temperature increase.

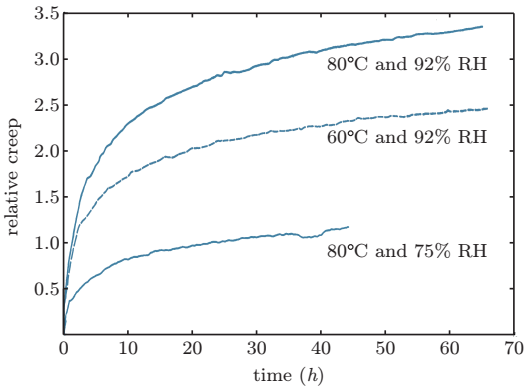

Figure 18 Temperature and moisture dependency of creep in the tangential direction of Scots pine (Svensson, 1996).

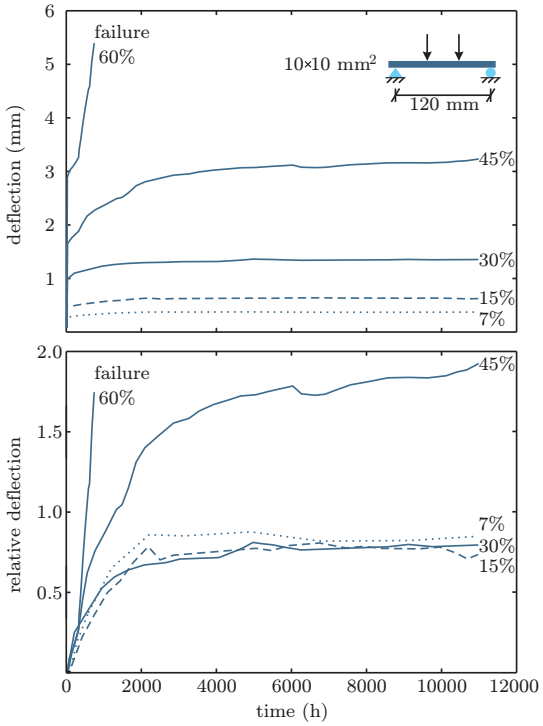

Figure 19 Deflection over time due to creep at different load levels in a four-point bending of Scots pine (*Pinus Sylvestris*) specimens Liu et al. (1992).

When the load exceeds 30-50% of the ultimate load, damage is accumulated in the microfibrils when loaded to the creep limit. The matrix material still provide resistance during moulding and the response is still viscous but not linear. An example of this is shown in Figure 19, where the three lowest load levels up to 30% of the ultimate load provides similar relative deflections (viscoelastic deflection normalized with respect to the elastic deflection), whereas at higher load levels results in non-linear creep, and for the highest load level results in failure within the time-limit of the experiment.

The different types of creep are called primary for the linear visco-elastic creep, secondary for the non-linear constant rate creep, and tertiary for the non-linear and accelerating creep.

As the load is removed the load bearing structure deforms elastically towards the origin. Again, a remolding of the matrix delays the response. In most cases the elastic potential energy stored in the fibers, the microfibrils, is insufficient to overcome the inertness of the molding of the matrix. Thus, complete recovery is not obtained.

By cycling, the relative humidity in the ambient air and hereby the moisture content in the considered specimen, complete recovery can almost be obtained, see e.g. (Mohager, 1987). This is due to unlocking of the inertness by swelling and shrinkage in the matrix structure. The unlocking due to moisture changes, the so-called mechano-sorption, is the subject of the next section.

That complete recovery can be obtained, when wood has experienced primary creep

alone shows that the bearing structure of the material remains undamaged. Thus slippage of hydrogen bonds cannot stem from this part of the composite structure since that would lead to a irrecoverable deformation component.

4.3 Mechano-sorptive creep

The deformation occurring in a wood specimen exposed to sustained load is promoted further by a moisture content variation (Figure 20). As mentioned, this is due to slippage and rebonding of hydrogen bonds between the matrix material constituents. These are in moisture *variations* extensively reorganized due to swelling and shrinkage.

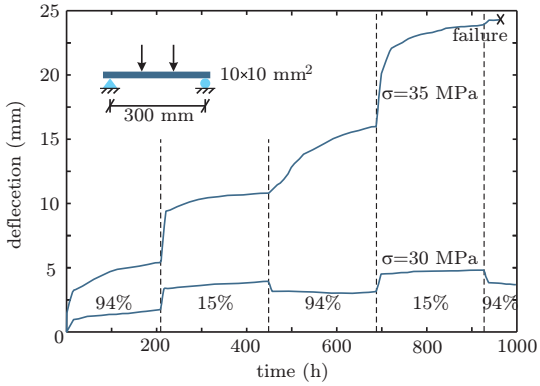

Figure 20 Deflection over time due to creep and mechano-sorption at two load levels in a four point bending of Scots pine (*Pinus Sylvestris*) specimens (Mohager, 1987).

Although creep and mechano-sorptive creep classically has been assumed to be independent phenomena, some experiments indicate that these are due to the same molecular mechanisms although the activation for the two differs. Indications of interaction between the two phenomena are observed and discussed in (Hanhijärvi and Hunt, 1998; Hunt, 1999). Some interaction is also seen in the experiment by Mohager (1987), where creep is found to be almost reversible if exposed to cycling moisture conditions.

Recovery for mechano-sorption longitudinal to the fibers has also been observed to be almost recoverable, as seen in Figure 21.

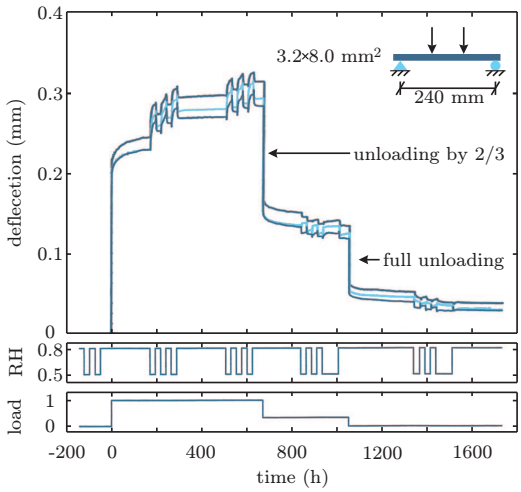

Figure 21 Deflection over time due to creep and mechano-sorption in a four point bending of three Scots pine *Pinus sylvestris* specimens (Hanhijärvi, 1995). The relative humidity variations (RH) and load are indicated below. The load is normalized with respect to the largest load, which provides a nominal edge stress of 6.9 MPa.

More irreversible damage was observed in the experiments on Norway spruce loaded in the tangential direction by Svensson and Toratti (2002). This is most likely due to occurrence of a higher degree of creep.

Even though a number of researchers have worked with phenomenological and to some extent quantification of mechano-sorption, this field is to the authors opinion still open for much interesting research.

Orthotropic creep

For different directions of load, different distribution paths of the stresses in a composite structure occur. For instance, if the cell is tensed in longitudinally, the cell is stretched and due to Poisson's effect in the cell wall, and the cell radius will diminish. In the different directions of deformation the composition of matrix material and the reinforcing microfib-

ril fibers are different. Thus, the rate of deformation in the different directions will be correspondingly distinct.

This results in e.g. time dependent Poisson's ratios as measured by Schniewind and Barrett (1972) (Figure 22). The strain variations leading to the varying PR in Figure 22 are, however, questionable, since they indicate that creep recovery occurs in the transverse direction simultaneously with creep in the longitudinal direction. Some of Schniewind and Barett's (1972) experiments show that the opposite trend of creep occurs in the transverse direction. However, the details on these are limited.

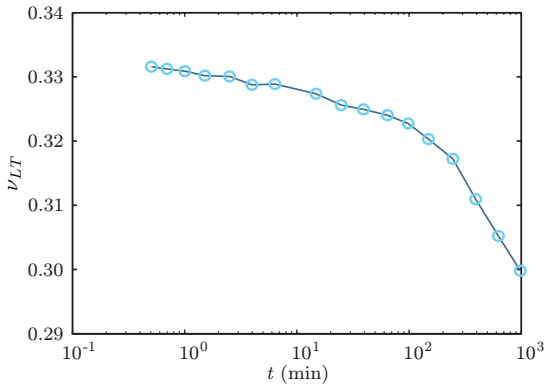

Figure 22 Varying PR from contractions tangential to the fiber loaded in the longitudinally in the experiment by Schniewind and Barrett (1972).

Although other models for orthotropic creep (more details below) have been proposed, the author has knowledge of only one experimental study of orthotropic creep, i.e., Schniewind and Barrett (1972). For connectors and other structural parts where multi-axial states of stress occur and the deformation is restrained, the coupling effects have great significance.

With regard to the pioneering work by Schniewind and Barrett (1972) it must be concluded that the uncertainty arising from this deviating behavior calls for a further investigation of the phenomenon.

4.4 Modeling of creep and mechano-sorption

The approaches for modeling creep and mechano-sorption are quite similar. Roughly speaking, the increments with time are replaced by increments of moisture content (the absolute value), see e.g (Takemura, 1967; Ranta-Maunus, 1975; Salin, 1992). So in the following modeling of the two phenomena will be referred to as creep. For a detailed review of various constitutive models, see e.g. (Hanhijärvi, 1995). In (Hanhijärvi, 1995) a new type of model based on deformation kinetics was applied with good results as well.

Constitutive modeling of the creep response can be done by two approaches, either:

- by purely mathematical expressions for the creep curve, e.g. the power law, or
- by a mechanical analogy involving springs and dashpots.

Both approaches have been widely applied to duration of load problems, shape stability and wood drying. For a recent review of duration of load models, see (Svensson, 2007). For shape stability there is a tendency of application of the latter approach (Hanhijärvi and Mackenzie-Helnwein, 2003; Ormarsson, 1999; Svensson, 2002). The reason for this may be the physical interpretability of the different rheological components involved.

A rheological system is constituted by springs and dashpots, and these are typically arranged in chains of so-called Maxwell or Kelvin elements. The response of such a system can be represented by the heredity integral approach, a set of first order differential equations, or a higher order differential equation. Of these the two former are more suitable for implementation into a numerical method, see e.g. (Ormarsson, 1999; Ottosen and Ristinmaa, 2005).

The classical approach for modeling the time dependent orthotropic response of wood is the hereditary approach also known as

the convolution integral approach, see e.g. (Schniewind and Barrett, 1972; Mårtensson, 1992; Ormarsson, 1999) and for a large displacement formulation (Mauget and Perré, 1999).

Another approach for obtaining an orthotropic creep model suitable for implementation into a numerical method is by formulating a set of first order differential equations, see e.g. (Hanhijärvi and Mackenzie-Helnwein, 2003).

The cited references all apply Kelvin series generalized to include more dimensions to model the time dependent orthotropic response of wood. In these the creep compliances to model the creep in the direction of the load can be determined from uniaxial experiments. For the transverse coupling creep, different assumptions have been made.

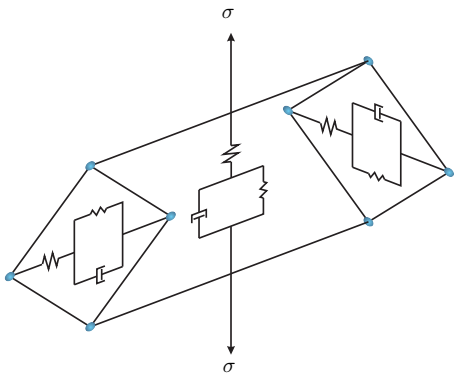

Figure 23 Parallel coupled rheological systems modeling strain and strain rate in various directions due to a longitudinal stress.

In Paper VII (Frandsen et al., 2007b) the transverse coupling creep in multidimensional modeling of creep is treated. Various assumptions about the transverse coupling creep compliances are reviewed. The transverse coupling creep rate differs from the creep rate in the direction of the load (Figure 22), and an orthotropic creep model should reflect this.

Upon that, a new constitutive model for orthotropic creep, which gives resemblance to deformation of the cellular structure of wood, is proposed. In Figure 2 a simple variant of the proposed orthotropic creep model with three coupled rheological systems is shown.

The center system models the deformation in the direction of the load. The two outer systems are connected to the direction of load by lattices, which resemble the distribution of stress in the cellular structure. The stress is hereby transferred in the cellular structure to deformations orthogonal to its direction. For simplicity only one spring modeling the elastic response and one Kelvin element modeling the creep are illustrated, but a generalization of the rheological systems are readily put forth.

Creep is in Paper VII considered as one phenomenon and the complexity of the couplings to temperature and moisture are temporarily disregarded. The considerations are, however, general, and the complexities mentioned are accounted for within the framework.

The object of the research is to establish a correspondence between the material parameters and the structure of wood and thus to contribute with general considerations on the mechanical couplings.

The theoretical considerations will be complemented by ongoing experimental work. In Paper VII (Frandsen et al., 2007b) the experimental procedure is presented. Furthermore, two approaches for implementing the proposed constitutive model into a finite element model are treated.

5 Conclusions

In order to describe shape stability an extensive amount of research has been carried out. In this introductory paper the aim has been to draw a connecting thread through research on shape stability to the research presented in this thesis.

Introducing the structure and composition of wood, the present knowledge on physical and chemical phenomena leading to the hygromechanical response of wood are presented. Hereby the background for the models pre-

sented in the present work is provided as well.

It has been realized by researches within the field that an essential segment of describing the hygromechanical distortions is having an accurate moisture transport model. A substantial part of the present work addresses this issue. Previous research has shown that at higher relative humidities, the moisture transport cannot be described by a Fickian moisture transport model, wherefore the observed phenomena have been referred to as non-Fickian. In the present thesis a so-called multi-Fickian moisture-transport model that describes transport in several phases is corrected and refined. The embedded sorption rate function, which is an essential part of the moisture transport model, is studied and revised. Furthermore, a generalization of the model to describe desorption is proposed. In the same paper the boundary conditions for the multi-Fickian model is discussed as well. It is believed that with this model the moisture transport in wood can be described with a higher accuracy.

Further to the non-Fickian behavior, the complexity of hysteresis also influences the moisture content of wood and thus also the hygromechanical response. In this work a new hysteresis model, suitable for implementation into a numerical method is developed. In this model the prevailing scanning curves are provided as closed-form expressions, which only depend on the current moisture content and relative humidity. Hence, no history of relative humidity variations or other storage parameters are necessary. Furthermore, the scanning curves are modeled independently of the boundary curves by a normalization. This makes the model applicable to different species and materials. The independency also allows temperature variations of the boundary curves to be taken into account.

In the present work it is also described how hysteresis and multi-Fickian moisture transport interact, and a mathematical model describing this interaction is provided. In the implementation of the hysteresis model into the multi-Fickian model a great advantage of the hysteresis model developed becomes evident. Accounting for the history of relative humidity variations can be done by a state variable in preference to e.g. an entire independent domain.

Finally, the temperature dependencies of the multi-Fickian moisture transport model with hysteresis is discussed, and a fully coupled heat and mass transport model is formulated. The model takes the phase changes between water vapor and bound water into consideration in the mass transportation as well as heat transportation. That these couplings exist has been shown in the literature by various experiments. However, no experiment provides evidence of all couplings at the same time.

Beyond addressing moisture transport, the present work also treats transverse creep in an orthotropic material. In experiments, Poisson's ratios have been observed to be time-dependent, and this observation is well supported by theoretical considerations. Therefore, investigations of the transverse couplings in existing models for creep of wood have been conducted. The most common approaches are investigated on this basis. Typically the models explicitly or implicitly provide a constant Poisson ratio over time. Consequently, a new approach that can describe variations of Poisson's ratio is proposed. Parallel to this work an experimental study is currently being carried out at Oregon State University. In this thesis the experimental procedure and setup of this study are described.

6 Perspectives

For the different topics addressed in this thesis a number assumptions and indirect investigations have been made. To substantiate the theories in this work further, a number of investigations and experiments can be made. These and ideas for continued research within the field are given in this section.

6.1 Multi-phase moisture transport

The multi-Fickian moisture transport model consists of more sub-models for phenomena, which have been investigated for different species and at different temperatures through the years. Although good results have been obtained by assumptions on the constitutive models for sorption and water-vapor diffusion, experiment for one species and matching specimens would substantiate the results found in this thesis.

The sorption rate in wood has received very little attention, and to the author's knowledge only one paper by Christensen (1965) addresses the topic. The slow sorption rate at higher relative humidity steps has great significance for the non-Fickian behavior observed. Thus, to gain general knowledge on the sorption rate and to substantiate this important part of the multi-Fickian model, the sorption rate should be investigated at different relative humidity steps and at different temperatures for one chosen species.

The method for measuring the sorption rate used by Christensen (1965) provides seemingly easy interpretable results. A stagnant boundary layer is avoided by conducting the experiments in a vacuum chamber, and diffusion can be neglected due to the spatial extent of the specimens used in the experiments.

Stamm (1959, 1960a) measured the bound-water diffusion in wood by filling the pores with a low melting alloy. The bound-water diffusion at different temperatures and at different moisture content levels can be obtained from this type of experiment given a known sorption rate.

Experimental quantification of the water-vapor diffusion in the cellular structure of wood seems difficult. Maybe water vapor could be substituted by a gas with the same physical characteristics but chemically inert with the cell wall. However, since many pits are aspirated and the vapor diffusion probably to some extent depends on adsorption and desorption through the cell walls, this type of experiment might not provide the desired results.

If the water-vapor diffusion cannot be measured by a clean cut experiment as described above, measuring some segments of the convoluted response is a secondary choice. In the measurements of weight increase by Wadsö (1994b) the weight of the entire specimen was measured over time. Although much has been learnt from this experiment, the total weight does not provide information of spatial distribution in various phases over time. The bound-water concentration can be obtained by measuring the weight, but also x-ray tomography (Lindgren et al., 1992) and Raman spectroscopy (Gierlinger et al., 2006) may turn out to be useful tools here. Furthermore, use of different experimental stages with different ambient climates as e.g. in (Koponen and Liu, 2001) could also be useful in this pursuit. As an example measuring the weight gain of a specimen in a cup and the relative humidity in the cup at different relative humidity steps could be used for studying the relation between sorption rate and vapor diffusion. It is left to the reader to construct an ingenious experiment, which can serve as a further study of multi-phase moisture transport.

6.2 Hysteresis

The temperature dependency of hysteresis has been investigated to some extent as the boundary curves for different species have been measured (see section 3.4). The temperature dependency of the scanning curves has not been investigated. This can be done by performing experiments similar to those conducted by Peralta (1995b) at different temperatures. This experiment could be combined with the experiment conducted by Christensen (1965) to obtain both the sorption rate and the hysteresis equilibrium path.

6.3 Orthotropic creep and mechanosorption

Further research on the transverse orthotropic couplings in creep has been planned, and an experimental study of the couplings are in

progress at Oregon State University.

The theoretical considerations on the transverse orthotropic couplings in creep can be generalized to take mechanosorption into consideration as well. Such a generalization and similar experiments for mechanosortption are at hand. First, a qualitative investigation and comparison with results observed in creep and subsequently a quantitative investigation could be performed.

References

Absetz, I. and Koponen, S. (1997). Fundamental diffusion behaviour of wood. In Hoffmeyer, P., editor, *Proceedings of the International Conference on Wood-Water Relations, Copenhagen*, volume E8, pages 89–106.

Ahlgren, L. (1972). *Moisture fixation in porous building materials.* Division Of Building Technology, The Lund Institute Of Technology.

Andersen, T., Fynholm, P., Hansen, M. H., and Nicolajsen, A. (2002). Fugtsikre træfacader - fugtindhold i højisolerede træfacader. Technical report, By og Byg.

Avramidis, S. (1997). The basics of sorption. In Hoffmeyer, P., editor, *Proceedings Of International Conference On Wood-Water Relations, Copenhagen*, volume E8, pages 1–16.

Avramidis, S., Kuroda, N., and Siau, J. F. (1987). Experiments in nonisothermal diffusion of moisture in wood, part 2. *Wood and Fiber Science*, 19(4):407–413.

Avramidis, S. and Siau, J. F. (1987). Experiments in nonisothermal diffusion of moisture in wood, part 3. *Wood Science and Technology*, 21(4):329–334.

Avramidis, S. and Wu, H. (2007). Artificial neural network and mathematical modeling comparative analysis of nonisothermal diffusion of moisture in wood. *Holz als Roh- und Werkstoff*, 65(2).

Babiak, M. (1990). Wood-water system. *Vedecké Pedagickeé Aktuality. Technical University In Zvolen.*

Bandyopadhyay, A., Radhakrishnan, H., Ramarao, B. V., and Chatterjee, S. G. (2000). Moisture sorption response of paper subjected to ramp humidity changes: Modeling and experiments. *Industrial and Engineering Chemistry Research*, 39(1):219–226.

Barber, N. (1968). Theoretical model of shrinking wood. *Holzforschung*, 22(4):97–103.

Briggs, G. E. (1967). Movement of water in plants. *Botanical Monographs, Davis, Philadelphia*, 7.

Choong, E. T. (1963). Movement of moisture through a softwood in the hygroscopic range. *Forest products journal*, 13(11):489–498.

Christensen, G. N. (1965). The rate of sorption by thin materials. In Wexler, A. and Winn, P. A., editors, *Humidity and Moisture*, volume 4, pages 279–293. Reinhold Publishing Corporation.

Crank, J. (1967). *The mathematics of diffusion.* Oxford Science Publications, London.

Crank, J. and Park, G. S. (1951). Diffusion in high polymers - some anomalies and their significance. *Transactions of the Faraday Society*, 47(10):1072–1084.

Cunningham, M. J. (1994). A model to explain "anomalous" moisture sorption in wood under step function driving forces. *Wood and Fiber Science*, 27(3):265–277.

Dinwoodie, J. M. (2000). *Timber: Its Nature and Behavior.* E & Fn Spon.

Eriksson, J., Ormarsson, S., and Petersson, H. (2006). Finite-element analysis of coupled nonlinear heat and moisture transfer in wood. *Numerical Heat Transfer*, 50(9):851–864.

Everett, D. H. (1954). A general approach to hysteresis. part 3. a formal treatment of the independent domain model of hysteresis. *Trans. Faraday Soc.*, 50:1077–1096.

Everett, D. H. (1955). A general approach to hysteresis. part 4. an alternative formulation of the domain model. *Transactions of the Faraday Society*, 51:1551–1557.

Everett, D. H. and Smith, F. W. (1954). A general approach to hysteresis. part 2. development of the domain theory. *Trans. Faraday Soc.*, 50:187–197.

Everett, D. H. and Whitton, W. I. (1952). A general approach to hysteresis. *Trans. Faraday Soc.*, 48:749–757.

Foss, W. R., Bronkhorst, C. A., and Bennett, K. A. (2003). Simultaneous heat and mass transport in paper sheets during moisture sorption from humid air. *International Journal of Heat and Mass Transfer*, 46(15):2875–2886.

Frandsen, H. L. (2005). Modeling of moisture transport in wood. In *Wood Science and Timber Engineering*. Department of Structural Engineering and Building Technology, Aalborg University, Aalborg.

Frandsen, H. L. (2007). Influence of temperature on hysteretic multi-fickian moisture transport in wood. *To be submitted*.

Frandsen, H. L. and Damkilde, L. (2006). A sorption hysteresis model for cellulosic materials. In *Proceedings of the 19th Nordic Seminar on Computational Mechanics, Lund, Sweden*, pages 77–80.

Frandsen, H. L., Damkilde, L., and Svensson, S. (2007a). A revised multi-fickian moisture transport model to describe non-fickian effects in wood. *Holzforschung*, 61(5):563–572.

Frandsen, H. L., Muszynski, L., and Svensson, S. (2007b). Couplings in orthotropic creep of wood. *To be submitted*.

Frandsen, H. L. and Svensson, S. (2007). Implementation of sorption hysteresis in multi-fickian moisture transport. *Holzforschung*, 61(6):693–701.

Frandsen, H. L., Svensson, S., and Damkilde, L. (2007c). A hysteresis model suitable for numerical simulation of moisture content in wood. *Holzforschung*, 61(2):175–181.

Gierlinger, N., Schwanninger, M., Reinecke, A., and Burgert, I. (2006). Molecular changes during tensile deformation of single wood fibers followed by raman microscopy. *Biomacromolecules*, 7(7):2077–2081.

Håkansson, H. (1994). *Experimentiella studier av transient sorption i cellvägen i trä*. Report tabk-94/3021, Lund Institute of Technology, Lund University, Sweden.

Hanhijärvi, A. (1995). *Modelling of creep deformation mechanisms in wood*. PhD thesis, Technical Research Centre of Finland, Espoo.

Hanhijärvi, A. and Hunt, D. G. (1998). Experimental indication of interaction between viscoelastic and mechano-sorptive creep. *Wood Science and Technology*, 32(1):57–70.

Hanhijärvi, A. and Mackenzie-Helnwein, P. (2003). Computational analysis of quality reduction during drying of lumber due to irrecoverable deformation - part i: Orthotropic viscoelastic-mechanosorptive-plastic material model for the transverse plane of wood. *ASCE Journal of Engineering Mechanics*, 129:996–1005.

Hearmon, R. F. S. and Paton, J. M. (1964). Moisture content changes and creep in wood. *Forest Product Journal*, 14(8):357.

Huang, H. C., Tan, Y. C., Liu, C. W., and Chen, C. H. (2005). A novel hysteresis model in unsaturated soil. *Hydrological Processes*, 19(8):1653–1665.

Hunt, D. G. (1999). A unified approach to creep of wood. *Royal Society of London Proceedings Series A*, 455(1991):4077–4095.

Kelsey, K. E. (1956). The sorption of water vapor by wood. *Australian Journal Of Applied Science*, 8(1):42–54.

Kollmann, F. F. P. and Côté, W. A. (1968). *Principles of wood science and technology.* Springer Verlag.

Kool, J. B. and Parker, J. C. (1987). Development and evaluation of closed-form expressions for hysteretic soil hydraulic properties. *Water Resources Research*, 23(1):105–114.

Koponen, S. and Liu, K. (2001). Moisture transport in wood through cell structure - transient-cup test and results. Technical report, Laboratory of Structural Engineering and Building Physics, Helsinki University of Technology.

Krabbenhøft, K. and Damkilde, L. (2004). A model for non-fickian moisture transfer in wood. *Materials and Structures*, 37(273):615–622.

Launay, J. (1987). Mesure des constantes élastiques d'un épicéa par goniométrie ultrasonore. Technical report, Rapport ESEM pour le CTBA, Contrat de programme M.R.E.S.

Lindgren, O., Davis, J., Wells, P., and Shadbolt, P. (1992). Nondestructive wood density distribution measurements using computed-tomography. *Holz als Roh- und Werkstoff*, 50:295–299.

Liu, T., Toratti, T., and Ödeen, K. (1992). Creep of wood under long-term loads in constant and varying environments. In *TRITA-BYMA*, volume 4, page 79. Deparment of Building Materials, The Royal Institute of Technology, Sweden.

Mandelkern, L. and Long, F. A. (1951). Rate of sorption of organic vapors by films of cellulose acetate. *Journal of Polymer Science*, 6(4):457–469.

Mårtensson, A. (1992). *Mechanical behavior of wood exposed to humidity variations.* Ph.d. thesis, Lund Institute of Technology.

Massoquete, A., Lavrykov, S., and Ramarao, B. V. (2005). Non-fickian behaviour of moisture diffusion in paper. *Journal of Pulp and Paper Science*, 31(3):121–127.

Mauget, B. and Perré, P. (1999). A large displacement formulation for anisotropic constitutive laws. *European Journal of Mechanics a-Solids*, 18(5):859–877.

Meylan, B. A. (1972). The influence of microfibril angle on the longitudinal shrinkage-moisture content relationship. *Wood Science and Technology*, 6(4):293–301.

Mohager, S. (1987). Studier av krypning hos trä (studies of creep in wood). In *TRITA-BYMA*, volume 1. Department of Building Materials, The Royal Institute of Technology, Sweden.

Mualem, Y. (1973). Modified approach to capillary hysteresis based on a similarity hypothesis. *Water Resources Research*, 9(5):1324–1331.

Mualem, Y. (1974). Conceptual model of hysteresis. *Water Resources Research*, 10(3):514–520.

Nelson, R. M. (1986). Diffusion of bound water in wood. *Wood Science and Technology*, 20(4):309–328.

Nelson, R. M. (1991). Heats of transfer and activation energy for bound-water diffusion in wood. *Wood Science and Technology*, 25:193–202.

Nyman, U., Gustafsson, P. J., Johannesson, B., and Hagglund, R. (2006). A numerical

method for the evaluation of non-linear transient moisture flow in cellulosic materials. *International journal for numerical methods in engineering*, 66(12):1859–1883.

Ormarsson, S. (1999). *Numerical Analalysis of Moisture-Related Distortions in Sawn Timber*. PhD thesis, Department of Structural Mechanics, Chalmers University of Technology.

Ottosen, N. S. and Ristinmaa, M. (2005). *The Mechanics of Constitutive Modeling*. Elsevier Science.

Pang, S. (2002). Predicting anisotropic shrinkage of softwood. part 1: Theories. *Wood Science and Technology*, 36:75–91.

Pedersen, C. R. (1990). *Combined heat and moisture transfer in build constructions*. PhD thesis, Thermal Insulation Laboratory, Technical University of Denmark, Denmark.

Peralta, P. N. (1995a). Modelling wood moisture sorption hysteresis using the independent-domain theory. *Wood and Fiber Science*, 27(3):250–257.

Peralta, P. N. (1995b). Sorption of moisture by wood within a limited range of relative humidities. *Wood and Fiber Science*, 27(1):13–21.

Peralta, P. N. (1996). Moisture sorption hysteresis and the independent-domain theory: The moisture distribution function. *Wood and Fiber Science*, 28(4):406–410.

Peralta, P. N. and Bangi, A. P. (1998a). Modeling wood moisture sorption hysteresis based on similarity hypothesis. Part 1. direct approach. *Wood and Fiber Science*, 30(1):48–55.

Peralta, P. N. and Bangi, A. P. (1998b). Modeling wood moisture sorption hysteresis based on similarity hypothesis. Part 2. capillary-radii approach. *Wood and Fiber Science*, 30(2):148–154.

Perré, P. and Degiovanni, A. (1990). Control-volume formulation of simultaneous transfers in anisotropic porous media: Simulations of softwood drying at low and high temperature. *International Journal of Heat and Mass Transfer*, 33(11):2463–2478.

Perré, P. and Turner, I. W. (1996). *Mathematical Modeling and Numerical Techniques in Drying Technology*, chapter The use of macroscopic equations to simulate heat and mass transfer in porous media. Marcel Dekker, New York,.

Perré, P. and Turner, I. W. (1999). A 3-d version of transpore: a comprehensive heat and mass transfer computational model for simulating the drying of porous media. *International Journal of Heat and Mass Transfer*, 42(24):4501–4521.

Ranta-Maunus, A. (1975). The viscoelasticity of wood at varying moisture content. *Wood Science and Technology*, 9:189–205.

Rosen, H. N. (1978). The influence of external resistance on moisture adsorption rates in wood. *Wood and Fiber Science*, 10(3):218–228.

Salin, J.-G. (1992). Numerical prediction of checking during timber drying and new mechano-sorptive creep model. *Holz als Roh- und Werkstoff*, 50:195–200.

Salin, J.-G. (1996). Mass transfer from wooden surfaces and internal moisture non-equilibrium. *Drying Technology*, 14(10):2213–2224.

Schirmer, R. (1938). Die diffusionszahl von wasserdampf-luftgemischen und die verdampfungsgeschwindigkeit. *VDI Beihaft Verfahrestechnik*, 6:170.

Schniewind, A. P. and Barrett, J. D. (1972). Wood as a linear orthotropic viscoelastic material. *Wood Science and Technology*, 6(1):43–57.

Scott, P. S., Farquhar, G. J., and Kouwen, N. (1983). Hysteretic effects on net infiltration. *Advances in Infiltration*, 11(83):163–170.

Siau, J. F. (1982). Chemical potential as a driving force for nonisothermal moisture movement in wood. *Wood Science and Technology*, 17(2):101–105.

Siau, J. F. (1984). *Transport Processes in Wood*. Springer-Verlag, Heidelberg.

Siau, J. F. (1995). *Wood: Influence of moisture on physical properties*. Department Of Wood Science and Forrest Products, Virginia polytechnic Institute and State University.

Siau, J. F. and Avramidis, S. (1993). Application of a thermodynamic model to nonisothermal diffusion of moisture in wood. *Wood Science and Technology*, 27(2):95–114.

Siau, J. F., Bao, F., and Avramidis, S. (1986). Experiments in nonisothermal diffusion of moisture in wood. *Wood and Fiber Science*, 18(1):84–89.

Skaar, C. and Siau, J. F. (1981). Thermal diffusion of bound water in wood. *Wood Science and Technology*, 15(2):105–112.

Stamm, A. J. (1959). Bound-water diffusion into wood in the fiber direction. *Forest Product Journal*, 9:27–32.

Stamm, A. J. (1960a). Bound-water diffusion into wood in the across-the-fiber directions. *Forest Product Journal*, 10:524–528.

Stamm, A. J. (1960b). Combined bound-water and water vapor diffusion into sitka spruce. *Forest Product Journal*, 10:644–648.

Stamm, A. J. and Nelson, R. M. (1961). Comparison betweeen measured and theoretical drying diffusion coefficients for southern pine. *Forest Product Journal*, pages 536–543.

Svensson, S. (1996). Strain and shrinkage force in wood under kiln drying conditions. ii: Strain, shrinkage and stress measurements under controlled climate conditions. *Holzforschung*, 50:463–469.

Svensson, S. (2002). *Internal Stress in Wood Caused by Climate Variations*. PhD thesis, Division of Structural Engineering, Lund University.

Svensson, S. (2007). Duration of load effects of solid wood; methods and models. In *COST E55 Workshop "Performance of Timber Structures", Graz, Austria*.

Svensson, S. and Toratti, T. (2002). Mechanical response of wood perpendicular to grain when subjected to changes of humidity. *Wood Science and Technology*, 36(2):145–156.

Takemura, T. (1967). Plastic properties of wood in relation to the non-equilibrium states of moisture content. *Mokuzai Gakkaishi*, 6:77–81.

USDA (1974). *Wood Handbook. Wood as an engineering material*. US Forest Product Laboratory.

Wadsö, L. (1994a). Describing non-fickian water-vapor sorption in wood. *Journal of Material Science*, 29:2367–2372.

Wadsö, L. (1994b). Unsteady-state water-vapor adsorption in wood: An experimental-study. *Wood and Fiber Science*, 26(1):36–50.

Whitaker, S. (1977). *Advances in heat transfer*, volume 13, chapter Simultaneous heat, mass, and momentum transfer in porous media: A theory of drying, pages 119–203. Academic Press, New York.

Whitaker, S. (1998). *Advances in heat transfer*, volume 31, chapter Coupled transport in multiphase systems: A theory of drying, pages 1–104. Academic Press, New York.

Yamamoto, H. (1999). A model of the anisotropic swelling and shrinking process of wood. Part 1. generalization of Barber's

wood fiber model. *Wood Science and Technology*, 33:311–325.

Paper II

A revised multi-Fickian moisture transport model to describe non-Fickian effects in wood

Holzforschung vol. 61 issue 5, pp. 563-572, 2007

Paper II

A revised multi-Fickian moisture transport model to describe non-Fickian effects in wood

Henrik Lund Frandsen[1] Lars Damkilde[2] and Staffan Svensson[3]
[1]*Department of Civil Engineering, Aalborg University, Denmark*
[2]*Esbjerg Institute of Technology, Aalborg University, Denmark*
[3]*Department of Civil Engineering, Technical University of Denmark, Denmark*

Abstract
This paper presents a study and a refinement of the sorption rate model in a so-called multi-Fickian or multi-phase model. This type of model describes the complex moisture transport system in wood, which consists of separate water-vapor and bound-water diffusion interacting through sorption. At high relative humidities, the effect of the complex moisture transport system becomes apparent, and since a single Fickian diffusion equation fails to model the behavior, it has been referred to as non-Fickian or anomalous behavior. At low relative humidities, slow bound-water transport and fast sorption allow a simplification of the system to be modeled by a single Fickian diffusion equation. To determine the response of the system, the sorption rate model is essential. Here the function modeling the moisture-dependent adsorption rate is investigated based on existing experiments on thin wood specimens. In these specimens diffusion is shown to be negligible, allowing a separate study of the adsorption rate. The desorption rate has been observed to be slower at higher relative humidities as well, and an expression analogous to the adsorption rate model is proposed. Furthermore, the boundary conditions for the model are discussed, since discrepancies from corresponding models for moisture transport in paper products have been found.

Key words: adsorption, boundary conditions, desorption, diffusion, multi-Fickian, multi-phase, non-Fickian, slow sorption, sorption rate.

1 Introduction

Moisture transport in wood below the fiber saturation point is a process governed by three phenomena: (1) bound-water diffusion, (2) water-vapor diffusion (Stamm, 1959, 1960a; Stamm and Nelson, 1961), and (3) the coupling between the two phases of water.

A change of vapor pressure in the ambient air results in diffusion of water vapor, J_v, in wood, sorption of bound-water, and consequential, bound-water diffusion, J_b. In Figure 1 the time-dependent processes of the phenomenon, i.e., diffusion in wood in the two phases and the sorption coupling, are schematically illustrated. It is important to recognize that the time-dependent sorption plays a significant role in this phenomenon.

At low relative humidities, bound-water dif-

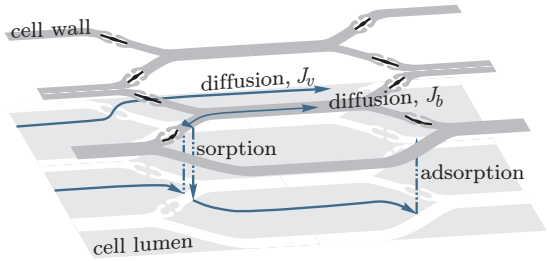

Figure 1 Various time-dependent processes responsible for moisture transport in the cellular structure of wood.

fusion is a relatively slow process, and the moisture transport in wood is governed by water-vapor diffusion, which is evident from the ratio between the diffusion coefficients: $D_v/D_b \simeq 1 : 4 \cdot 10^{-6}$ (Schirmer, 1938; Siau, 1995). Subsequently, relatively fast sorption of bound water commences. Hence, the process governing the combined process is water-vapor diffusion and moisture transport is often modeled by a single Fickian diffusion equation.

At higher relative humidities, bound-water diffusion becomes more significant ($D_v/D_b \simeq 1 : 2 \times 10^{-5}$) and the sorption slows down (Christensen, 1965). This combined phenomenon of two-phase diffusion and sorption has characteristics that cannot be described by a single diffusion equation (Krabbenhøft and Damkilde, 2004). Therefore, it has been referred to as anomalous behavior ornon-Fickian effects (Crank and Park, 1951; Wadsö, 1994a).

For a single diffusion equation to model one-dimensional diffusion, the fractional weight increase, E, as a function of time, t, for different specimen thickness, a, is identical when time is normalized by $t^{1/2}/a$ (Crank 1967). The fractional weight increase is given by:

$$E(t) = \frac{w(t) - w_0}{w_\infty - w_0}, \tag{1}$$

where w_0 and w_∞ are the initial and final weight, respectively, and $w(t)$ is the weight at the time t. Note that surface resistance here is assumed to be negligible because of sufficient convection at the surface. Efforts to ensure this condition were made in the experiments mentioned in the following.

The first researchers to report the non-Fickian effects were Crank and Park (1951) for long polymers and Mandelkern and Long (1951) for cellulose acetate. Wadsö (1994b; 1994a) measured uptake of bound water in pine (*Pinus silvestris*) specimens of various widths, a, and different material directions at high relative humidity steps, i.e., 54–75% and 75–84% relative humidity. The specimens were exposed on two symmetrically oriented surfaces in a ventilated climate chamber humidified using salt solutions. The air velocity was approximately 3 m s^{-1}, so that effects from the boundary layer can be assumed to very small (Rosen, 1978). Figure 2 shows the fractional weight increase for diffusion in the tangential direction in some of these measurements is shown. During the first relative humidity step (54-75%) the thick specimen shows a slightly higher rate of fractional weight increase. In the second relative humidity step (75-84%) the thick specimen gains weight significantly faster. Besides, these fractional weight increase curves do not show the Fickian characteristic of an initial almost linear increase succeeded by an abrupt bend into a horizontal asymptote, but are smoother.

Thus, it can be concluded that the observed phenomenon cannot be modeled by a single Fickian diffusion equation. In the following, the development of a moisture transport model capturing this behavior is presented.

2 Development of the multi-Fickian model

As early as the 1960s, a detailed model that considered several moisture transport routes was suggested by Stamm (1960b), and Siau (1984) presented a simpler, but similar model. In these models, the resistances to diffusion from cell walls and lumens are parallel and serially connected. The underlying assumption connecting these resistances is instantaneous sorption or immediate equilibrium between the

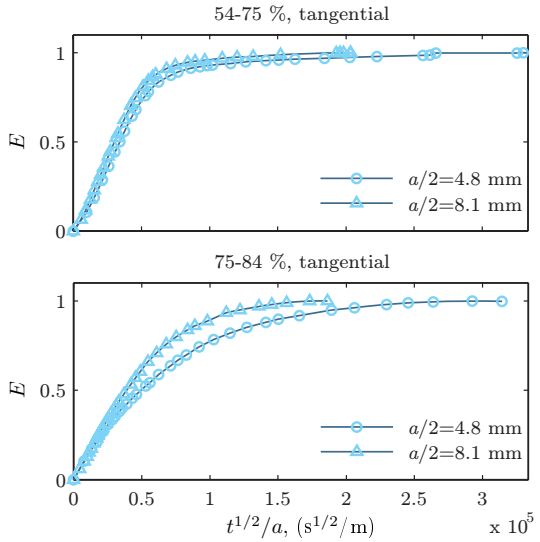

Figure 2 Fractional weight increase, E, in pine specimens over time normalized with respect to specimen thickness a from measurements by Wadsö (1994b).

water vapor and bound water. Thus, the time dependence of sorption, i.e., the vertical process in Figure 1, is neglected. Therefore this type of model cannot describe the non-Fickian behavior caused partly by slow sorption.

Consequently, the transport of water vapor and bound water must be modeled in separate phases connected through a phase change, i.e., time-dependent sorption. Here, this type of model is referred to as a multi-Fickian model, since bound-water and water-vapor transport are described by two coupled Fickian diffusion equations, one for each phase.

To the best of our knowledge, the first researcher to follow up on Wadsö's experiments with this type of mathematical model was Cunningham (1994). The differential equations posed were solved analytically, so that a number of simplifications of the physics were made, i.e., bound-water diffusion (J_b in Figure 1) was neglected and the sorption isotherm was assumed linear. However, with the equation-solving tool available, this approach gave quite good results when comparing to *one* of Wadsö's experiments.

Salin (1996) included the bound-water diffusion and solved the problem analytically, so the isotherm was again assumed to be linear. Again, relatively good results were obtained using an analytical solution. Salin correctly indicated the applied sorption function to be the reason why his model deviates from Wadsö's measurements at higher relative humidities. Salin assumed that the sorption rate function, which is independent of the moisture content. This dependency becomes clear when studying the experiments by Christensen (1965), and is further discussed below.

Absetz and Koponen (1997) modeled multi-Fickian moisture transport in laminated veneer lumber (LVL) parallel to grain in specimens of different thickness. Since all experiments were performed at the same relative humidity step, a moisture-independent sorption rate was sufficient to obtain good results. Furthermore, Absetz and Koponen provided an important discussion of the magnitude of different parameters involved in their model, but without identifying them.

Krabbenhøft and Damkilde (2004) discussed and identified some of these physical constants, introduced an expression for moisture-dependent sorption rate and applied a non-linear isotherm. Furthermore, the two diffusion equations were formulated in terms of concentration of bound-water and water-vapor pressure in preference to concentrations only (Cunningham, 1994; Salin, 1996) or pressures only (Absetz and Koponen, 1997). An overview of the model development is provided in Table 1.

Parallel to this line of research, the type of models has also been applied on moisture transport in paper stacks; see e.g. (Bandyopadhyay et al., 2000; Foss et al., 2003; Massoquete et al., 2005).

The present paper refines the work of Krabbenhøft and Damkilde (2004) and previous researchers with studies on the so far undocumented, but essential, sorption rate func-

	Cunningham (1994)	Salin (1996)	Absetz and Koponen (1997)	Krabbenhøft and Damkilde (2004)
Water-vapor diff., J_v	√	√	√	√
Bound-water diff., J_b		√	√	√
Non-linear isotherm				√
Moist. dep. sorp. rate				√
Pressure and conc.				√

Table 1 Progress of the multi-Fickian model refinement.

tion in relation to the multi-Fickian model. The studies on the sorption rate function are based on measurements by Christensen (1965). Initially, the coupled diffusion equations that constitute the mathematical framework are derived. The boundary conditions for the problem are presented and discussed based on differences in similar models for moisture transport in paper stacks. Finally, results from the revised model are compared with the measurements by Wadsö (1994b).

3 Diffusion processes

As mentioned, transport in the two phases (bound water and water vapor) takes place by diffusion. The diffusion equations are initially stated in terms of concentrations of water in each phase relative to the dry volume of wood. Thus, effects arising from volume changes due to swelling are omitted from the mass balance.

The flux vectors of the bound water, $\mathbf{J}_b$, and water vapor, $\mathbf{J}_v$, are given by the constitutive equations (Fick's first law):

$$\mathbf{J}_b = -\mathbf{D}_b \boldsymbol{\nabla} c_b \quad , \quad \mathbf{J}_v = -\mathbf{D}_v \boldsymbol{\nabla} c_v \tag{2}$$

where c_b and c_v are the concentration of water in the bound-water and water-vapor phase, respectively, with the dry volume of wood as reference (kg m^{-3}). The matrices $\mathbf{D}_b$ and $\mathbf{D}_v$ contain the temperature and moisture-dependent diffusion coefficients for the different material directions in the diagonal (m^2 s^{-1}). $\boldsymbol{\nabla}$ is the spatial gradient operator.

Since the dry volume has been chosen as reference for concentrations, the mass conservation equations for each phase are:

$$\frac{\partial c_b}{\partial t} + \boldsymbol{\nabla} \cdot (\mathbf{J}_b) = \dot{c} \ , \ \frac{\partial c_v}{\partial t} + \boldsymbol{\nabla} \cdot (\mathbf{J}_v) = -\dot{c}. \tag{3}$$

These deviate from the standard Fickian mass conservation equation, with the right-hand side containing the sorption rate, $\dot{c}$. Through this term, the water is allowed to change phase. For a positive value of $\dot{c}$, water is adsorbed from the vapor phase to the bound-water phase. Eliminating the fluxes $\mathbf{J}_b$ and $\mathbf{J}_v$ from Eqs. (2) and (3) provides the governing equations:

$$\frac{\partial c_b}{\partial t} = \boldsymbol{\nabla} \cdot (\mathbf{D}_b \boldsymbol{\nabla} c_b) + \dot{c} \tag{4}$$

$$\frac{\partial c_v}{\partial t} = \boldsymbol{\nabla} \cdot (\mathbf{D}_v \boldsymbol{\nabla} c_v) - \dot{c}. \tag{5}$$

The water-vapor diffusion equation is based on concentration, whereas the amount of water vapor in the ambient air is quantified in terms of partial gas pressure, p_v, and hence it is advantageous to shift the independent variable by applying the ideal gas law:

$$p_v = \frac{n_v}{V_{\text{lumens}}} RT = c'_v \frac{RT}{M_{\text{H}_2\text{O}}}, \tag{6}$$

where c'_v is the concentration of water vapor based on the volume of the cell lumens, V_{lumens} (m^3), R the universal gas constant (J mol^{-1}K^{-1}), T the temperature (K) and $M_{\text{H}_2\text{O}}$ the molecular mass of water (kg mol^{-1}). The relationship between the concentration c_v, which is based on total volume, and c'_v is:

$$\varphi = \frac{V_{\text{lumens}}\, w_v}{V_{\text{total}}\, w_v} = \frac{c_v}{c'_v}, \tag{7}$$

where φ is the porosity and w_v is the mass of water vapor. Inserting Eqs. (6) and (7) into

Eq. (5) yields:

$$\frac{\partial}{\partial t}\left(p_v \frac{\varphi M_{\mathrm{H_2O}}}{RT}\right) = \boldsymbol{\nabla}\cdot\left(\mathbf{D}_v\boldsymbol{\nabla}\left(p_v\frac{\varphi M_{\mathrm{H_2O}}}{RT}\right)\right) - \dot{c}. \tag{8}$$

For an isothermal case, where no gradients in temperature are present, Eq. (8) simplifies to:

$$\varphi\frac{\partial p_v}{\partial t} = \boldsymbol{\nabla}\cdot(\varphi\mathbf{D}_v\boldsymbol{\nabla}p_v) - \frac{RT}{M_{\mathrm{H_2O}}}\dot{c}. \tag{9}$$

Eq. (9) differs from Eq. (11) in (Krabbenhøft and Damkilde, 2004) with the fraction $RT/M_{\mathrm{H_2O}}$. However, in their numerical simulations this fraction was accounted for.

Diffusion in the cell lumens is assumed to be similar to diffusion in stagnant air, but compensated for the geometry of the lumens and resistance at the narrow passages of the pits. Diffusion of water vapor in bulk air is estimated by the empirical expression by Schirmer (1938):

$$\mathbf{D}_v = \boldsymbol{\xi}\underbrace{\left(2.31\times10^{-5}\frac{p_{\mathrm{atm}}}{p_{\mathrm{atm}}+p_v}\left(\frac{T}{273K}\right)^{1.81}\right)}_{\text{Schirmer}}, \tag{10}$$

where p_{atm} is the atmospheric pressure and p_v the partial vapor pressure. The matrix $\boldsymbol{\xi}$ contains the estimated reduction factors, due to hindrance of the diffusion in the cellular structure. The reduction factors for the different directions are located in the diagonal of the matrix.

For typical softwoods, the diffusion of water vapor longitudinal to the tracheid fibers is governed by the partly interconnected lumens. In the tangential direction, diffusion is significantly hindered by the narrow passages at the intertracheid pits and bordering pits, so that the reduction here is expected to be more substantial. The reduction factors applied, reflecting diffusion through pits as well, are identified from the experiments carried out by Wadsö (1994b) as $\xi_L = 0.9$ and $\xi_T = 0.03$.

Diffusion in the cell walls can be determined using an expression of Skaar and Siau (1981). They derived a bound-water diffusion coefficient of the Arrhenius type for bound-water diffusion transverse to the fiber direction based on the measurements made by Stamm (1959). The bound-water diffusion coefficient in the longitudinal direction is estimated to be 2.5 times greater than that in the tangential direction (Siau, 1995). Thus, the matrix with the diffusion coefficients is written as:

$$\mathbf{D}_b = \mathbf{D}_0\exp\left(\frac{-E_b}{RT}\right), \tag{11}$$

where E_b is the activation energy for bound-water diffusion (J mol^{-1}). The diagonal terms of $\mathbf{D}_0$, i.e., D_T^0 and D_L^0 are equal to 7×10^{-6} m^{2}s^{-1} and 17.5×10^{-6} m^{2}s^{-1}, respectively, for a two-dimensional case (Siau 1984). The activation energy may be approximated by the linear expression $E_b = (38.5-29m)\times10^3$ J mol^{-1} (Siau, 1995), where $m = c_b/\rho_0$ is the moisture content and ρ_0 is the dry density of wood. The decrease in activation energy with moisture content is due to the decrease in bonding energy at the sorption sites.

4 Sorption

Sorption is a phase change between water vapor and bound water, which occurs when the driving potentials in the two phases are not in equilibrium. The driving potentials are the water-vapor pressure p_v and the bound-water concentration c_b. Comparison requires conversion to the same basis through the sorption isotherm, which represents equilibrium.

Either the water-vapor pressure p_v is converted to a saturated bound-water concentration c_{bs}, or the bound-water concentration c_b is converted into a wood vapor pressure that is in equilibrium with it p_{vw} (Figure 3). The first approach was chosen in (Frandsen, 2005), but better results have been obtained with the latter, which is applied here.

The Hailwood-Horrobin isotherm is applied

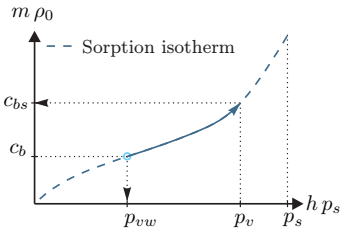

Figure 3 Conversion of driving potentials through the sorption isotherm to determine sorption.

in the model:

$$m(h) = \frac{h}{f_1 + f_2\,h + f_3\,h^2}, \tag{12}$$

where m is the moisture content, h is the relative humidity and the shape factors are $f_1 = 2.22$, $f_2 = 15.7$ and $f_3 = -14.0$ (all non-dimensional).

Since sorption ceases at equilibrium, the sorption rate is modeled as being proportional to the difference between the driving vapor pressure in ambient air p_v and the vapor pressure corresponding to the bound-water concentration in wood p_{vw} (Figure 3):

$$\dot{c} = H(p_v - p_{vw}), \tag{13}$$

where H is a moisture-dependent reaction rate function specifying the rate of the sorption (kg m^{-3}Pa^{-1}s^{-1}). The model describes the decreasing sorption rate $\dot{c}$ when equilibrium is approached ($p_{vw} \to p_v$) (Figure 3).

When equilibrium is approached at high relative humidities, the sorption slows down significantly. To model the decrease, Krabbenhøft and Damkilde (2004) applied the upper half of the following expression for adsorption $p_{vw} < p_v$:

$$H = \begin{cases} C_1 \exp\left(-C_2 \left(\frac{p_{vw}}{p_v}\right)^{C_3}\right) + C_4 & p_{vw} < p_v \\ C_1 \exp\left(-C_2 \left(2 - \frac{p_{vw}}{p_v}\right)^{C_3}\right) + C_4 & p_{vw} > p_v \end{cases} \tag{14}$$

where C_i are the vapor pressure or relative humidity dependent variables. In particular, C_2, has great significance for the onset of slow sorption (Figure 4).

The lower half of Eq. (14) describes the sorption rate in desorption ($p_{vw} > p_v$) by assuming decreasing desorption rate similar to that of adsorption as equilibrium is approached (Figure 4).

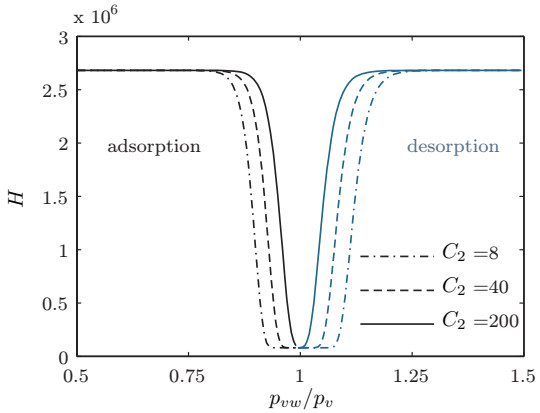

Figure 4 Variation of H with relative saturation $p_{vw}//p_v$ in adsorption and desorption for different values of C_2. C_1, C_3 and C_4 is presented in Table 2

This hypothesis is supported by measurements of slower desorption (lower $\dot{c}$) at the higher relative humidity steps by Håkansson (1994).

The fractional weight decrease, $E(t)$, shown in Figure 5 in these measurements is calculated as:

$$E(t) = \frac{w_\infty - w(t)}{w_\infty - w_0}. \tag{15}$$

Note that the trend of slower desorption at higher relative humidities corresponds to that for adsorption in the experiments by (Wadsö, 1994b) (Figure 2).

The non-linearity of the sorption rate expressed through Eq. (14) most likely relates to the slower binding of the outer molecules on a sorption site, because of the smaller amount of potential energy associated with that bond.

However, no theories have been proposed for the rate.

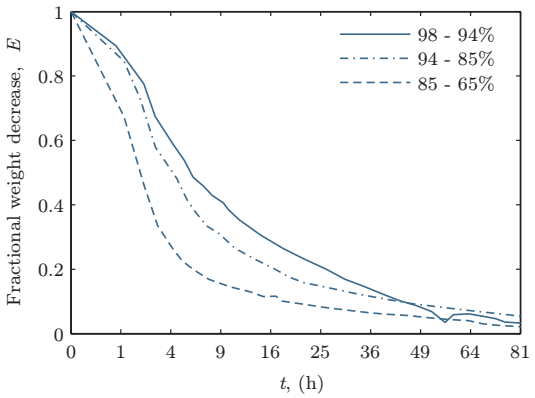

Figure 5 Measurements of fractional weight decrease over time for 3 different relative humidity steps by Håkansson (1994).

Krabbenhøft and Damkilde (2004) calibrated the H-function to the experiments by Wadsö (1994b). They found no noteworthy variation of the C_1, C_3 and C_4 parameters in the two intervals of relative humidity of the experiments (54-75% and 75-84%). Therefore, they assumed C_1, C_3 and C_4 to be constant. The parameter C_2 was found to depend on moisture content, but in their model it was assumed to be constant within each of the two relative humidity steps. The values applied by Krabbenhøft and Damkilde (2004) are provided in Table 2.

C_1 ($\mathrm{Pa^{-1}s^{-1}}$)	C_2 54-75%	C_2 75-84%	C_3	C_4 ($\mathrm{Pa^{-1}s^{-1}}$)
2.6×10^{-6}	8	40	50	8.0×10^{-8}

Table 2 The c_{2j}-coefficients of the $C_2(h)$-functions in the multi-Fickian model (Krabbenhøft and Damkilde, 2004)

From Table 2 it is seen that the C_2 parameter increases quite rapidly at higher relative humidities. To model the rapid increase, the following continuous variation of C_2 has been assumed here:

$$C_2(h) = c_{21} \exp(c_{22}\, h), \tag{16}$$

where the shape parameters c_{21} and c_{22} are calibrated to the measurements made by Wadsö (1994b) to 5.22×10^{-6} and 19.0, respectively. This continuous variation is illustrated in Figure 6 as the dot-and-dash line together with the two constant levels applied by Krabbenhøft and Damkilde (2004) (marked with $\star$ and $+$). As shown in Figure 11, good results can be obtained by applying Eq. (16). However, the magnitude and variation of the C_i parameters and the H-function have not been documented. In the following we consider a sorption experiment carried out by Christensen (1965) to investigate the magnitude and variation of the parameters of the sorption rate model.

4.1 Study of sorption experiments

Christensen (1965) investigated the rate of sorption for thin araucaria specimens (*Araucaria klinkii* Lauterb.) in the absence of air at 40°C. She measured the sorption rate for different specimen thickness and directions to grain for the following three thin specimen types:

- 1 mm thick, cut across grain
- 1 mm thick, cut parallel to grain
- 20 μm thick, cut parallel to grain

The weight gains of all the specimen types for different moisture steps were almost identical, and the influence of the boundary layer was eliminated by the absence of air. It can therefore be concluded that the spatial process of vapor diffusion into the wood lumens is instantaneous or negligible. Thus, adsorption governs the processes leading to the weight increase measured. For the second type of specimen (1 mm thick, cut parallel to grain) the mass change over time was measured at different relative vapor pressure steps (Figure 7).

Note that at higher relative humidity from approximately 55% and up, a radical decrease

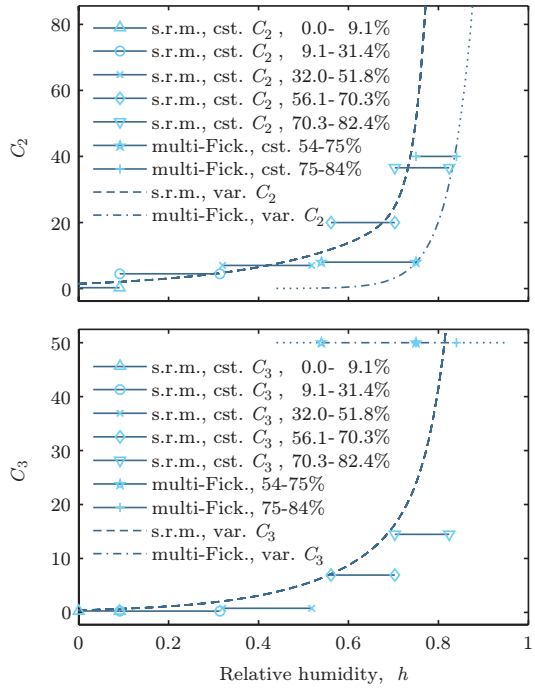

Figure 6 Variation of the parameters C_2 and C_3 with relative humidity applied in the *s*orption *r*ate *m*odel to klinki pine and in the sorption rate model embedded in the multi-Fickian model to pine.

in sorption rate occurs after 30-40 min of sorption. This is one of the phenomena causing the so-called non-Fickian behavior (Wadsö, 1993). Hence, these experiments show the same tendency as the experiments by Wadsö (1994b).

Since vapor diffusion and thus also the spatial variation of bound-water concentration can be neglected, the bound-water concentration can be obtained by integrating the sorption rate $\dot{c}$ with respect to time:

$$c_b(t) = c_{b0} + \int_0^t \dot{c}(\tau) d\tau, \qquad (17)$$

where c_{b0} is the initial bound-water concentration. Without a spatial variation of concentration, the fractional weight increase can be obtained by Eq. (1) as

$$E(t) = \frac{c_b(t)V - c_{b0}V}{c_{b\infty}V - c_{b0}V} = \frac{c_b(t) - c_{b0}}{c_{b\infty} - c_{b0}}, \qquad (18)$$

where V is the volume of the specimen.

By Eqs. (17) and (18) the sorption rate model Eq. (14) can be calibrated against the measurements. This calibration was conducted in two ways.

First, the coefficients C_1, C_2, C_3 and C_4 were assumed to be constant within each relative humidity step resulting in the solid lines in Figure 7. This quite good fit shows a variation of the constants C_i with relative humidity. In Figure 6, this variation is shown as the five first discontinuous, marked lines, and the values are provided in Table 3. Perturbations of C_1 from the constant value 2.0×10^{-3} do not influence the result of this calibration significantly, so the parameter is chosen to be constant.

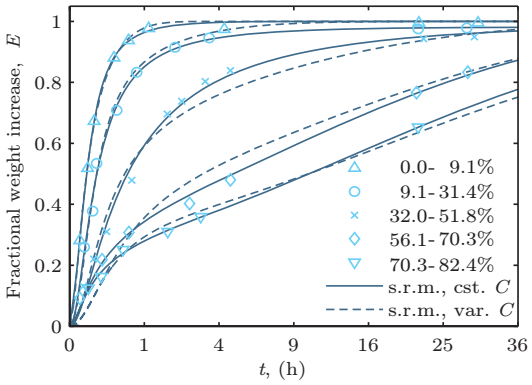

Figure 7 Fractional weight increase of thin specimens of klinki pine measured by Christensen (1965) and calibrations of the **s**orption **r**ate **m**odel in (14) with **c**on**s**tant and variable C_i.

Second, a variation identical to Eq. (16) of the $C_i(h)$ parameters with relative humidity is assumed:

$$C_i(h) = c_{i1} \exp(c_{i2}\, h) + c_{i3} \exp(c_{i4}\, h). \qquad (19)$$

This function is chosen to model the radical increase of C_2 and C_3 with relative humidity (Figure 6).

Calibration of Eqs. (14) and (19) to the measurements with the $C_i(h)$ parameters as a function of relative humidity yields the dashed

	0.0 - 9.1%	9.1 - 31.4%	32.0 - 51.8%	56.1 - 70.3%	70.3 - 82.4%
C_1	2.0e-3	2.0e-3	2.0e-3	2.0e-3	2.0e-3
C_2	2.54e-1	4.48	7.00	20.0	36.6
C_3	0.252	0.239	0.767	6.91	14.5
C_4	-1.55e-3	-2.31e-5	-1.77e-6	3.60e-7	4.04e-7

Table 3 The constant C_i parameters for the different relative humidity steps in the experiments by Christensen (1965). The unit of C_1 and C_4 is $\mathrm{Pa}^{-1}\mathrm{s}^{-1}$.

lines in Figures 6 and 7. The c_{ij}-coefficients obtained are shown in Table 4.

Hence, the H-functions vary with the degree of saturation p_{vw}/p_v, through the $C_i(h)$ parameters, and also with relative humidity $h = p_{vw}/p_s$. In Figure 8 the H-function is plotted against these two variables.

C_i	c_{i1}	c_{i2}	c_{i3}	c_{i4}
C_1	8.90e-5	0	0	0
C_2	1.44	3.76	1.77e-11	37.39
C_3	0.409	5.074	1.16e-7	23.57
C_4	2.37e-4	-41.96	2.83e-7	0.268

Table 4 The c_{ij}-coefficients in the $C_i(h)$-functions in the experiments by Christensen (1965). The unit of c_{11}, c_{13}, c_{41} and c_{43} is $\mathrm{Pa}^{-1}\mathrm{s}^{-1}$.

The markers in Figure 8 are the H-function extracted from the measurements by Christensen (1965). From the slope between two successive measurements at the times $\{t_k\}$ and $\{t_k + \Delta t_k\}$, respectively, the discrete points of the H-function have been extracted by the following central difference discretization of Eq. (13):

$$H\left\{t_k + \tfrac{\Delta t_k}{2}\right\} = \frac{\dot{c}_b\{t_k + \Delta t_k/2\}}{p_v\{t_k + \Delta t_k/2\}} \tag{20}$$

where

$$\dot{c}_b\left\{t_k + \tfrac{\Delta t_k}{2}\right\} = \frac{c_b\{t_k + \Delta t_k\} - c_b\{t_k\}}{\Delta t_k} \tag{21}$$

$$p_v\left\{t_k + \tfrac{\Delta t_k}{2}\right\} = \frac{p_v\{t_k\} + p_v\{t_k + \Delta t_k\}}{2}. \tag{22}$$

The bound-water concentrations c_b are evaluated from the sorption isotherm fitted with Eq. (12) to the measurements (Figure 9). For klinki pine at 40 ° C: $f_1 = 1.81$, $f_2 = 14.7$ and $f_3 = -12.6$.

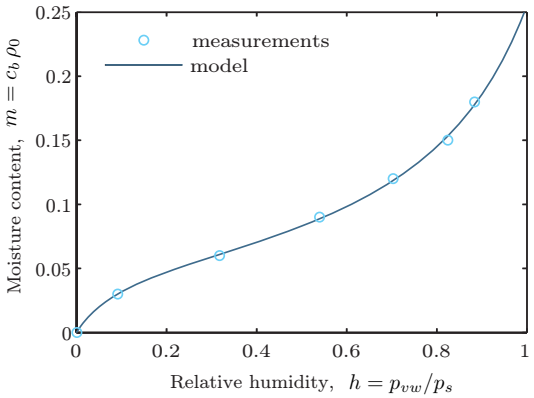

Figure 9 Sorption isotherm for klinki pine at 40°C calibrated to the measurements by Christensen (1965).

From this investigation it can be concluded that the H-function applied to the multi-Fickian model has the same magnitude as the H-function computed from the measurements by Christensen (1965). Furthermore, the variation of the $C_2(h)$-function, which governs the initialization of slow sorption, has the same trend and magnitude for both types of experiment and species.

5 Boundary conditions

Water vapor is diffusing through a boundary layer of stagnant and slower moving air and into the wood (Figure 10).

If the airflow at the wood surface is slow, the boundary layer provides resistance to diffusion. The flux vector of vapor $\mathbf{J}_v$ perpendicular to the surface, with the normal vector $\mathbf{n}$, $\mathbf{n} \cdot \mathbf{J}_v$ is driven by the difference in vapor pressure over the boundary layer. Thus, the following Neumann boundary condition can be stated:

$$\mathbf{n} \cdot \mathbf{J}_v = k_v(p_v^s - p_v^a), \tag{23}$$

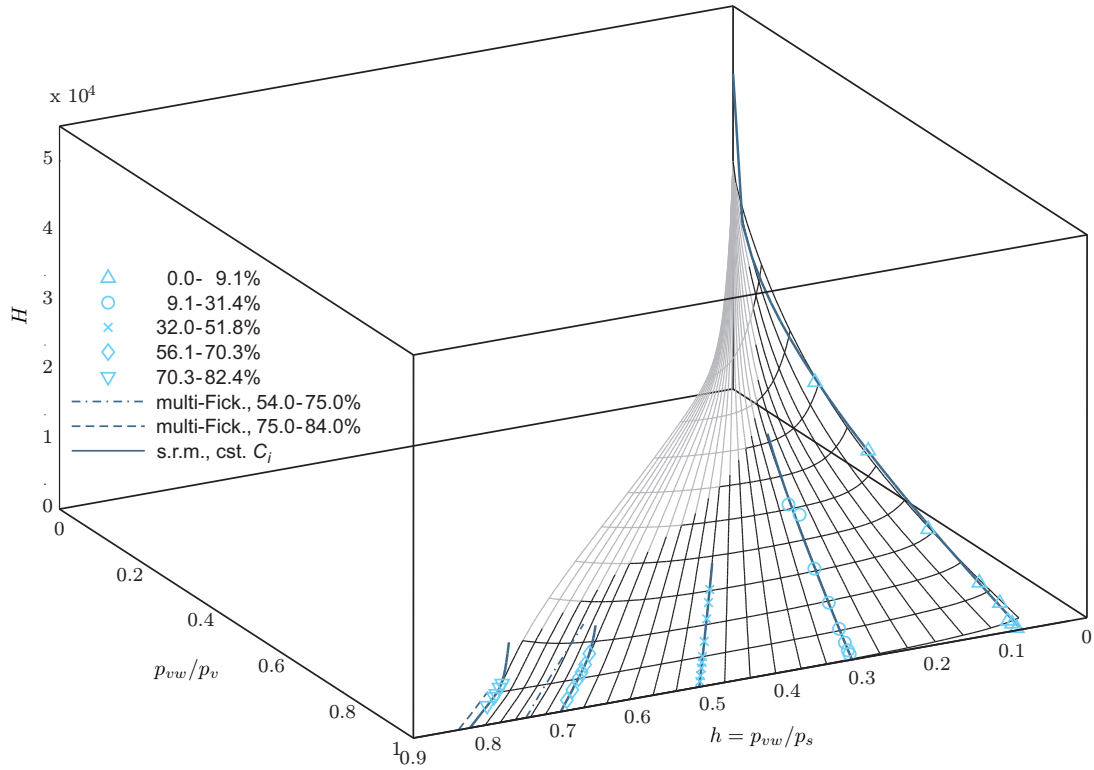

Figure 8 Variation of the H-function with degree of saturation (p_{vw}/p_v) and relative humidity h. The markers indicate the measurements on klinki pine carried out by Christensen (1965). The dashed and the dot-and-dash lines are the H-functions applied to the multi-Fickian model for the measurements on pine. The thick solid lines are the H-function with constant C_i-coefficients and the mesh with varying $C_i(h)$-functions computed from the measurements on klinki pine. The gray part of the mesh is not verified by measurements.

where p_v^s and p_v^a are the vapor pressures at the surface and in the ambient air, respectively. k_v is the mass transfer coefficient of the boundary layer.

At higher air velocities, the resistance from this layer may be assumed to be negligible, see e.g. (Rosen, 1978), and the partial vapor pressure at the surface can be assumed to be identical to the partial vapor pressure in the ambient air; thus the following Dirichlet boundary condition can be stated:

$$p_v^s = p_v^a. \tag{24}$$

Additional bound water can only be added to the system by adsorption. Since bound water is restricted to the solid medium (wood), it does obviously not move through the surface, i.e., $\mathbf{n} \cdot \mathbf{J}_b = 0$ (Figure 10). The common approach for modeling moisture transport in a paper stack is to assume the outermost sheet of paper is in equilibrium with the ambient air $c_b^s = c_b^a$ (Bandyopadhyay et al., 2000; Foss et al., 2003; Massoquete et al., 2005). However, for the concentration of bound water in the sheet to remain constant at arbitrarily large amounts of bound-water transport from the sheet, this assumption implies instantaneous sorption of water from the air to the sheet. This is not the case; sorption is a time-dependent process, as discussed in the previous section. Hence, the correct boundary condition for paper and wood must be:

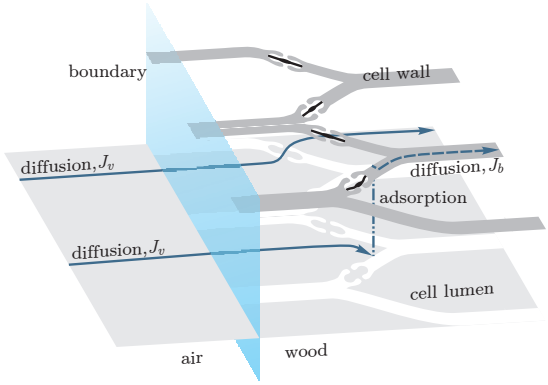

Figure 10 Movement of water vapor through the boundary between air and wood with consequential sorption and bound-water diffusion.

$$\mathbf{n} \cdot \mathbf{J}_b = 0. \tag{25}$$

6 Simulations of experiments

In the following, simulations of the measurements by Wadsö (1994b) using the model implemented into a commercial software (Comsol Multiphysics^{TM}) are presented. In the experiments, the different specimens's mass gain during two almost instantaneous steps of relative humidity was measured, i.e., 54-75% and 75-84% relative humidity. Equilibrium was ensured before initiation of each step. Thus, the specimens have a uniform initial vapor pressure distribution and a corresponding uniform bound-water concentration distribution. As the steps are initialized, Eq. (25) is applied as the bound-water boundary condition. The air velocity in the experiment is about 3 ms^{-1}, which allows Eq. (24) to be applied as the vapor pressure boundary condition. The transient problem is calculated by the following equations:

- Diffusion: Egs. (5), (8), (10) and (11); and
- Sorption: Eqs. (12), (13) and (16),

where the C parameters applied are stated in Table 2 apart from C_2, which depends on the relative humidity according to Eq. (16). The mass gain and fractional weight increase is evaluated for each time step by integrating the bound-water concentration over the volume. The fractional weight increase in the simulations is compared with the measurements by Wadsö (1994b) in Figure 11.

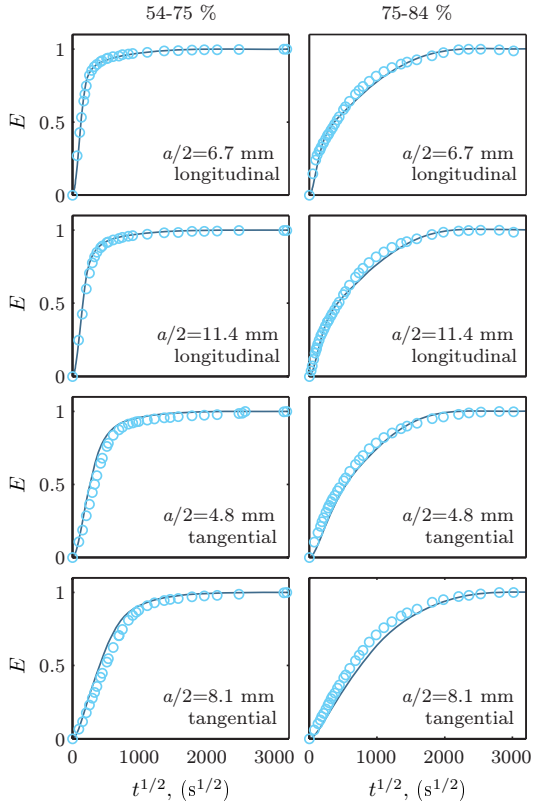

Figure 11 The variation of fractional weight increase E over time. The circles indicate the measurements by Wadsö (1994b) and the solid lines indicate the simulations by the multi-Fickian model.

From Figure 11 it can be concluded that the major feature of a characteristic drops in fractional weight increase rate for high relative humidities is captured by the model. For most practical applications, the model provides adequate results for different material directions and thickness.

An example of the distribution of bound-water concentration and water-vapor pressure

in the simulations is presented in Figure 12, from which the effect of the boundary conditions discussed can be observed. Water vapor diffuses into the specimen and adsorbs into bound water, which therefore falls behind. Another consequence of the combined transport system and boundary conditions is the smaller gradients of bound-water concentration close to the boundary compared to a Fickian model. The large gradients in moisture content predicted by a Fickian model would result in large gradients in moisture induced stresses and consequently in cracks for even a small increase in relative humidity. These smaller gradients in a multi-Fickian model could explain why cracks do not appear during smaller changes in relative humidity in the ambient air.

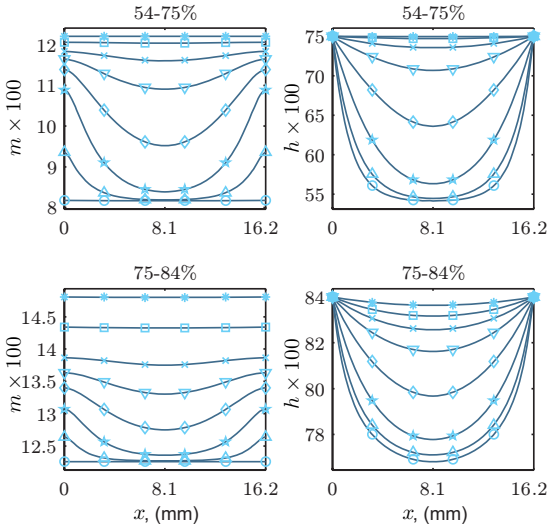

Figure 12 Distribution of bound water in terms of moisture content $m = c_b/\rho_0$ and vapor pressure in terms of relative humidity $h = p_v/p_s$ in the simulation of the experiment on the tangential 8.1 mm specimen. ○: 1/2 min, △: 2h, ⋆: 10h, ◇: 40h, ▽: 4days, ×: 7days, □: 14days, ∗: 29days.

7 Discussion

With this presentation of the multi-Fickian model, a more realistic sorption rate function has been introduced, and thus a certain level of complexity has been chosen. In this section the level of complexity and validity of the presented model are discussed.

The multi-Fickian model relies on three physiochemical phenomena, i.e., bound-water diffusion, water-vapor diffusion and sorption. The transport of bound water was measured by Stamm (1960a), as mentioned in the introduction. By filling the capillaries with a molten metal alloy containing bismuth, which expands during solidification, the diffusion of water vapor was prevented. Transport into clear wood occurs at a much higher rate, which indicates that water vapor in the lumens is the main transportation path. The experiments by Christensen (1965) prove that sorption is a time-dependent process. Hence, it is reasonable to assume that all the considered phenomena occur in wood. However, the question arises as to whether any of the phenomena can be neglected.

Slow sorption cannot be the only explanation for the non-Fickian effects observed by Wadsö (1994b,a), since the experiments would yield identical results for different specimen thickness, which is not the case (cf. Figure 2).

Although the presented multi-Fickian model takes a number of phenomena into account, it does of course have limitations. Here, a simple S-shaped sorption isotherm has been applied, but sorption is hysteretic, and Eq. (12) can be replaced by a hysteretic sorption function. For further details on implementation of hysteresis into a multi-Fickian model, see (Frandsen and Svensson, 2007). Furthermore, temperature variations have not been discussed in this paper, but the Soret effect influences the bound-water transport, see e.g. (Skaar and Siau, 1981; Siau and Avramidis, 1993). Temperature variations can be taken into account as well by including coupling terms to heat transfer in the constitutive relations supplemented with a multi-phase energy balance equation and a constitutive model for heat transfer, see e.g. (Whitaker, 1977).

8 Conclusions

In the present paper, the following new findings for a multi-Fickian model to describe moisture transport in wood are presented:

- The sorption rate model embedded in the multi-Fickian model is refined to be a vapor pressure-dependent continuous function, whereas it in previous work was assumed to be a discontinuous function.
- The parameters involved in the sorption rate model have been calibrated against the measurements made by Wadsö (1994b). These are compared to those found in sorption experiments carried out by Christensen (1965). The variation of the parameters with relative humidity in the two investigations is observed to be similar.
- To make the theory applicable to desorption, a desorption rate function, which is analogous to that of the adsorption rate, is proposed. This hypothesis is supported by measurements of slow desorption at high relative humidities performed by Håkansson (1994), which display analogous behavior as those on adsorption by Christensen (1965).
- The boundary conditions used for moisture transport in paper were found to imply an immediate equilibrium for sorption of bound water at the boundary with the ambient air, regardless of the internal moisture transport. This cannot be true, since sorption is a time-dependent process. Thus, the boundary conditions typically applied in multi-Fickian models for moisture transport in wood should be sustained.

Finally, the multi-Fickian model was compared with the measurements by Wadsö (1994b). The model captured the characteristic drop in the fractional weight increase rate for the high relative humidities range as well as regular Fickian behavior in the low range. This observation is valid for different material directions and specimen sizes.

Acknowledgements

This work has been funded in part by the Danish Forest and Nature Agency and in part by the Danish Research Agency under Project no. 2020-00-0017. Their financial support is gratefully acknowledged.

References

Absetz, I. and Koponen, S. (1997). Fundamental diffusion behaviour of wood. In Hoffmeyer, P., editor, *Proceedings of the International Conference on Wood-Water Relations, Copenhagen*, volume E8, pages 89–106.

Bandyopadhyay, A., Radhakrishnan, H., Ramarao, B. V., and Chatterjee, S. G. (2000). Moisture sorption response of paper subjected to ramp humidity changes: Modeling and experiments. *Industrial and Engineering Chemistry Research*, 39(1):219–226.

Christensen, G. N. (1965). The rate of sorption by thin materials. In Wexler, A. and Winn, P. A., editors, *Humidity and Moisture*, volume 4, pages 279–293. Reinhold Publishing Corporation.

Crank, J. and Park, G. S. (1951). Diffusion in high polymers - some anomalies and their significance. *Transactions of the Faraday Society*, 47(10):1072–1084.

Cunningham, M. J. (1994). A model to explain "anomalous" moisture sorption in wood under step function driving forces. *Wood and Fiber Science*, 27(3):265–277.

Foss, W. R., Bronkhorst, C. A., and Bennett, K. A. (2003). Simultaneous heat and mass transport in paper sheets during moisture sorption from humid air. *International Journal of Heat and Mass Transfer*, 46(15):2875–2886.

Frandsen, H. L. (2005). Modeling of moisture transport in wood. In *Wood Science and Timber Engineering*. Department of Structural

Engineering and Building Technology, Aalborg University, Aalborg.

Frandsen, H. L. and Svensson, S. (2007). Implementation of sorption hysteresis in multi-fickian moisture transport. *Holzforschung*, 61(6):693–701.

Håkansson, H. (1994). *Experimentiella studier av transient sorption i cellvägen i trä*. Report tabk-94/3021, Lund Institute of Technology, Lund University, Sweden.

Krabbenhøft, K. and Damkilde, L. (2004). A model for non-fickian moisture transfer in wood. *Materials and Structures*, 37(273):615–622.

Mandelkern, L. and Long, F. A. (1951). Rate of sorption of organic vapors by films of cellulose acetate. *Journal of Polymer Science*, 6(4):457–469.

Massoquete, A., Lavrykov, S., and Ramarao, B. V. (2005). Non-fickian behaviour of moisture diffusion in paper. *Journal of Pulp and Paper Science*, 31(3):121–127.

Rosen, H. N. (1978). The influence of external resistance on moisture adsorption rates in wood. *Wood and Fiber Science*, 10(3):218–228.

Salin, J.-G. (1996). Mass transfer from wooden surfaces and internal moisture non-equilibrium. *Drying Technology*, 14(10):2213–2224.

Schirmer, R. (1938). Die diffusionszahl von wasserdampf-luftgemischen und die verdampfungsgeschwindigkeit. *VDI Beihaft Verfahrestechnik*, 6:170.

Siau, J. F. (1984). *Transport Processes in Wood*. Springer-Verlag, Heidelberg.

Siau, J. F. (1995). *Wood: Influence of moisture on physical properties*. Department Of Wood Science and Forrest Products, Virginia polytechnic Institute and State University.

Siau, J. F. and Avramidis, S. (1993). Application of a thermodynamic model to non-isothermal diffusion of moisture in wood. *Wood Science and Technology*, 27(2):95–114.

Skaar, C. and Siau, J. F. (1981). Thermal diffusion of bound water in wood. *Wood Science and Technology*, 15(2):105–112.

Stamm, A. J. (1959). Bound-water diffusion into wood in the fiber direction. *Forest Product Journal*, 9:27–32.

Stamm, A. J. (1960a). Bound-water diffusion into wood in the across-the-fiber directions. *Forest Product Journal*, 10:524–528.

Stamm, A. J. (1960b). Combined bound-water and water vapor diffusion into sitka spruce. *Forest Product Journal*, 10:644–648.

Stamm, A. J. and Nelson, R. M. (1961). Comparison betweeen measured and theoretical drying diffusion coefficients for southern pine. *Forest Product Journal*, pages 536–543.

Wadsö, L. (1993). *Studies of water vapor transport and sorption in wood*. PhD thesis, Building Materials, Lund University, Sweden.

Wadsö, L. (1994a). Describing non-fickian water-vapor sorption in wood. *Journal of Material Science*, 29:2367–2372.

Wadsö, L. (1994b). Unsteady-state water-vapor adsorption in wood: An experimental-study. *Wood and Fiber Science*, 26(1):36–50.

Whitaker, S. (1977). *Advances in heat transfer*, volume 13, chapter Simultaneous heat, mass, and momentum transfer in porous media: A theory of drying, pages 119–203. Academic Press, New York.

Paper III

A hysteresis model suitable for numerical simulation of moisture content in wood

Holzforschung vol. 61 issue 2, pp. 175-181, 2007

Paper III

A hysteresis model suitable for numerical simulation of moisture content in wood

Henrik Lund Frandsen[1] Staffan Svensson[1] and Lars Damkilde[2]
[1]*Department of Civil Engineering, Aalborg University, Denmark*
[2]*Esbjerg Institute of Technology, Aalborg University, Denmark*

Abstract
The equilibrium moisture content in wood depends not only on the current relative humidity in ambient air, but also on the history of relative humidity variations. This hysteresis dependence of sorption in wood implies that in the worst case the moisture content for a given relative humidity may deviate by 30-35%. While researchers seem to have reached a general agreement on the hypothesis for the sorption hysteresis phenomenon, only a few models describing the phenomenon are available. Current models such as the independent domain model have numerical deficiencies and drawbacks. This paper presents a new hysteresis model, which mathematically resolves in closed-form expressions, with the current relative humidity and moisture content as the only input parameters. Furthermore, the model has the advantage of being applicable to different sorption isotherms, i.e., different species and different temperatures. These features make the model relatively easy to implement into a numerical method such as the finite element method.

Key words: hysteresis; independent domain model; moisture content; numerical method; sorption.

1 Introduction

Variation of the relative humidity in ambient air causes variations in the moisture content of wood. However, a given relative humidity does not uniquely define the equilibrium moisture content. The history of the variations must also be taken into account. Figure 1 illustrates the dependence of moisture content, m, using a sequence of relative humidity, h, variations.

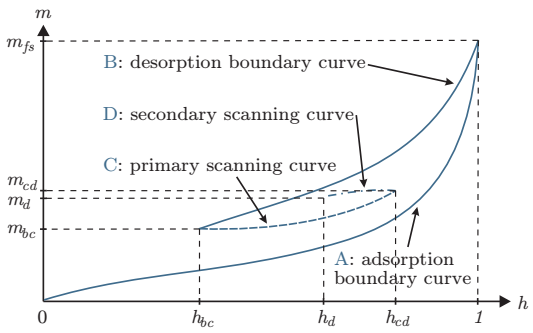

Figure 1 Various boundary and scanning curves.

The explanation for the sorption hysteresis phenomenon is found in the chemical behavior and complex structure of wood. The glucane chains of cellulose within the microfibrils are organized into crystalline and paracrystalline regions. There are more intermolecular hydrogen bonds (to the OH groups of the neighboring chains) in the former than in the latter. The non-participating OH groups are also called sorption sites, since they have great affin-

ity for water and are responsible for sorption in wood (Avramidis, 1997; Dinwoodie, 2000). Adsorption of water leads to swelling of the cell wall and breaking of hydrogen bonds, and thus more available sorption sites become unbound. The hydrogen bonds are re-established during desorption, but this process is delayed, since water molecules now occupy the sorption sites. Hence, wood contains more water at a given relative humidity during desorption than during adsorption. For an arbitrary variation in the relative humidity, conditions between pure adsorption and pure desorption depend on the availability of sorption sites. The terminology is presented in Figure 1.

Using initial conditions of the dry state with a moisture content (MC) and relative humidity (RH) equal to zero and increasing the RH to 100% provides the so-called adsorption boundary curve, A. Decreasing the RH also decreases the MC along the desorption boundary curve, B. An increase in RH before reaching the dry state again results in movement along a so-called scanning curve, C, which gradually approaches the adsorption boundary curve. This type of scanning curve is called a primary scanning curve, and a scanning curve taking origin in this is called a secondary scanning curve, D, etc. The points at which a shift from a desorption curve to an adsorption curve occurs $\{h_{bc}, m_{bc}\}$, or the reverse $\{h_{cd}, m_{cd}\}$, are called reversal points.

In the following section an evaluation of the existing models and requirements for a model suitable for numerical implementation is provided. A new model fulfilling these requirements is then presented and the model is fitted to existing experimental data. Finally, examples to illustrate the procedure of the model are outlined.

2 Existing hysteresis models

A classical approach for modeling sorption hysteresis is the independent domain (ID) model developed by Everett and co-workers (Everett and Whitton, 1952; Everett and Smith, 1954; Everett, 1954, 1955). The model was applied to wood by Peralta (1995b,a, 1996) and improved further by Peralta and Bangi (1998a,b). This and a model by Pedersen (1990) are discussed in the following.

2.1 The independent domain model

In the ID model the amount of activated sorption sites is figuratively accounted for in an ID, Ω. Likewise, the function over this domain, w, may be interpreted as the amount of water molecules bound at each sorption site (Figure 2). This function may be obtained indirectly by measurements of a series of scanning curves.

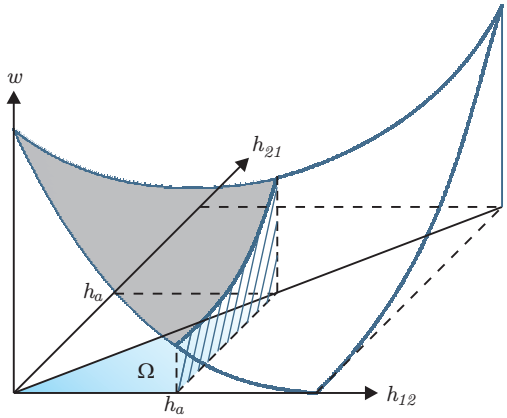

Figure 2 The w-function over the ID Ω. The domain Ω is here bounded by h_{21}=0, $h_{12} = h_a$ and always bounded by $h_{12} = h_{21}$.

Thus, the volume integral of this function over the domain Ω provides the present MC, m:

$$m = \int_{\Omega} w(h_{12}, h_{21}) d\Omega \qquad (1)$$

where h_{12} and h_{21} are the adsorption and desorption relative humidities, respectively. The domain is from the dry condition during adsorption expanded to vertical lines intersecting at h_{12}. During desorption, the domain is reduced along horizontal lines intersecting at h_{21}.

Figure 3 illustrates changes in ID due to the changes in RH in Figure 1.

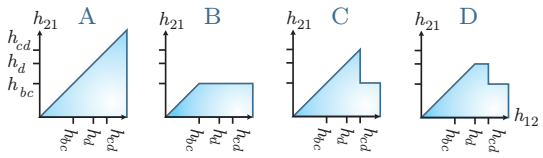

Figure 3 Changes in ID due to changes in the RH in Figure 1.

Measurements of sorption hysteresis in yellow poplar (*Liriodendron tulipifera* L.) were presented by Peralta (1995b), which involved successful application of a method that was a discretization of the ID model in Peralta (1995a). However, the discretization only allowed steps between the RH values 0%, 11%, 32%, 53%, 75%, 92% and 100%.

Thus, Peralta (1996) refined the model to take smaller RH steps into account. However, this refinement violates the original method of Everett (Everett and Whitton, 1952; Everett and Smith, 1954; Everett, 1954, 1955), and in the general case, some subdomains are omitted, leading to a loss of water in the accounting. As an example of this, consider the sequence of RH changes 100%, 60% and 40%. As observed in Figure 4c, some of the original domain in Figure 4a is omitted.

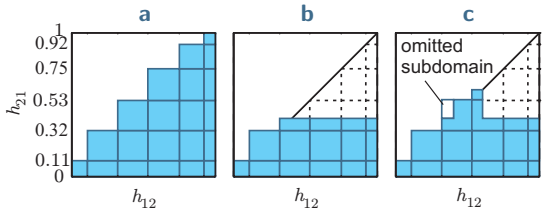

Figure 4 RH changes in the refined discretized ID by Peralta (1996) leading to "loss of water".

To generalize the measurements from a given isotherm for a given species, and thus avoid extensive experimental work, Peralta and Bangi (1998a,b) presented two models based on the work of Mualem (1973, 1974). On simplifying assumptions made on the w-function, the first paper presents an analytical model for determining the scanning curves from the adsorption and desorption boundary curves. The second paper is based on a more physical approach, but involves a more complicated structure for changes in the ID. Both of the models still involve accounting for an entire domain or entire history of RH variations to obtain the MC.

In addition to the accounting complications, the ID model has another major numerical drawback for isotherms with a slope different from zero in the dry condition. Thus, here it implicitly involves singularities in the w-function at the acute-angled corners of domain Ω, as shown in Appendix A.

2.2 Pedersen's model

Pedersen (1990) presented a model in which the slopes of the scanning curves are determined as a weighted average of the slopes of the adsorption boundary curve $\xi_a = \partial m_a/\partial h$ and desorption boundary curve $\xi_d = \partial m_d/\partial h$. The slopes of the adsorption scanning ξ_a^{scc} and desorption scanning ξ_d^{scc} curves by Pedersen have been generalized by Frandsen (2005) to:

$$\xi_a^{\mathrm{scc}} = \frac{(m_d - m)^b \xi_a + a(m - m_a)^b \xi_d}{(m_d - m_a)^b} \tag{2a}$$

$$\xi_d^{\mathrm{scc}} = \frac{a(m_d - m)^b \xi_a + (m - m_a)^b \xi_d}{(m_d - m_a)^b}, \tag{2b}$$

where $a$and b are species-independent shape parameters.

This formulation provides a differential equation that must be solved numerically in the $h-m$ domain for each step in time in a numerical method. Frandsen (2005) applied this model successfully to the measurements performed by Peralta (1995b) on yellow poplar (*Liriodendron tulipifera* L.) at 30°C and to measurements on Norway spruce (*Picea abies*) at 20°C performed by Ahlgren (1972).

2.3 Evaluation of existing models

Besides the two models described above, models for describing sorption hysteresis in unsaturated soil have been proposed (Scott et al., 1983; Kool and Parker, 1987; Huang et al., 2005). The physics are different from sorption hysteresis in wood, since the driving forces of sorption in wood are primarily of a chemical nature compared to the capillary force-driven sorption in porous materials (Avramidis, 1997). Mathematically, however, the models are more similar. The model by Huang et al. (2005) has the advantage of describing the scanning curves using closed-form expressions, with the two previous reversal points as input. A drawback is that the model for the scanning curves is not naturally bounded by the boundary curves.

The ID models and Pedersen's model are both very cumbersome to implement into a numerical method such as the finite element method, since the prevailing scanning curve must be evaluated numerically for each step forward in time.

A closed-form expression for the scanning curve would be advantageous for implementation into a numerical method. Being able to predict the scanning curve from the current condition $\{h_0, m_0\}$, thereby avoiding accounting for the entire history of RH variations, as shown in Figure 5a, would also be a great advance. Finally, temperature variations should easily be included in the hysteresis model.

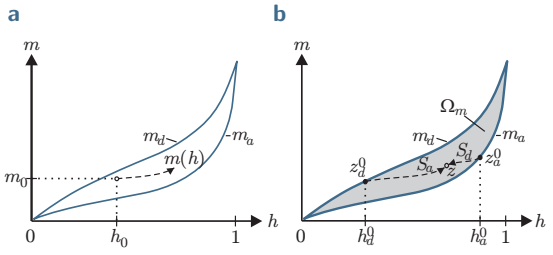

Figure 5 (a) Prediction of the scanning curve from the current condition $\{h_0, m_0\}$. (b) A sorption isotherm with symbols as used in the text.

In the next section a new model fulfilling these requirements is proposed.

3 Proposed exploited sorption site model

A new approach for describing sorption hysteresis is developed through the following steps:

- It is reasoned that a scanning curve is uniquely defined by the prevailing state. Thus, it is possible to find a closed-form expression for a scanning curve tracing through the state.
- The model is generalized by normalization to modeling different sorption isotherms for different species and temperatures.
- Finally, the proposed mathematical model is stated as closed-form expressions, which use the current state as the only input parameter.

In the following, the wood specimen's current condition or so-called state is defined as a point on an RH-MC graph $z = \{h, m\}$, since m is not uniquely defined by h. The feasible states z lie in the domain Ω_m, which is bounded by the adsorption and desorption boundary curves $m_a(h)$ and $m_d(h)$ (Figure 5b).

4 Uniqueness of the scanning curves

A state z within the domain Ω_m can be reached by either an adsorption path, S_a, or a desorption path, S_d, from the desorption or adsorption boundary curve in states z_d^0 and z_a^0, respectively (Figure 5b). Superscript zero indicates the initial state.

The states z_d^0 and z_a^0 must be the only origins on the boundary curves that will lead to state z by pure adsorption or desorption. This may be realized by considering, for example, a desorption scanning curve originating on the adsorption boundary curve with perturbation Δh from the original: $z_a^{0\prime} = \{h_a^0 + \Delta h, m_a(h_a^0 + \Delta h)\}$. In this initial state, more sorption sites

will be activated, and therefore the wood specimen will be able to contain more water and hence follow another desorption path, S'_d, to a final state of higher MC.

Thus, domain Ω_m must be covered by an infinite number of desorption scanning curves that do not intersect. The same arguments hold for the adsorption scanning curves.

Thus, the adsorption and desorption scanning curves originating from state z_0 must be uniquely defined by the state itself, since it is part of the adsorption or desorption scanning curve tracing through the state. This statement of uniqueness is used to predict the paths of the scanning curves.

5 Generalization for different sorption isotherms

To generalize the model to different species and temperatures, the domain Ω_m is normalized by transformation of the MC, $m(h)$, to the parameter $s(h)$:

$$s(h) = \frac{m(h) - m_a(h)}{m_d(h) - m_a(h)} \tag{3}$$

Thus, the species-and temperature-dependent boundary curves $m_a(h)$ and $m_d(h)$ are only implicitly included in the model formulation.

The parameter s may also be interpreted in a physical sense as the fractional amount of sorption sites exploited at the current RH.

This normalization involves transforming the gray domain Ω_m in Figure 5b to the 1×1 square shown in Figure 6b.

Figure 6a presents the boundary curves and an adsorption scanning curve measured by Ahlgren (1972). The same measurements of the adsorption scanning curve are shown in the normalized domain, together with the measurements of desorption scanning curves by Peralta (1995b), in Figure 6b.

At $h \to 0$ and $h \to 1$, the deviations of the measurements appear larger, since the denominator of s approaches zero ($m_a \simeq m_d$).

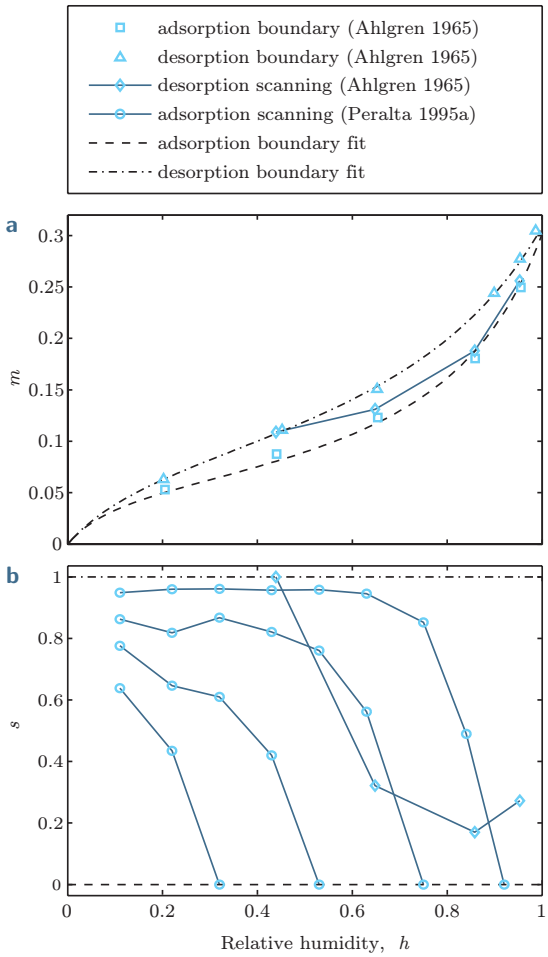

Figure 6 (a) Measurements of the boundary curves and a single adsorption scanning curve by Ahlgren (1972). (b) The same adsorption scanning curve and desorption scanning curves (Peralta 1995a) in the s-space.

6 The mathematical model

As observed in Figure 6b, the slope of the desorption scanning curves originating at the adsorption boundary curve ($s = 0$) will approach the desorption boundary curve ($s = 1$) asymptotically. Similar observations are made for the adsorption scanning curves.

The properties of the desorption scanning

curves may be formulated as:

$$h = h_a^0 \quad \text{for} \quad s = 0 \tag{4a}$$

$$\frac{\partial s}{\partial h} \to 0^- \quad \text{for} \quad s \to 1 \tag{4b}$$

and the properties of the adsorption scanning curves as:

$$h = h_d^0 \quad \text{for} \quad s = 1 \tag{5a}$$

$$\frac{\partial s}{\partial h} \to 0^- \quad \text{for} \quad s \to 0, \tag{5b}$$

where the initial relative humidities on the desorption and adsorption boundary curve are denoted h_d^0 and h_a^0, respectively.

One solution is the mathematical model in Eqs. (6a)–(6d), which implicitly fulfills these requirements and implies that the scanning curves are uniquely defined by their origins h_a^0 and h_d^0 (Figure 5a):

$$s = -1 + 2^{\left(\frac{1-h}{1-h_d^0}\right)^{\left(\frac{d_1}{\ln(d_2(1-h_d^0))}\right)}}, \quad \dot{h} > 0 \wedge s_0 > 0 \tag{6a}$$

$$s = 2 - 2^{\left(\frac{h}{h_a^0}\right)^{\left(\frac{d_1}{\ln(d_2\, h_a^0)}\right)}}, \quad \dot{h} < 0 \wedge s_0 < 1 \tag{6b}$$

$$s = 0, \quad \dot{h} > 0 \wedge s_0 = 0 \tag{6c}$$

$$s = 1, \quad \dot{h} < 0 \wedge s_0 = 1, \tag{6d}$$

where d_1 and d_2 are shape parameters. Eqs. (6a) and (6b) model the scanning curves during adsorption ($\dot{h} > 0$) and during desorption ($\dot{h} < 0$), respectively. Eq. (6c) simply states that a state with origin on the adsorption boundary curve ($s_0 = 0$) will follow the adsorption boundary curve if adsorption is taking place ($\dot{h} > 0$), and similarly for desorption in Eq. (6d). h_a^0 and h_d^0 are determined h_0 and s_0, and the concept is illustrated for an adsorption scanning curve in Figure 7.

Since the scanning curves are known to trail through the initial state $z_0 = \{h_0, m_0\}$, the expressions for h_a^0 and h_d^0 can be obtained by solving (6a) and (6b) for h_a^0 and h_d^0, respectively:

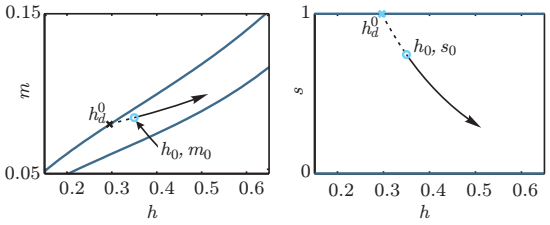

Figure 7 Close-up of an arrow-marked scanning curve in the m-space and s-space.

$$h_a^0 = h_0(d_2 h_0)^{q_1} \tag{7a}$$

$$h_d^0 = 1 - (1 - h_0)(d_2(1 - h_0))^{q_2}, \tag{7b}$$

where

$$q_1 = -\frac{\ln(\ln(2)) - \ln(\ln(2 - s_0))}{\ln(\ln(2)) - \ln(\ln(2 - s_0)) - d_1} \tag{8a}$$

$$q_2 = -\frac{\ln(\ln(2)) - \ln(\ln(1 + s_0))}{\ln(\ln(2)) - \ln(\ln(1 + s_0)) - d_1}. \tag{8b}$$

Note the symmetry of the two sets of equations, i.e., one set may be obtained from the other by replacing h by $1 - h$ and s by $1 - s$.

An alternative to the second criterion for s_0 in (6a)-(6d), which determines movements along boundary or scanning curves, are criteria based on h_a^0, h_d^0 and h i.e., $h_0 < h_d^0$, $h_0 > h_a^0$, $h_0 = h_d^0$ and $h_0 = h_a^0$, respectively. However, here h_a^0 and h_d^0 must be determined before choice of the curve in (6a)-(6d).

By a reverse mapping, the result in the s-space can be obtained in the m-space:

$$m(h) = \big(m_d(h) - m_a(h)\big)s(h) + m_a(h). \tag{9}$$

This closed-form formulation of the scanning curves easily provides an analytical expression for the derivative and easy time integration in a numerical method.

7 Fitting of the model

Simulations of the measurements of scanning curves by Peralta and Ahlgren in the s-space are presented in Figure 8.

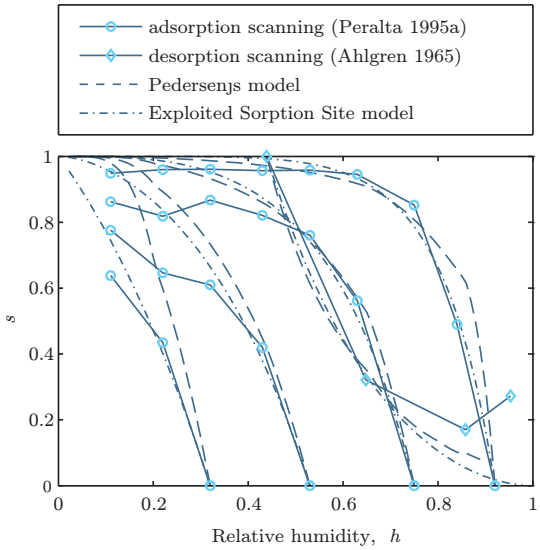

Figure 8 Measurements by Peralta (1995b) and Ahlgren (1972) plotted in the s-space with simulations by Pedersen's model and the new model.

From Figure 8 it is evident that the proposed exploited sorption site model fits the measurements slightly, but not significantly better than Pedersen's model. It should be noted, however, that the shape parameters d_1 and d_2 in the new model are the same for both sets of curves (Table 1), in contrast to those of Pedersen's model. This suggests that in the s-space the scanning curves for different species might be identical. However, further measurements and experiments must be performed to verify this hypothesis.

d_1	d_2
-1.32	0.88

Table 1 Scanning curve shape parameters applied to yellow poplar and Norway spruce.

A simulation of Ahlgren's experiment is transformed back into the m-space in Figure 9. The small deviation observed in the s-space in Figure 8 is negligible in the m-space in Figure 9.

In the simulation shown in Figure 9, the

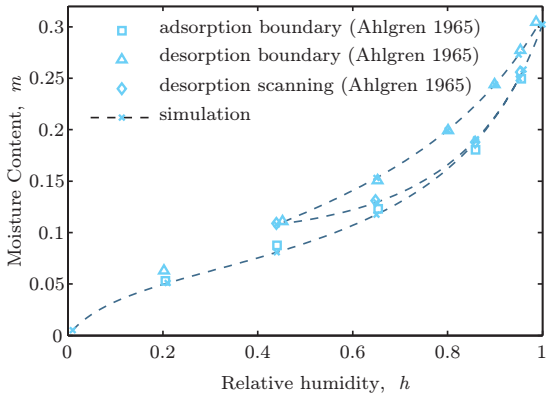

Figure 9 A simulation of the measurements by Ahlgren (1972) starting at $z = \{0, 0\}$, followed by adsorption to the fiber saturation point, desorption to 43.9% RH, and finally adsorption along a scanning curve to 95.3% RH.

following simple expression for the boundary curves is used:

$$m_\alpha(h) = \frac{h}{f_1^\alpha + f_1^\alpha h + f_1^\alpha h^2}, \qquad (10)$$

where $\alpha \in \{a, d\}$ designates either adsorption or desorption. The shape parameters f_i^α are given in Table 2.

α	f_1^α	f_2^α	f_3^α
a	1.804	13.63	-12.12
d	1.886	7.884	-6.526

Table 2 Shape parameters of the boundary curve measurements by Ahlgren (1972).

8 Examples

8.1 Example 1

Consider the sequence of changes in RH $h = \{0.30, 0.60, 0.35, 0.50\}$, with an initial MC of 0.0625 corresponding to a state on the adsorption boundary curve. This sequence is illustrated in the m-space and s-space in Figure 10.

The first step from 30% to 60% RH is trivial, since this adsorption process initiates on the adsorption boundary curve. This is modeled by Eq. (6c).

The second step from 60% to 35% RH is a primary desorption scanning curve, i.e., it initiates on the adsorption boundary curve with $s_0 = 0$ and $h_a^0 = h_0$. The scanning curve is modeled by Eq. (6b). This step leads to $s = 0.745$ and $m = 0.0853$.

The last step from 35% to 50% RH is a secondary scanning curve and is modeled by (6a). The point of origin on the desorption boundary curve h_d^0 of the scanning curve, tracing through the point ($h_0 = 0.35$, $s_0 = 0.745$), is determined by Eqs. (7b) and (8b) as 0.296.

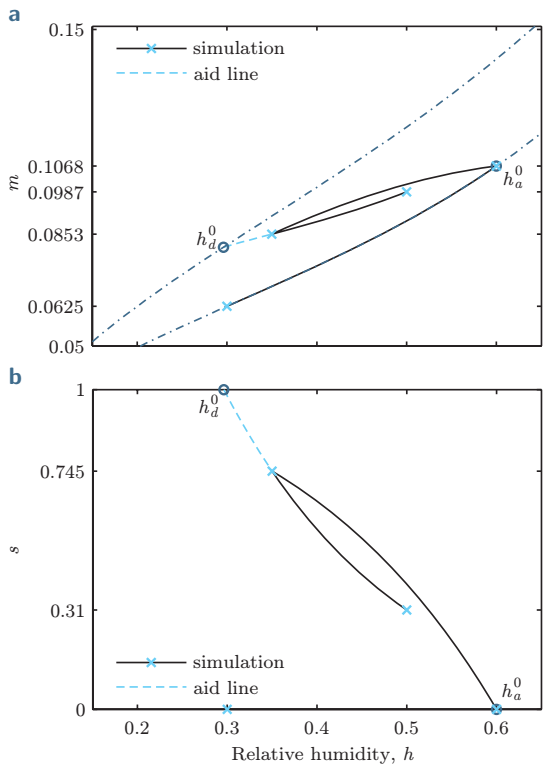

Figure 10 Hysteretic variation of moisture due to variation in RH in the example plotted in the m-space and s-space.

8.2 Example 2

This example concerns variations in MC in a thin wood sample exposed to RH oscillations around the set point in an "on-off"-controlled climate chamber. In this example the wood sample is assumed to be only a couple of millimeters thick, so diffusion can be neglected and equilibrium is obtained almost instantaneously. The simulation is initiated at the adsorption boundary curve at a set point of 60% RH and the amplitude chosen for illustration is 5% RH. The model then yields the MC variation shown in Figure 11.

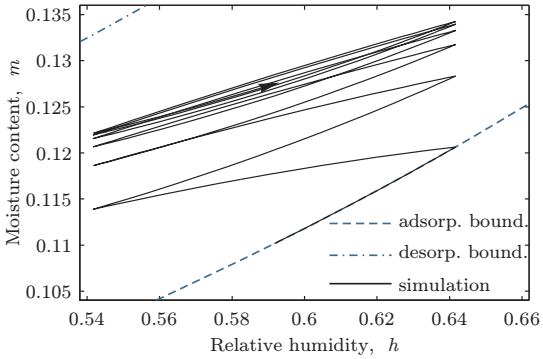

Figure 11 Variation in MC exposed to an oscillating variation in RH.

As observed from Figure 11, the MC tends toward the mean of the two boundary curves corresponding to an s-value of 0.5. The reason is found in Figure 8, where the scanning curves are obviously steeper near their origin. This provides a sliding effect towards $s = 0.5$.

The tendency for an initial gradual moisture increase and stabilization at a given moisture level during RH oscillation has also been observed in experiments by Fan et al. (1999) and Chomcarn and Skaar (1983).

9 Conclusions

The present paper proposes a sorption hysteresis model, which has the following advantages:

- The scanning curves are modeled as closed-form expressions depending only on the current moisture content and relative humidity. This makes the model much more convenient

for implementation into a numerical method such as the finite element method.

- By normalization, the scanning curves of the proposed method are modeled independently of the isotherms. Thus, the method may be applied to any species, and variations in temperature can easily be taken into account.

Formulating the model independently of the sorption isotherms for a given species and temperature, the two shape parameters of the model seem to be independent of temperature and species. However, this hypothesis needs verification with more experimental data.

Acknowledgements

This work has been funded in part by the Danish Forest and Nature Agency and in part by the Danish Research Agency under project no. 2020-00-0017. The financial support is gratefully acknowledged.

Appendix A

The adsorption scanning curve is determined from the integral (Figure 2):

$$m_a = \int_0^{h_a} \int_0^{h_a} w(h_{12}, h_{21}) dh_{21} dh_{12}. \quad (11)$$

The slope of the adsorption boundary curve at h_a can be determined by differentiation of Eq. (11) with respect to the adsorption RH h_{12}:

$$\left.\frac{\partial m_a}{\partial h_{12}}\right|_{h_{12}=h_a} = \int_0^{h_a} w(h_a, h_{21}) dh_{21}. \quad (12)$$

This corresponds to the vertically hatched cross-sectional area of the w-function shown in Figure 2. The slope of the adsorption boundary curve $\partial m_a / \partial h_{12}$ near the dry condition, i.e., as ha approaches zero, is non-zero for wood. Since the integration length $[0\ h_a]$ in Eq. (12) goes to zero as h_a approaches zero, the w-function must tend towards infinity for the slope of the adsorption boundary curve to be non-zero. A similar singularity can be proven to exist at the other acute-angled corner. These singularities will cause problems in a numerical model.

References

Ahlgren, L. (1972). *Moisture fixation in porous building materials.* Division Of Building Technology, The Lund Institute Of Technology.

Avramidis, S. (1997). The basics of sorption. In Hoffmeyer, P., editor, *Proceedings Of International Conference On Wood-Water Relations, Copenhagen*, volume E8, pages 1–16.

Chomcarn, A. and Skaar, C. (1983). Dynamic sorption and hygroexpansion of wood wafers exposed to sinusoidally varying humidity. *Wood Science and Technology*, 17:259–277.

Dinwoodie, J. M. (2000). *Timber: Its Nature and Behavior.* E & Fn Spon.

Everett, D. H. (1954). A general approach to hysteresis. part 3. a formal treatment of the independent domain model of hysteresis. *Trans. Faraday Soc.*, 50:1077–1096.

Everett, D. H. (1955). A general approach to hysteresis. part 4. an alternative formulation of the domain model. *Transactions of the Faraday Society*, 51:1551–1557.

Everett, D. H. and Smith, F. W. (1954). A general approach to hysteresis. part 2. development of the domain theory. *Trans. Faraday Soc.*, 50:187–197.

Everett, D. H. and Whitton, W. I. (1952). A general approach to hysteresis. *Trans. Faraday Soc.*, 48:749–757.

Fan, M. Z., Dinwoodie, J. M., Bonfield, P. W., and Breese, M. C. (1999). Dimensional instability of cement-bonded particleboard: Behavior of cement paste and its contribution to the composite. *Wood and Fiber Science*, 31:306–318.

Frandsen, H. L. (2005). Modeling of moisture transport in wood. In *Wood Science and Timber Engineering*. Department of Structural Engineering and Building Technology, Aalborg University, Aalborg.

Huang, H. C., Tan, Y. C., Liu, C. W., and Chen, C. H. (2005). A novel hysteresis model in unsaturated soil. *Hydrological Processes*, 19(8):1653–1665.

Kool, J. B. and Parker, J. C. (1987). Development and evaluation of closed-form expressions for hysteretic soil hydraulic properties. *Water Resources Research*, 23(1):105–114.

Mualem, Y. (1973). Modified approach to capillary hysteresis based on a similarity hypothesis. *Water Resources Research*, 9(5):1324–1331.

Mualem, Y. (1974). Conceptual model of hysteresis. *Water Resources Research*, 10(3):514–520.

Pedersen, C. R. (1990). *Combined heat and moisture transfer in build constructions*. PhD thesis, Thermal Insulation Laboratory, Technical University of Denmark, Denmark.

Peralta, P. N. (1995a). Modelling wood moisture sorption hysteresis using the independent-domain theory. *Wood and Fiber Science*, 27(3):250–257.

Peralta, P. N. (1995b). Sorption of moisture by wood within a limited range of relative humidities. *Wood and Fiber Science*, 27(1):13–21.

Peralta, P. N. (1996). Moisture sorption hysteresis and the independent-domain theory: The moisture distribution function. *Wood and Fiber Science*, 28(4):406–410.

Peralta, P. N. and Bangi, A. P. (1998a). Modeling wood moisture sorption hysteresis based on similarity hypothesis. Part 1. direct approach. *Wood and Fiber Science*, 30(1):48–55.

Peralta, P. N. and Bangi, A. P. (1998b). Modeling wood moisture sorption hysteresis based on similarity hypothesis. Part 2. capillary-radii approach. *Wood and Fiber Science*, 30(2):148–154.

Scott, P. S., Farquhar, G. J., and Kouwen, N. (1983). Hysteretic effects on net infiltration. *Advances in Infiltration*, 11(83):163–170.

Paper IV

A sorption hysteresis model for cellulosic materials

Proceedings of the 19th Nordic Seminar on Computational Mechanics
Lund, Sweden, 2006, pp. 77-80

Paper IV

A sorption hysteresis model for cellulosic materials

Henrik Lund Frandsen[1] and Lars Damkilde[2]
[1]*Department of Civil Engineering, Aalborg University, Denmark*
[2]*Esbjerg Institute of Technology, Aalborg University, Denmark*

Abstract
The equilibrium concentration of adsorbed water in cellulosic materials is dependent on the history of the variations of vapor pressure in the ambient air, i.e., sorption hysteresis. Existing models to describe this phenomenon such as the independent domain theory have numerical drawbacks and/or imply accounting for the entire history variations of every material point. This paper presents a sorption hysteresis model based on a state formulation and expressed in closed-form solutions, which makes it suitable for implementation into a numerical method.

1 Introduction

Cellulosic materials adsorb water from the ambient air by binding of the water molecules to hydroxyl groups on cellulose. The amount of adsorbed water is dependent on the relative humidity of the air and on the amount of hydroxyl groups available, which again is dependent on the variation of the relative humidity. Hence, at a given relative humidity a cellulosic material may contain more or less water dependent on the preceding path of the relative humidity variations, see figure 2. During adsorption the material swells and more hydroxyl groups become available for adsorption. Since water occupies the hydroxyl groups, hydrogen bonds between the cellulose molecules are prevented from re-establishment during desorption. Thus, more hydroxyl groups are available during desorption than during adsorption. For an arbitrary variation of the relative humidity, more or less hydroxyl groups may be available leading to conditions between pure adsorption and pure desorption on so-called scanning curves.

In figure 1 the terminology is presented by the variation of relative humidity in the ambient air, h, and moisture content in wood, m (=concentration of water /dry density of cellulosic material).

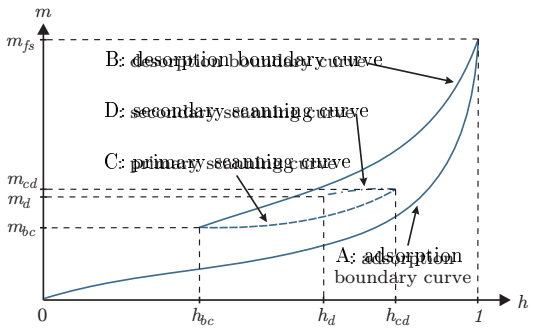

Figure 1 The terminology of sorption hysteresis.

2 Existing models

A classical approach for modeling sorption hysteresis is the independent domain model devel-

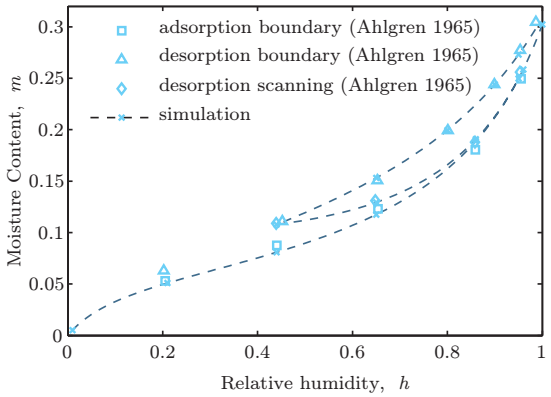

Figure 2 Measurements of boundary and an adsorption scanning curve in Norway Spruce (Ahlgren, 1972).

oped by Everett (1955), refined to require less calibration measurements by Mualem (1974), and applied to wood and paper by Peralta and Bangi (1998) and Chatterjee et al. (1997), respectively. The independent domain theory involves complicated accounting for a volume integral of a function over a varying 2D-domain for each point in a material to obtain the moisture content. Additionally it implicitly involves singularities of the function over the domain, as shown in (Frandsen et al., 2007).

A simpler model by Pedersen (1990), stated as a set of differential equations, provides a good alternative. Though, the differential equation in h and m must be solved numerically in the vicinity of the actual state for each step in time.

3 The proposed model

The proposed sorption hysteresis model has the following advantages:

- Formulated in terms of current state, thus no accounting for the history of the relative humidity variations is required.
- Formulated as closed-form expressions enabling easy time integration.
- Generalizes the scanning curves to be independent of the temperature dependent boundary curves by a normalization .

3.1 Uniqueness of scanning curves

In (Frandsen et al., 2007) it is argued that adsorption scanning curves originating at different points will not intersect and likewise for the desorption scanning curves, see figure 3. Hence, a state within the boundary curves are uniquely defined by the origin of the scanning curve leading to the state, i.e., $z_a^0 = \{h_a^0, m_a^0\}$ and $z_d^0 = \{h_d^0, m_d^0\}$, see figure 4.

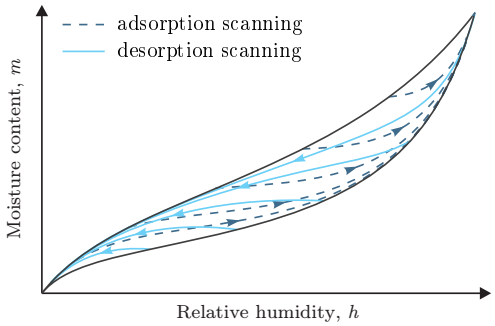

Figure 3 Grid of non-intersecting adsorption scanning curves and non-intersecting desorption scanning curves.

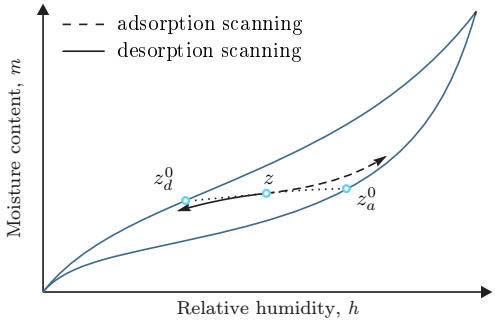

Figure 4 Definition of a state z from the scanning curves origin states z_a^0 and z_d^0.

3.2 Generalization of scanning curves

The expression for the scanning curves will be stated in the normalized parameter $s(h)$, which is the fractional amount of exploited hydroxyl

groups at the given relative humidity

$$s(h) = \frac{m(h) - m_a(h)}{m_d(h) - m_a(h)}. \tag{1}$$

Hereby the material-, species- and temperature-dependent boundary curves $m_a(h)$ and $m_d(h)$ are excluded from the expression for the scanning curves. In figures 5 and 6, some scanning curves from the different measurements are presented in the 1 by 1 normalized domain.

3.3 The mathematical model

As seen in figures 5 and 6, the slope of the desorption scanning curves originating at the adsorption boundary curve ($h = h_a^0$, $s = 0$) will approach the desorption boundary curve ($s = 1$) asymptotically, i.e., $\partial s/\partial h \to 0^-$. Similar observations are made for the adsorption scanning curves originating at the desorption boundary curve ($h = h_d^0$, $s = 1$), i.e., $\partial s/\partial h \to 0^-$ for $s \to 0$.

The mathematical model in equation Eq. (2) implicitly fulfills these requirements and implies the scanning curves to be uniquely defined by their origins h_a^0 and h_d^0, see figure 4

$$s(h) = \begin{cases} -1 + 2^{\left(\frac{1-h}{1-h_d^0}\right)^{\left(\frac{d_1}{\ln(d_2(1-h_d^0))}\right)}} & \dot{h} > 0 \ \wedge \ s_0 > 0 \\ 2 - 2^{\left(\frac{h}{h_a^0}\right)^{\left(\frac{d_1}{\ln(d_2 h_a^0)}\right)}} & \dot{h} < 0 \ \wedge \ s_0 < 1 \\ 0 & \dot{h} > 0 \ \wedge \ s_0 = 0 \\ 1 & \dot{h} < 0 \ \wedge \ s_0 = 1 \end{cases} \tag{2}$$

where d_1 and d_2 are shape parameters. Equations (2a) and (2b) model the scanning curves during adsorption ($\dot{h} > 0$) and during desorption ($\dot{h} < 0$), respectively. Equation (2c) simply states that a state with origin on the adsorption boundary curve ($s = 0$) will follow the adsorption boundary curve if adsorption is taking place ($\dot{h} > 0$) and similarly for desorption in equation (2d). Since the scanning curves are known to trail through the initial state $z_0 = \{h_0, m_0\}$, the expressions for h_a^0 and h_d^0 can be obtained by solving (2a) and (2b) for h_a^0 and h_d^0, respectively

$$h_a^0 = h_0(d_2 h_0)^{q_1} \tag{3a}$$

$$h_d^0 = 1 - (1 - h_0)(d_2(1 - h_0))^{q_2}, \tag{3b}$$

where

$$q_1 = -\frac{\ln(\ln(2)) - \ln(\ln(2 - s_0))}{\ln(\ln(2)) - \ln(\ln(2 - s_0)) - d_1} \tag{4a}$$

$$q_2 = -\frac{\ln(\ln(2)) - \ln(\ln(1 + s_0))}{\ln(\ln(2)) - \ln(\ln(1 + s_0)) - d_1}. \tag{4b}$$

The result in terms of $m(h)$ can be obtained by the reverse mapping $m(h) = (m_d(h) - m_a(h))s(h) + m_a(h)$. An analytical expression for the derivative for time integration into a numerical method is also easily obtained.

4 Fitting of the model

In figures 5, 7 and 2, measurements of scanning curves for sorption in Yellow Poplar by Peralta (1995) and Norway Spruce by Ahlgren (1972) are simulated by the proposed model. The scanning curves for sorption in a bleached-kraft paperboard measured by Chatterjee et al. (1997) are simulated in figures 6 and 8. The applied shape parameters d_1 and d_2 for wood and paper are shown in table 1.

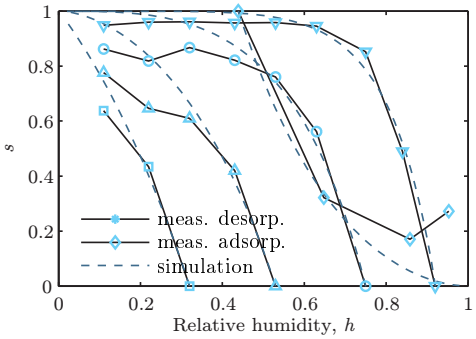

Figure 5 Scanning curves from sorption in Norway Spruce (Ahlgren, 1972) and Yellow Poplar (Peralta, 1995).

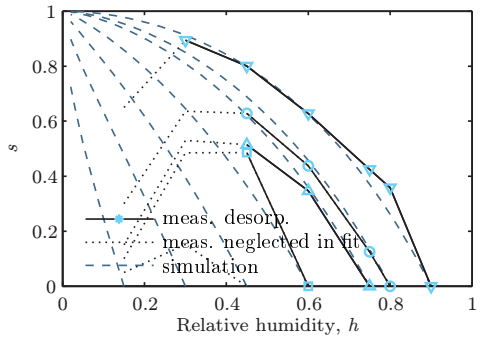

Figure 6 Desorption scanning curves from sorption in bleached-kraft paperboard (Chatterjee et al., 1997).

In figures 5 and 6 at $h \to 0$ and at $h \to 1$, the deviations of the measurements displayed with s as a function of h appear larger, since the denominator of s approaches zero ($m_a \approx m_d$).

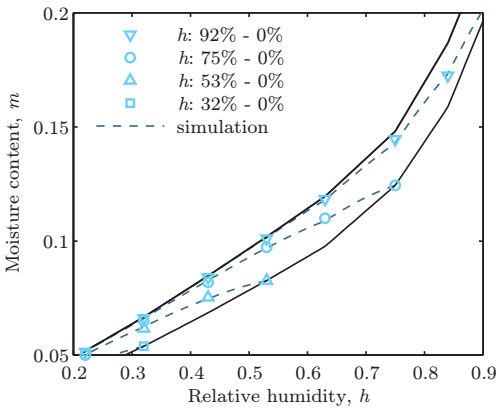

Figure 7 Desorption scanning curves from sorption in Yellow Poplar (Peralta, 1995).

	Yellow poplar and Norway spruce	Bleached-kraft paperboard
d_1	-1.32	-1.28
d_2	0.88	0.57

Table 1 Shape parameters of the scanning curves.

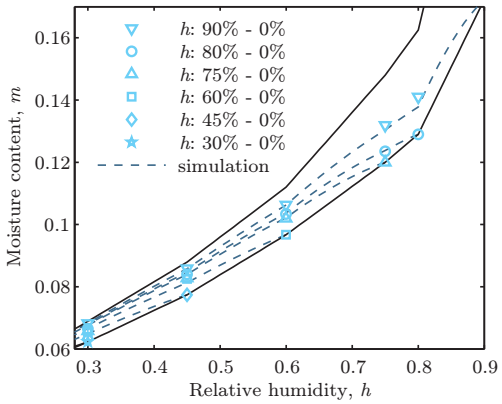

Figure 8 Desorption scanning curves from sorption in bleached-kraft paperboard (Chatterjee et al., 1997).

5 Conclusion

The present paper proposes a sorption hysteresis model, which offers advantages for implementation in a numerical method. Easy time integration is obtained by expressing the scanning curves in closed-form solutions with the current state as the only input parameter. General applicability is provided by excluding the material, wood-species and temperature dependent boundary curves boundary curves from the hysteresis scanning curves.

References

Ahlgren, L. (1972). *Moisture fixation in porous building materials.* Division Of Building Technology, The Lund Institute Of Technology.

Chatterjee, S. G., Ramarao, B. V., and Tien, C. (1997). Water-vapour sorption equilibria of a bleached-kraft paperboard - a study of the hysteresis region. *Jour. of Pulp and Paper Science*, 23(8):366–373.

Everett, D. H. (1955). A general approach to hysteresis. part 4. an alternative formulation of the domain model. *Transactions of the Faraday Society*, 51:1551–1557.

Frandsen, H. L., Svensson, S., and Damkilde,

L. (2007). A hysteresis model suitable for numerical simulation of moisture content in wood. *Holzforschung*, 61(2):175–181.

Mualem, Y. (1974). Conceptual model of hysteresis. *Water Resources Research*, 10(3):514–520.

Pedersen, C. R. (1990). *Combined heat and moisture transfer in build constructions*. PhD thesis, Thermal Insulation Laboratory, Technical University of Denmark, Denmark.

Peralta, P. N. (1995). Sorption of moisture by wood within a limited range of relative humidities. *Wood and Fiber Science*, 27(1):13–21.

Peralta, P. N. and Bangi, A. P. (1998). Modeling wood moisture sorption hysteresis based on similarity hypothesis. Part 2. capillary-radii approach. *Wood and Fiber Science*, 30(2):148–154.

Paper V

Implementation of sorption hysteresis in multi-Fickian moisture transport

Holzforschung vol. 61 issue 6, pp. 693-701, 2007

Paper V

Implementation of sorption hysteresis in multi-Fickian moisture transport

Henrik Lund Frandsen[1] and Staffan Svensson[2]
[1]*Department of Civil Engineering, Aalborg University, Denmark*
[2]*Department of Civil Engineering, Technical University of Denmark, Denmark*

Abstract
In the cellular structure of wood, bound-water diffusion and water-vapor diffusion interact via sorption in a complex moisture transportation system. At low relative humidities moisture-transport may be modeled by a Fickian diffusion equation with a good approximation. At higher relative humidities, slow sorption and faster bound-water diffusion cause effects, which have been referred to as non-Fickian or anomalous, as they cannot be modeled by one Fickian diffusion equation. Previous research has demonstrated that a set of coupled diffusion equations, namely the multi-Fickian model, can represent this behavior. The multi-Fickian model describes the combined transport of bound water and vapor and their interaction through sorption. The bound-water concentration is also influenced by sorption hysteresis. In the worst case sorption hysteresis may result in deviations of up to 30-35% in moisture content. Hence, for a precise moisture content computation, sorption hysteresis must be taken into account. The present paper explains the relation between sorption hysteresis and multi-Fickian moisture transport, and clarifies how models for the two phenomena are coupled. To illustrate the effects, a finite element simulation, which is based on the combined model, is presented.

Key words: hysteresis, moisture transport, multi-Fickian, multi-phase, non-Fickian, sorption.

1 Introduction

When creep and mechanosorptive creep in wood are calculated, an accurate estimation of moisture content distribution is important to avoid inaccuracies, because even small changes of the moisture content may accelerate the creep considerably.

This paper adresses modeling of moisture content in wood and more specifically the combined effect of sorption hysteresis and the so-called non-Fickian effects. Both influence the moisture content in wood, but this aspect is often neglected, as the combined effect is undocumented.

In this paper, we describe the basics and a model that describes both phenomena and their interaction. The combined effect will be illustrated by simulations, which relies on a finite element model.

1.1 Multi-Fickian moisture transport

Moisture transport in wood below the fiber saturation point is a process governed by diffusion of bound-water and water-vapor diffusion (Stamm, 1959) and the coupling between the two phases of water, i.e., sorption.

A change of vapor pressure in the ambient air results in diffusion of water vapor

into wood, sorption of bound-water and, consequently, bound-water diffusion. In Figure 1, the time-dependent processes of these phenomena, i.e., diffusion into wood in the two phases and the sorption coupling, are schematically illustrated. It is important to recognize that the time dependency on the sorption plays a significant role.

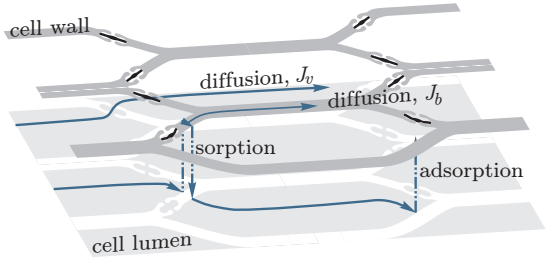

Figure 1 Various time-dependent processes responsible for moisture transport in the cellular structure of wood. J_v and J_b are the water-vapor and bound-water fluxes, respectively.

At low relative humidities, bound-water transport is a relatively slow process and the moisture transport in wood is governed by water-vapor diffusion and, subsequently, a relatively fast sorption to bound water. When evaluated against vapor diffusion, bound-water diffusion and sorption can be neglected. Therefore, moisture transport is customarily modeled by a single Fickian equation describing vapor diffusion.

At higher relative humidities, bound-water diffusion becomes more substantial and the sorption rate decreases (Christensen, 1965; Frandsen et al., 2007a). This combined two-phase diffusion and sorption phenomenon has characteristics which cannot be described by a single diffusion equation and has been referred to as anomalous behavior (Crank and Park, 1951) and non-Fickian effects (Wadsö, 1994).

The phenomenon was reported by Crank and Park (1951) for long polymers and Mandelkern and Long (1951) for cellulose acetate. Wadsö (1994) measured the bound-water uptake in pine (*Pinus silvestris*) specimens of various thicknesses and directions to the grain at high relative humidity (RH) steps, i.e., at 54-75% and 75-84% RH. The specimens were exposed by humid air (climate chamber with a salt solution, ventilated with an air velocity on 3 $\mathrm{m\,s^{-1}}$) on two accessible and symmetrically oriented surfaces, and therefore it can be assumed that the effects from the boundary layer can be neglected (Rosen, 1978). The mass was measured over time, from which the fractional weight increase was calculated by:

$$E(t) = \frac{w(t) - w_0}{w_\infty - w_0}, \tag{1}$$

where w_0 and w_∞ are the initial and final weight, respectively, and $w(t)$ is the weight at the time t. Measurements for two specimens with different widths but identical direction of diffusion from this experiment are presented in Figure 2.

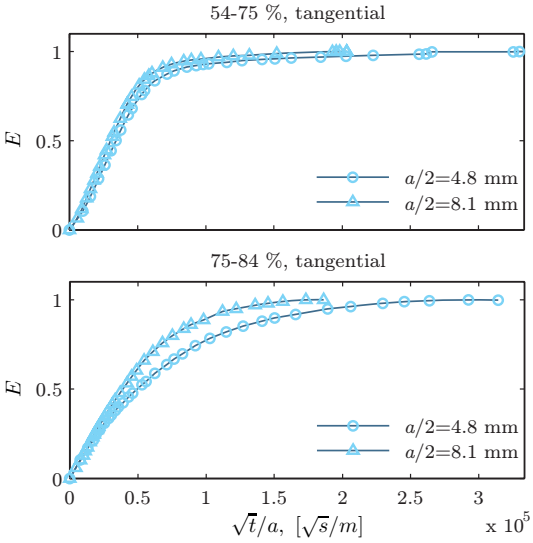

Figure 2 Fractional weight increase, E, in pine specimens over time normalized with respect to specimen thickness a in the experiments by Wadsö (1994).

Obtaining the diffusion coefficients by fitting a Fickian model not only leads to moisture, but also specimen-length dependent diffusion coefficients. This is seen in Figure 2b, where

the $\sqrt{t}/a$ normalization of the axis of abscissa should result in identical curves for different specimen lengths, even for moisture dependent diffusion coefficients (Crank, 1967). A dependency on length of the diffusion coefficients has no physical motivation, and consequently the phenomenon cannot be modeled by one Fickian diffusion equation.

Therefore, a new moisture transport model, which describes the combined bound-water and water-vapor transport and their interaction through sorption, has been developed. The solution of the coupled differential equation set of this model has gone from being analytical to being numerical. This has allowed for inclusion of more non-linear dependencies of, e.g., diffusion coefficients, sorption isotherm and sorption rate (Cunningham, 1994; Salin, 1996; Absetz and Koponen, 1997; Krabbenhøft and Damkilde, 2004). An overview of the development of the model is provided by Frandsen et al. (2007a). The authors also discuss and revise the embedded sorption rate model, and addresses the boundary conditions for the problem.

Parallel to this line of research on multi-Fickian models in wood, similar models have been investigated for modeling moisture transport in paper stacks (Bandyopadhyay et al., 2000; Massoquete et al., 2005; Nyman et al., 2006).

1.2 Sorption hysteresis

Variation of the RH in the ambient air causes variations of the moisture content (MC) in wood. But a given RH does not uniquely define the equilibrium MC. The history of the variations must be taken into account. This is illustrated in Figure 3, where the dependency on MC, m, of a sequence of RH, h, variations is shown. Furthermore, the terminology of sorption hysteresis is presented in Figure 3.

The explanation for the sorption hysteresis phenomenon is found in the chemical behavior and complex structure of the wood cell wall. The glucane chains of the cellulose within the microfibrils are organised in crystalline and

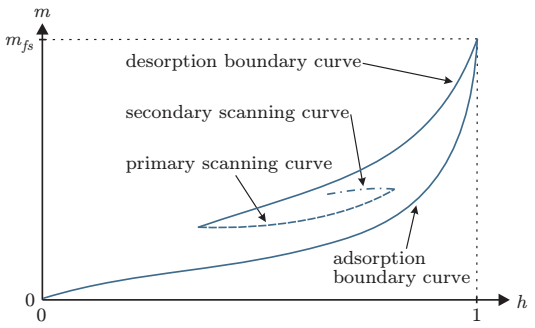

Figure 3 Various boundary and scanning curves.

paracrystalline regions. There are more intermolecular hydrogen bonds (bounds between neighbor chains) in the former than in the latter. The non-participating hydroxyl groups are also called sorption sites, because they have great affinity to water and are responsible for sorption in wood (Avramidis, 1997).

Adsorption of water leads to swelling of the cell wall and breaking of hydrogen bonds, and thus more available sorption sites become available. The hydrogen bonds are re-established during desorption, but this process is delayed, because water molecules now occupy the sorption sites. Hence, wood contains more water at a given RH during desorption than during adsorption. For an arbitrary variation of the RH, conditions in between pure adsorption and pure desorption depending on availability of sorption sites are obtained.

A classical approach for modeling sorption hysteresis is the independent domain model developed by Everett (1954, 1955). The model was applied to wood by Peralta (1995b,a, 1996) and improved by Peralta and Bangi (1998a,b). The independent domain theory involves complications on accounting for activated domains. Moreover, it also has another major numerical drawback for wood and other materials with isotherms, which have an initial slope different from zero, because it implicitly involves singularities in the function spanning over the independent domain (Frandsen et al., 2007b).

Another approach, which involves numerical solution of a partial differential equation for each increment forward in time, is provided by Pedersen (1990). The different approaches are discussed by Frandsen et al. (2007b). These authors also presented a model suitable for numerical simulations. This model is applied in the present work and is described in the section "Sorption" below.

1.3 Interaction of the phenomena

Both hysteresis and multi-phase moisture transport obviously influence the moisture content of wood. The multi-phase moisture transport influences it in time and space, and hysteresis provides the MC by the preceding RH variations. The sorption takes place inside the wood specimen between air in the lumens and the cell wall. For a point in a cell wall, the increase of MC along an adsorption scanning curve in time can be illustrated, as in Figure 4.

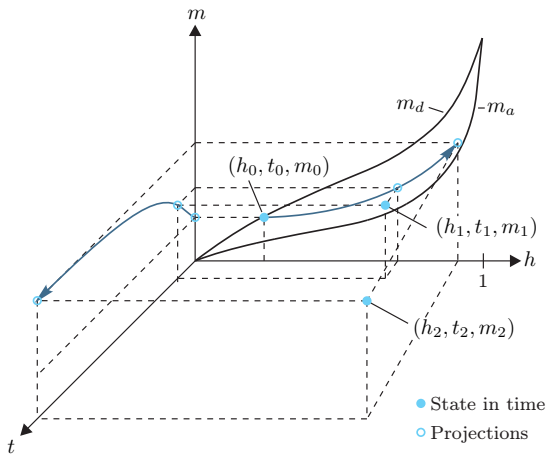

Figure 4 The increase of MC, m, over time, t, along an adsorption scanning curve, due to an increase of RH, h.

Exposed to an increase in RH from h_0 to h_2, the MC will trace along the adsorption scanning curve to the equilibrium point (h_2,t_2,m_2) over time. Hence, the equilibrium MC, which influences the sorption rate, is governed by hysteresis.

The sorption rate, diffusion of vapor and bound water to the point determine the rate, by which the state moves along the scanning curve. Here, the two diffusion processes influences the initial state and the set-point of the sorption process and, hereby, also the rate the state moves along the scanning curve.

In the following, a mathematical and physical model for these relations is presented.

2 Modeling of the diffusion processes

The bound-water and water-vapor diffusion is modeled by the two coupled diffusion equations:

$$\frac{\partial c_b}{\partial t} = \boldsymbol{\nabla} \cdot (\mathbf{D}_b \boldsymbol{\nabla} c_b) + \dot{c} \tag{2}$$

$$\frac{\partial c_v}{\partial t} = \boldsymbol{\nabla} \cdot (\mathbf{D}_v \boldsymbol{\nabla} c_v) - \dot{c}, \tag{3}$$

where c_b and c_v are the concentration of water in the bound-water and water-vapor phases, respectively, with the dry volume of wood as a reference. The matrices $\mathbf{D_b}$ and $\mathbf{D}_v$ contain the diffusion coefficients for the different material directions in the diagonal. $\boldsymbol{\nabla}$ is the spatial gradient operator. $\dot{c}$ is the sorption rate, and within the time interval dt, the amount of water vapor adsorbed to bound water is $\dot{c}\,dt$.

Eq. (3) may be based on partial vapor pressure in preference to concentration via the ideal gas law (Frandsen et al., 2007a):

$$\frac{\partial}{\partial t}\left(p_v \frac{\varphi M_{\mathrm{H_2O}}}{RT}\right) = \boldsymbol{\nabla} \cdot \left(\mathbf{D}_v \boldsymbol{\nabla}\left(p_v \frac{\varphi M_{H_2O}}{RT}\right)\right) - \dot{c}, \tag{4}$$

where R is the universal gas constant (J mol^{-1}K^{-1}), T is the temperature (K), φ is the porosity and $M_{\mathrm{H_2O}}$ is the molar mass of water (kg mol^{-1}).

2.1 Diffusion coefficients

Diffusion in the cell walls can be determined by the expression in Skaar and Siau (1981):

$$\mathbf{D}_b = \mathbf{D}_0 \exp\left(\frac{-E_b}{RT}\right), \tag{5}$$

where E_b is the activation energy for bound-water diffusion (J mol^{-1}). The diagonal components of the matrix $\mathbf{D}_0$, i.e., D^0_{TT} and D^0_{LL} are equal to $7\times10^{-6}m^2s^{-1}$ and $17.5\times10^{-6}m^2s^{-1}$, respectively (Siau 1995). The activation energy may be approximated by the linear expression $E_b = (38.5 - 29m)\times10^3$J mol^{-1} (Siau, 1995), where $m = c_b/\rho_0$ is the MC and ρ_0 is the dry density of wood.

Diffusion in the cell lumens is assumed to be identical to diffusion in stagnant air, though compensated for by the resistance at the narrow passages of the pits and geometry of the lumens. Diffusion of water vapor in bulk air is estimated by the empirical expression by Schirmer (1938):

$$\mathbf{D}_v = \boldsymbol{\xi}\underbrace{\left(2.31\times10^{-5}\frac{p_{\text{atm}}}{p_{\text{atm}}+p_v}\left(\frac{T}{273K}\right)^{1.81}\right)}_{\text{Schirmer}}, \tag{6}$$

where p_{atm} is the atmospheric pressure and p_v is the partial vapor pressure. The matrix $\boldsymbol{\xi}$ contains the estimated reduction factors due to hindrance of the diffusion in the cellular structure for the different directions in the diagonal.

2.2 Boundary Conditions

The water vapor is diffusing through a boundary layer of stagnant and slower moving air at the wood surface. The flux vector of vapor $\mathbf{J}_v$ perpendicular to the surface, with the normal vector $\mathbf{n}$, $\mathbf{n}\cdot\mathbf{J}_v$ is driven by the difference in partial vapor pressure at the surface p^s_v and in the ambient air p^a_v

$$\mathbf{n}\cdot\mathbf{J}_v = k_v(p^s_v - p^a_v) \tag{7}$$

where k_v is the mass transfer coefficient of the boundary layer. At higher air velocities, the resistance from this layer may be assumed to be negligible and the partial vapor pressure at the surface is assumed to be identical to the partial vapor pressure in the ambient air (Frandsen et al., 2007a):

$$p^s_v = p^a_v. \tag{8}$$

Additional bound water can only be added to the system by adsorption. Since bound water is restricted to wood, it is obviously not moving through the surface (Frandsen et al., 2007a):

$$\mathbf{n}\cdot\mathbf{J}_b = 0. \tag{9}$$

3 Modeling of sorption

Sorption is a phase change between water vapor and bound water, which occurs when the driving potential in the two phases are not in equilibrium. The driving potentials are water-vapor pressure p_v and bound-water concentration c_b. Comparison requires conversion to the same basis (pressure or concentration) through the hysteric sorption isotherm, which represents equilibrium.

A key point for implementation of sorption hysteresis into a multi-Fickian model is accounting for hysteresis in all the material points. In the applied model hysteresis can be accounted for by storing the condition of wood as a state variable $\{p_{vw}, c_b\}$ in the hysteresis space (Figure 5). For example, similar accounting would in the independent domain model (Everett, 1954) would require storing an independent domain for each material point.

The state $\{p_{vw}, c_b\}$ only describes the condition of wood and do not relate to the vapor pressure in the lumens, p_v. To investigate if equilibrium is obtained p_v and p_{vw} can be compared. Alternatively, the bound-water concentration c_b can be compared to the bound-water concentration in equilibrium with the vapor pressure, p_v, which will be denoted c_{bl} (Figure 5).

It is beyond the scope of this paper to determine, which of the two mentioned approaches for determining equilibrium, i.e., comparing pressures or concentrations, is the better. The object is to open the opportunity for application of hysteresis with both approaches.

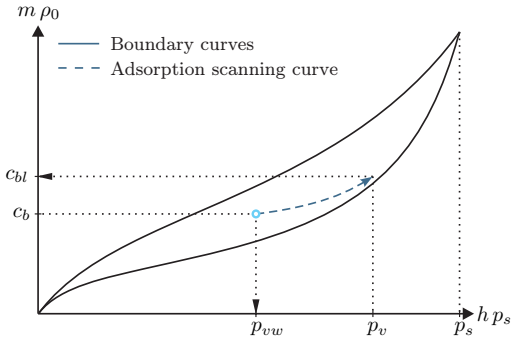

Figure 5 The relation between the different state variables through sorption hysteresis equilibrium path.

The sorption rate models of two different approaches, the chosen hysteresis model and their implementation into a multi-Fickian model are presented in the following sections.

3.1 Sorption rate

Sorption ceases at equilibrium, and therefore the sorption rate should go towards zero as equilibrium is approached. The sorption rate can therefore be described as a difference between the condition of the air in the lumens and the condition of the wood.

In the first approach with bound-water concentration as a reference, the sorption rate can be modeled by (Frandsen, 2005):

$$\dot{c} = \frac{\partial c_{\text{sorp}}}{\partial \text{t}} = H_c(c_{bl} - c_b). \tag{10}$$

The sorption rate function, H_c, has a steep drop as equilibrium is approached for higher relative humidities as seen in (Christensen 1965). Compared to the measurements by Wadsö (1994) reasonable results have been obtained in (Frandsen, 2005) by:

$$H_c = \begin{cases} C_1 \exp\left(-C_2 \left(\frac{c_b}{c_{bl}}\right)^{C_3}\right) + C_4 & c_b < c_{bl} \\ C_1 \exp\left(-C_2 \left(2 - \frac{c_b}{c_{bl}}\right)^{C_3}\right) + C_4 & c_b > c_{bl} \end{cases} \tag{11}$$

for adsorption ($c_b < c_{bl}$) and desorption ($c_b > c_{bl}$).

In the second approach with pressure as a reference, the sorption rate can be modeled by a similar expression (Frandsen et al., 2007a):

$$\dot{c} = \frac{\partial c_{\text{sorp}}}{\partial \text{t}} = H_p(p_v - p_{vw}). \tag{12}$$

The sorption rate function, H_p, has a similar steep drop as equilibrium is approached for higher relative humidities, and an expression analogous to Eq. (10) can be applied for modeling this (Frandsen et al., 2007a):

$$H_p = \begin{cases} C_1 \exp\left(-C_2 \left(\frac{p_{vw}}{p_v}\right)^{C_3}\right) + C_4 & p_{vw} < p_v \\ C_1 \exp\left(-C_2 \left(2 - \frac{p_{vw}}{p_v}\right)^{C_3}\right) + C_4 & p_{vw} > p_v \end{cases} \tag{13}$$

for adsorption ($p_{vw} < p_v$) and desorption ($p_{vw} > p_v$).

The variation of the shape parameters C_i with RH is discussed in (Frandsen et al., 2007a) and compared with measurements of sorption in thin specimens of klinki pine (*Araucaria Klinkii lauterb.*) at 40°C by Christensen (1965). The variation of the parameter C_2 can be modeled with the expression (Frandsen et al. 2007b):

$$C_2(h) = c_{21} \exp(c_{22} h) \tag{14}$$

where the shape c_{21} and c_{22} are given in Table 1.

3.2 Sorption hysteresis

A hysteresis model provides the equilibrium path along which the moisture condition of wood moves. The moisture condition is generally provided in terms of MC, m, as a function of the RH, h, variations. These two measures are normalized quantities of bound-water concentration and vapor pressure with respect to dry density, ρ_0, and saturated vapor pressure, p_s, respectively:

$$m = \frac{c}{\rho_0} \quad , \quad h = \frac{p}{p_s} \tag{15}$$

where c is bound-water concentration and p is vapor pressure. Note that the subscripts b, bl, v and vw have been omitted for generalization, since the conversion through the equilibrium path is independent of the medium, i.e., cell wall or air (Figure 5).

The chosen hysteresis model is derived in Frandsen et al. (2007b) and condensed in the following section. The model has the advantage that the scanning curves are given by closed-form expressions using the current state $z_0 = \{h_0, m_0\}$ as the only input. Thus, accounting for the entire RH history or storing another memory variable is avoided. The model can be applied to different species, and variations in temperature are relatively easy to take into account.

The generalization is obtained by expressing the model for the scanning curves in terms of a normalized the MC, $s(h)$:

$$s(h) = \frac{m(h) - m_a(h)}{m_d(h) - m_a(h)}. \tag{16}$$

Hereby, the species and temperature-dependent boundary curves $m_a(h)$ and $m_d(h)$ are only implicitly included in the model formulation.

The parameter, s, may also be interpreted in a physical sense as the fractional amount of sorption sites exploited at the current RH. The normalization implies the gray domain in Figure 6 for the scanning curves to be mapped into a 1×1 square.

Frandsen et al. (2007b) argued that the scanning curves are uniquely defined by their origin on one of the boundary curves (Figure 6).

Thus, the scanning curves can be explicitly formulated in terms of their origin on the boundary curves:

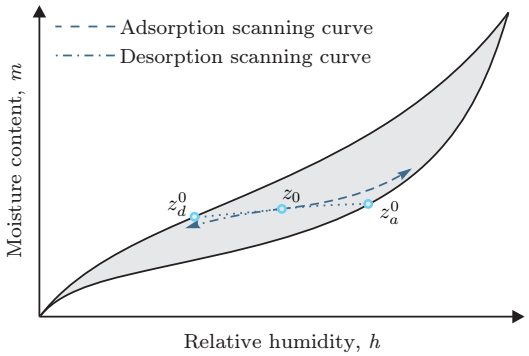

Figure 6 Prediction of the scanning curves from the current state z_0, and the origins of the scanning curves, z_a^0 and z_d^0.

$$s(h) = \begin{cases} -1 + 2^{\left(\frac{1-h}{1-h_d^0}\right)^{\left(\frac{d_1}{\ln(d_2(1-h_d^0))}\right)}} & \dot{h} > 0 \ \wedge \ s_0 > 0 \\ 2 - 2^{\left(\frac{h}{h_a^0}\right)^{\left(\frac{d_1}{\ln(d_2 h_a^0)}\right)}} & \dot{h} < 0 \ \wedge \ s_0 < 1 \\ 0 & \dot{h} > 0 \ \wedge \ s_0 = 0 \\ 1 & \dot{h} < 0 \ \wedge \ s_0 = 1 \end{cases} \tag{17}$$

where d_1 and d_2 are shape parameters. Eqs. (17a) and (17b) model the scanning curves during adsorption ($\dot{h} > 0$) and during desorption ($\dot{h} < 0$), respectively. (17c) simply expresses that a state with origin on the adsorption boundary curve ($s_0 = 0$) will follow the adsorption boundary curve if adsorption is taking place ($\dot{h} > 0$) and similarly for desorption in Eq. (17d). h_a^0 and h_d^0 are the RH at the origin of the desorption and adsorption scanning curve, respectively (Figure 6).

Because the scanning curves are known to trail through the current state $z_0 = \{h_0, m_0\}$, expressions for h_a^0 and h_d^0 can be obtained by solving Eq. (17a) and (17b) for h_a^0 and h_d^0, respectively, where $h = h_0$ and $s = s_0$:

$$h_a^0 = h_0 (d_2 h_0)^{q_1} \tag{18}$$

$$h_d^0 = 1 - (1 - h_0)(d_2(1 - h_0))^{q_2}, \tag{19}$$

where

$$q_1 = -\frac{\ln(\ln(2)) - \ln(\ln(2-s_0))}{\ln(\ln(2)) - \ln(\ln(2-s_0)) - d_1} \quad (20)$$

$$q_2 = -\frac{\ln(\ln(2)) - \ln(\ln(1+s_0))}{\ln(\ln(2)) - \ln(\ln(1+s_0)) - d_1}. \quad (21)$$

As seen from Eq. (17)-(21), the only input parameter to the model is the current state $z_0 = \{h_0, m_0\}$.

From Eq. (15) and (16) the bound-water concentration on the equilibrium path may be expressed as a function of vapor pressure:

$$c(h) = \rho_0 \left(s(h) \left(m_d(h) - m_a(h) \right) + m_a(h) \right), \quad (22)$$

where h is p/p_s and s is determined from Eqs. (17)-(21).

4 Implementation of sorption hysteresis

In the following section, the two approaches for modeling sorption rate by the hysteresis model are implemented into the multi-Fickian model.

The first concentration based approach has the governing Eqs.: (2), (4) and (10). The independent variables of the equation system are c_b and p_v. The variable c_{bl} in Eq. (10), depends on p_v through the equilibrium path and is therefore replaced by applying Eq. (22), which becomes:

$$c_{bl}(h) = \rho_0 \left(s(h) \left(m_d(h) - m_a(h) \right) + m_a(h) \right), \quad (23)$$

where h is p_v/p_s and s is determined from Eq. (17)-(21). This substitution enables solution of Eq. (2), (4) and (10) with respect to c_b and p_v.

The second pressure based approach has the governing Eqs.: (2), (4) and (12). The independent variables of the equation system are c_b and p_v. However, here the dependent variable p_{vw} cannot be replaced by the corresponding independent variable c_b by use of Eq. (21), since Eqs. (16)-(20) cannot be inverted, such that bound-water concentration becomes a function of vapor pressure $c_b(p_{vw})$.

The solution to the problem is to perform a shift from c_b to p_{vw} as an independent variable in Eq. (2) by applying the chain rule:

$$\frac{\partial c_b}{\partial p_{vw}} \frac{\partial p_{vw}}{\partial t} = \boldsymbol{\nabla} \cdot \left(\mathbf{D}_b \frac{\partial c_b}{\partial p_{vw}} \boldsymbol{\nabla} p_{vw} \right) + \dot{c}, \quad (24)$$

where the fraction $\partial c_b / \partial p_{vw} = C_{vw}$ is a RH dependent capacity corresponding to e.g. heat capacity in a heat transfer problem. For a consistent and simple notation the term $\mathbf{D}_b \partial c_b / \partial p_{vw}$ is replaced by a diffusion coefficient named $\mathbf{D}_{vw}$ and Eq. (24) becomes:

$$C_{vw} \frac{\partial p_{vw}}{\partial t} = \boldsymbol{\nabla} \cdot \left(\mathbf{D}_{vw} \boldsymbol{\nabla} p_{vw} \right) + \dot{c}. \quad (25)$$

The fraction $\partial c_b / \partial p_{vw}$ can be calculated from Eq. (22):

$$\frac{\partial c_b(h)}{\partial p_v} = \frac{\partial h}{\partial p_v} \frac{\partial c_b}{\partial h} = \frac{1}{p_s} \frac{\partial c_b}{\partial h}, \quad (26)$$

where

$$\begin{aligned} \frac{\partial c_b}{\partial h} =& \rho_0 \left(s \left(\frac{\partial m_d}{\partial h} - \frac{\partial m_a}{\partial h} \right) \right. \\ & \left. + \frac{\partial s}{\partial h} (m_d - m_a) + \frac{\partial m_a}{\partial h} \right) \end{aligned} \quad (27)$$

$$\frac{\partial s}{\partial h} = \begin{cases} \frac{-g_a 2^{g_a} d_1 \ln(2)}{\ln\left(d_2(1-h_d^0)\right)(1-h)} & \dot{h} > 0 \quad \wedge \quad s_0 > 0 \\ 0 & \dot{h} > 0 \quad \wedge \quad s_0 = 0 \\ \frac{-g_d 2^{g_d} d_1 \ln(2)}{\ln(d_2 h_a^0) h} & \dot{h} < 0 \quad \wedge \quad s_0 < 1 \\ 0 & \dot{h} < 0 \quad \wedge \quad s_0 = 1 \end{cases} \quad (28)$$

where

$$g_a = \left(\frac{1-h}{1-h_d^0} \right)^{\left(\frac{d_1}{\ln(d_2(1-h_d^0))} \right)} \quad (29)$$

$$g_d = \left(\frac{h}{h_a^0} \right)^{\left(\frac{d_1}{\ln(d_2 h_a^0)} \right)}. \quad (30)$$

Any expression for the boundary curves, which is differentiable with h at least once, can be applied. Here the Hailwood-Horrobin sorption isotherm is chosen:

$$m_\alpha(h) = \frac{h}{f_1^\alpha + f_2^\alpha h + f_3^\alpha h^2}, \quad (31)$$

where $\alpha \in \{a, d\}$ designates either adsorption or desorption and f_i^α are shape parameters. Differentiating Eq. (31) with respect to h yields:

$$\frac{\partial m_\alpha}{\partial h} = \frac{f_1^\alpha - f_3^\alpha h^2}{\left(f_1^\alpha + f_2^\alpha h + f_3^\alpha h^2\right)^2}. \qquad (32)$$

5 Simulations

To illustrate the effect of the combined model, two simulations of a specimen of wood exposed to a series of changes in RH are presented in the following section.

Both approaches have been successfully implemented into the commercial software Comsol Multiphysics^{TM}, but in the following only simulations with the vapor pressure based sorption rate approach are presented.

The material data for the multi-Fickian model have been obtained in Frandsen et al. (2007a) from experiments on pine at 23°C by Wadsö (1994). The material parameters of the sorption rate model in Eq. (13) are shown in Table 1. The reduction factor for diffusion of vapor in the cellular structure in the tangential direction ξ_T in Eq. (6) is 0.03, and the dry density ρ_0 is 500 kg m^{-3}.

c_1	c_{21}	c_{22}	c_3	c_4
2.6×10^{-6}	5.22×10^{-6}	19.0	50	8.0×10^{-8}

Table 1 Sorption rate constants (Frandsen et al., 2007a).

The shape parameters for the boundary curves in Eq. (31) are obtained from the measurements on pine at 20°C by Ahlgren (1972) are shown in Table 2. The shape parameters for the scanning curves are obtained from Ahlgren (1972) also to and $d_1 = -0.7$ and $d_2 = 1.0$.

α	f_1^α	f_2^α	f_3^α
a	0.947	15.93	-13.58
d	0.533	11.41	-8.725

Table 2 The shape parameters of the Hailwood-Horrobin isotherm calibrated to the measurements on pine at 20°C by Ahlgren (1972).

The specimen and setup are chosen to be identical to one of those in the experiment by Wadsö (1994). The 16.2 mm wide specimen is exposed on two adjacent tangential surfaces and insulated on the remaining surfaces (Figure 7).

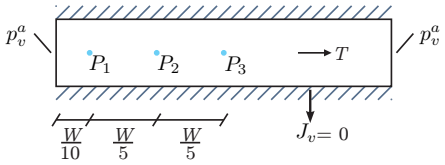

Figure 7 The setup of the specimen with the width, W=16.2 mm, used in the simulations.

5.1 Comparison with experimental data

In this simulation the model is compared with experiments to evaluate its ability to reproduce the observations. The RH is varied in three sequences:

1 adsorption boundary: 21%, 54%, 75%, 84%, 96%, 100% RH,

2 desorption boundary: 100%, 95%, 90%, 80%, 65%, 43% RH,

3 adsorption scanning: 43%, 65%, 86%, 95% RH,

which are similar to the measurements by Ahlgren (1972) except from the two steps 54-75% and 75-84% on the adsorption boundary curve, which correspond to the experiments by Wadsö (1994). For each step, equilibrium is ensured before initiation of the next, which also corresponds to the experiment by Ahlgren (1972). This implies that all points in the entire

specimen trace along the same scanning curves, however, not simultaneously.

In Figure 8, the variation of MC caused by the RH sequence is shown together with the measurements by Ahlgren (1972). The model reproduces the measured hysteresis effect successfully.

The fractional weight increase for each of the RH steps in the three sequences is shown in Figures 9a, b, c, respectively. In Figure 9a the measurements by Wadsö (1994) shown in Figure 2 are also displayed.

The simulated fractional weight increases are based on the sorption isotherm measured by Ahlgren (1972) and are shown in Figure 8. As this isotherm deviates from that of the specimen used by Wadsö (1994) the measured fractional weight increases in Figure 9a differ to some extent.

5.2 Variations before equilibrium

This simulation illustrates the effect of a variation of RH at the boundary before equilibrium is obtained at the internal material points.

From equilibrium on the adsorption boundary curve at 30% RH, the RH at the boundary is increased to 95% in two days and subsequently lowered and kept at 30% for three days.

Within the first RH step, all points in the specimen approach, but do not reach equilibrium. For illustrational purposes, the three points in the specimen shown in Figure 7 are observed. In Figures 10 and 11, the variation in the MC as a function of RH and time from this simulation are shown.

With the stepwise increase in RH, adsorption processes along the adsorption boundary curve takes place at all three points. As the boundary condition is changed before equilibrium is obtained, the three points observed have a different state in the hysteresis space. As observed in Figure 10, this results in individual scanning curves in the hysteresis space.

At two of the points, desorption processes initiate almost immediately with the new boundary condition of a 30% RH. However, at the third point the higher MC in the layers between the second and the third point results in continued moisture transport inwards for about half a day more. Subsequent desorption along

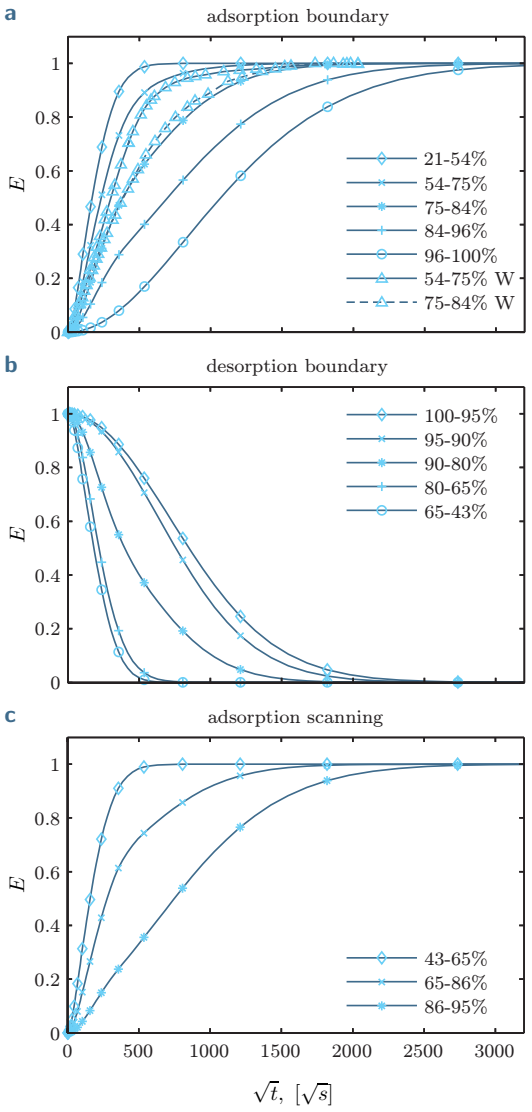

Figure 9 The simulated fractional weight increase with time for relative humidity steps along the (a) adsorption boundary curve, (b) desorption boundary curve and (c) adsorption scanning curve, respectively. The triangles in (a) represents the measurements by Wadsö (1994) (specimen width = 16.2 mm).

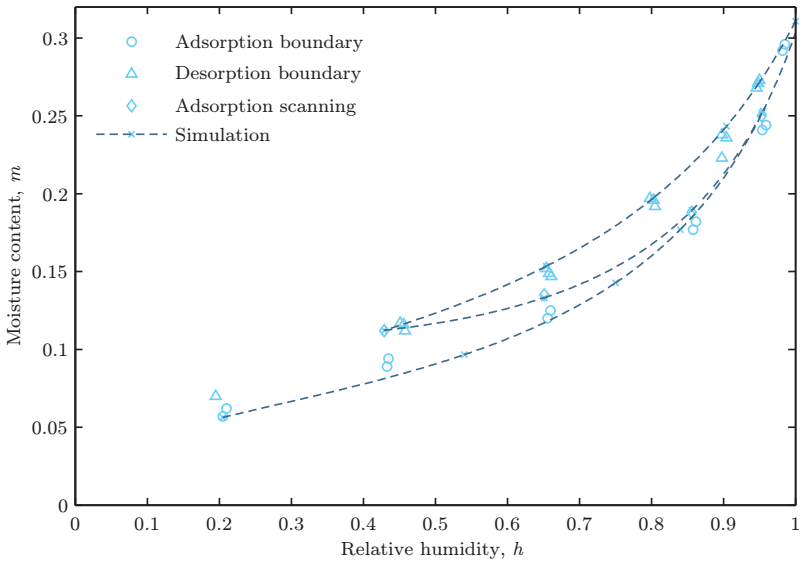

Figure 8 Variation of MC due to the RH sequence in the text compared with the measurements by Ahlgren (1972).

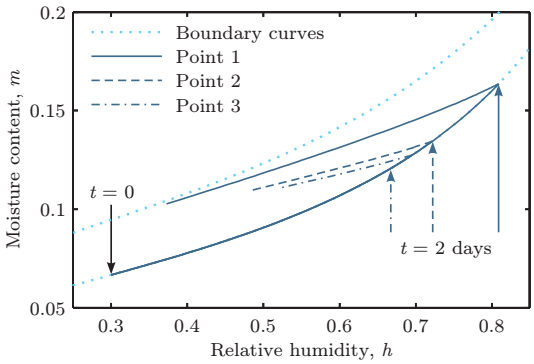

Figure 10 Individual equilibrium paths of the three points due to hysteresis.

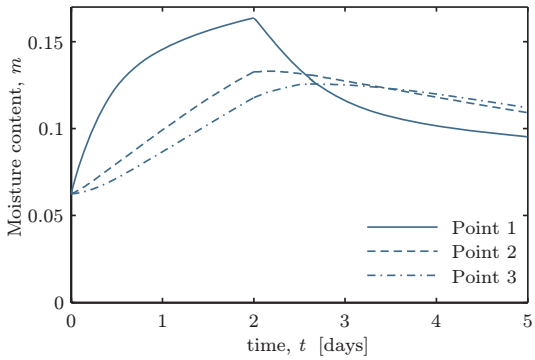

Figure 11 The variation of MC over time.

a scanning curve takes place here as well.

It should be noted that the MC after 3 days of drying does not reach equilibrium at 30% RH. This entrapment of moisture is partly due to the non-linear diffusion coefficient in Eq. (5). The diffusion coefficient decreases with the MC, leaving the outer dryer layers less permeable.

6 Conclusions

Whereas the multi-Fickian model describes the spatial variation, and transportation of bound water and water vapor, sorption hysteresis defines the interaction and equilibrium between the two phases. The present paper explains this interaction and provides a mathematical model to describe the interaction.

An essential part of the model is definition of the moisture condition in wood as a state

in preference to MC alone. This consideration allows a simple accounting for hysteresis effect at the individual points of the material. Furthermore, together with a similar state for the condition of the air in the lumens, it is used to describe sorption rate and hysteresis in terms of independent variables.

The sorption rate can be formulated in terms of vapor pressures or bound-water concentrations. Both approaches allow implementation of sorption hysteresis into a multi-Fickian moisture transport model. The implementation of a hysteresis model for both approaches is presented and tested in a finite element program. To illustrate the combined effect of the sorption hysteresis and multi phase moisture transport, simulations from one of these implementations are presented conclusively.

Acknowledgements

This work has been funded in part by the Danish Forest and Nature Agency and in part by the Danish Research Agency under Project no. 2020-00-0017. The financial support is gratefully acknowledged.

References

Absetz, I. and Koponen, S. (1997). Fundamental diffusion behaviour of wood. In Hoffmeyer, P., editor, *Proceedings of the International Conference on Wood-Water Relations, Copenhagen*, volume E8, pages 89–106.

Ahlgren, L. (1972). *Moisture fixation in porous building materials.* Division Of Building Technology, The Lund Institute Of Technology.

Avramidis, S. (1997). The basics of sorption. In Hoffmeyer, P., editor, *Proceedings Of International Conference On Wood-Water Relations, Copenhagen*, volume E8, pages 1–16.

Bandyopadhyay, A., Radhakrishnan, H., Ramarao, B. V., and Chatterjee, S. G. (2000). Moisture sorption response of paper subjected to ramp humidity changes: Modeling and experiments. *Industrial and Engineering Chemistry Research*, 39(1):219–226.

Christensen, G. N. (1965). The rate of sorption by thin materials. In Wexler, A. and Winn, P. A., editors, *Humidity and Moisture*, volume 4, pages 279–293. Reinhold Publishing Corporation.

Crank, J. (1967). *The mathematics of diffusion.* Oxford Science Publications, London.

Crank, J. and Park, G. S. (1951). Diffusion in high polymers - some anomalies and their significance. *Transactions of the Faraday Society*, 47(10):1072–1084.

Cunningham, M. J. (1994). A model to explain "anomalous" moisture sorption in wood under step function driving forces. *Wood and Fiber Science*, 27(3):265–277.

Everett, D. H. (1954). A general approach to hysteresis. part 3. a formal treatment of the independent domain model of hysteresis. *Trans. Faraday Soc.*, 50:1077–1096.

Everett, D. H. (1955). A general approach to hysteresis. part 4. an alternative formulation of the domain model. *Transactions of the Faraday Society*, 51:1551–1557.

Frandsen, H. L. (2005). Modeling of moisture transport in wood. In *Wood Science and Timber Engineering.* Department of Structural Engineering and Building Technology, Aalborg University, Aalborg.

Frandsen, H. L., Damkilde, L., and Svensson, S. (2007a). A revised multi-fickian moisture transport model to describe non-fickian effects in wood. *Holzforschung*, 61(5):563–572.

Frandsen, H. L., Svensson, S., and Damkilde, L. (2007b). A hysteresis model suitable for numerical simulation of moisture content in wood. *Holzforschung*, 61(2):175–181.

Krabbenhøft, K. and Damkilde, L. (2004). A model for non-fickian moisture transfer in wood. *Materials and Structures*, 37(273):615–622.

Mandelkern, L. and Long, F. A. (1951). Rate of sorption of organic vapors by films of cellulose acetate. *Journal of Polymer Science*, 6(4):457–469.

Massoquete, A., Lavrykov, S., and Ramarao, B. V. (2005). Non-fickian behaviour of moisture diffusion in paper. *Journal of Pulp and Paper Science*, 31(3):121–127.

Nyman, U., Gustafsson, P. J., Johannesson, B., and Hagglund, R. (2006). A numerical method for the evaluation of non-linear transient moisture flow in cellulosic materials. *International journal for numerical methods in engineering*, 66(12):1859–1883.

Pedersen, C. R. (1990). *Combined heat and moisture transfer in build constructions*. PhD thesis, Thermal Insulation Laboratory, Technical University of Denmark, Denmark.

Peralta, P. N. (1995a). Modelling wood moisture sorption hysteresis using the independent-domain theory. *Wood and Fiber Science*, 27(3):250–257.

Peralta, P. N. (1995b). Sorption of moisture by wood within a limited range of relative humidities. *Wood and Fiber Science*, 27(1):13–21.

Peralta, P. N. (1996). Moisture sorption hysteresis and the independent-domain theory: The moisture distribution function. *Wood and Fiber Science*, 28(4):406–410.

Peralta, P. N. and Bangi, A. P. (1998a). Modeling wood moisture sorption hysteresis based on similarity hypothesis. Part 1. direct approach. *Wood and Fiber Science*, 30(1):48–55.

Peralta, P. N. and Bangi, A. P. (1998b). Modeling wood moisture sorption hysteresis based on similarity hypothesis. Part 2. capillary-radii approach. *Wood and Fiber Science*, 30(2):148–154.

Rosen, H. N. (1978). The influence of external resistance on moisture adsorption rates in wood. *Wood and Fiber Science*, 10(3):218–228.

Salin, J.-G. (1996). Mass transfer from wooden surfaces and internal moisture non-equilibrium. *Drying Technology*, 14(10):2213–2224.

Schirmer, R. (1938). Die diffusionszahl von wasserdampf-luftgemischen und die verdampfungsgeschwindigkeit. *VDI Beihaft Verfahrestechnik*, 6:170.

Siau, J. F. (1995). *Wood: Influence of moisture on physical properties*. Department Of Wood Science and Forrest Products, Virginia polytechnic Institute and State University.

Skaar, C. and Siau, J. F. (1981). Thermal diffusion of bound water in wood. *Wood Science and Technology*, 15(2):105–112.

Stamm, A. J. (1959). Bound-water diffusion into wood in the fiber direction. *Forest Product Journal*, 9:27–32.

Wadsö, L. (1994). Unsteady-state water-vapor adsorption in wood: An experimental-study. *Wood and Fiber Science*, 26(1):36–50.

Paper VI

Influence of temperature on hysteretic multi-Fickian moisture transport in wood

A discussion paper

Paper VI

Influence of temperature on hysteretic multi-Fickian moisture transport in wood

- A discussion paper -

Henrik Lund Frandsen
Department of Civil Engineering, Aalborg University, Denmark

Abstract
Moisture transport in structural wood occurs in two phases, i.e., bound-water and water-vapor diffusion. The two phases interact by sorption in the transport process. The sorption between the two phases slows down at higher relative humidities and is hysteretic. Thus, the equilibrium bound-water concentration depends on the previous variations of vapor pressure. These interacting phenomena have been modeled by a coupled multi-Fickian moisture transport model, where the coupling consists of a sorption hysteresis model. This paper discusses the temperature dependency of these phenomena. The multi-Fickian moisture transport model couples to the heat transport by the so-called Soret and Dufour effect. However, in the considered system, the effects are influenced by transport of mass in multiple phases. The temperature dependency of sorption hysteresis model is included by utilizing independent formulation of the scanning curves. Thus, the temperature dependency of the sorption boundary curves is readily included.

Key words: Dufour effect, heat transport, hysteresis, moisture transport, multi-Fickian, Soret effect, sorption, temperature dependency.

1 Introduction

Moisture transport in structural wood can with a good approximation be modeled as coupled bound-water and water-vapor diffusion due to the absence of the convection caused by higher pressures and temperatures. Convection of gases and liquids should on the other hand be taken into consideration in modeling of kiln drying of wood, impregnation of wood with liquid preservatives, or impregnation of wood chips with pulping chemicals (Siau, 1984).

In the combined moisture transport system of bound-water and water-vapor diffusion, the latter is the more significant. At higher relative humidities the contribution from bound-water diffusion becomes more significant, and the rate of sorption between bound water and water vapor decreases significantly and causes the so-called non-Fickian effects (Wadsö, 1994; Frandsen et al., 2007a). However, multi-Fickian effects would be a more appropriate term for this phenomenon observed, since models with multiple Fickian diffusion equations and slow sorption have been shown to model it (Cunningham, 1994; Salin, 1996; Absetz and Koponen, 1997; Krabbenhøft and Damkilde, 2004; Frandsen et al., 2007a).

In these articles the sorption isotherm was

assumed to be either linear or in the best case a one-to-one S-shaped function, which uniquely defines the moisture content in wood by the current relative humidity. However, the sorption phenomenon in wood as well as some other materials (e.g. paper, soil and concrete) is hysteretic. In Frandsen et al. (2007b) sorption hysteresis models applied to wood are reviewed, and a new hysteresis model suitable for implementation into numerical methods is given. The interaction of sorption hysteresis and the multi-Fickian moisture transport is described in (Frandsen and Svensson, 2007) and two different approaches for implementing the hysteresis model into a multi-Fickian model are presented.

In the research mentioned, temperature variations were disregarded, although temperature influences both moisture transport and sorption hysteresis.

The influences of a spatially varying temperature field on moisture transport have been investigated experimentally by Choong (1963); Siau et al. (1986); Avramidis et al. (1987); Avramidis and Siau (1987) among others. The experiments showed the so-called Soret effect, i.e., the moisture diffuses from warmer to colder regions, i.e., along the imposed temperature gradient. Models to describe this phenomenon were proposed by Briggs (1967); Skaar and Siau (1981); Siau (1982); Nelson (1986, 1991), and the various models were reviewed in (Siau and Avramidis, 1993; Siau, 1995). The models are based on either activated bound water or free energy, but without taking account of the vapor diffusion and internal sorption. Numerical considerations for implementation of the model by Skaar and Siau (1981) in FEM are described in (Eriksson et al., 2006), and most recently also by a neural network in (Avramidis and Wu, 2007).

The temperature influences the moisture transport, but conversely the diffusion of molecules with a given enthalpy does also result in transport of energy. The moisture transport will therefore influence the temperature field as well, and a full coupled equation system must be invoked.

Whitaker (1977, 1998) proposed a theory for coupled heat, mass, and momentum transfer in porous media under the assumption of a rigid indeformable matrix. Previously, this formulation has been applied for modeling kiln drying of wood by Perré et al. (1990; 1996; 1999).

In the following, the theory by Whitaker (1977, 1998) is applied to modeling moisture transport in structural wood. Hence, absence of liquid water is assumed and convection is neglected, whereas transport of bound water has been included. Thus, for an isothermal case the model concurs with that derived in (Frandsen et al., 2007a; Frandsen and Svensson, 2007). Furthermore, in the proposed formulation, a hysteretic sorption model is applied. To include temperature variations the model derived in (Frandsen et al., 2007b) is applied.

Temperature dependency of hysteresis has, to the author's knowledge, never been explicitly experimentally investigated. The temperature dependency of the boundary curves has, however, been investigated by a number of authors. The desorption boundary curve of sitka spruce (*Picea sitchensis*) was measured at several temperatures by Hawley (1931), here cited from (Kollmann and Côté, 1968). Babiak (1990) calibrated the Anderson-McCarthy model to data from an unknown species at 21.1°C, 35.0°C, 43.3°C, 51.6°C and 71.1°C from data in the USDA Wood Handbook (1974). Choong (1963) measured both boundary curves of Western fir (*Abies nobilis*) at 25°C, 32.2°C, 40°C and 50°C. In Figure 1 measurements by Kelsey (1956) of klinki pine's (*Araucaria hunsteinii*) adsorption and desorption boundary curves at 10°C, 25°C, 40°C and 55°C are shown.

Now the question regarding the temperature dependency of the scanning curves remains. On this topic very sparse experimental data exist. However, it was observed in (Frandsen et al., 2007b) that the normalized shape of the scanning curves (explained further below) of yellow poplar (*Liriodendron tulipifera* L.) at 30°C and Norway spruce (*Picea abies*) at 20°C was quite

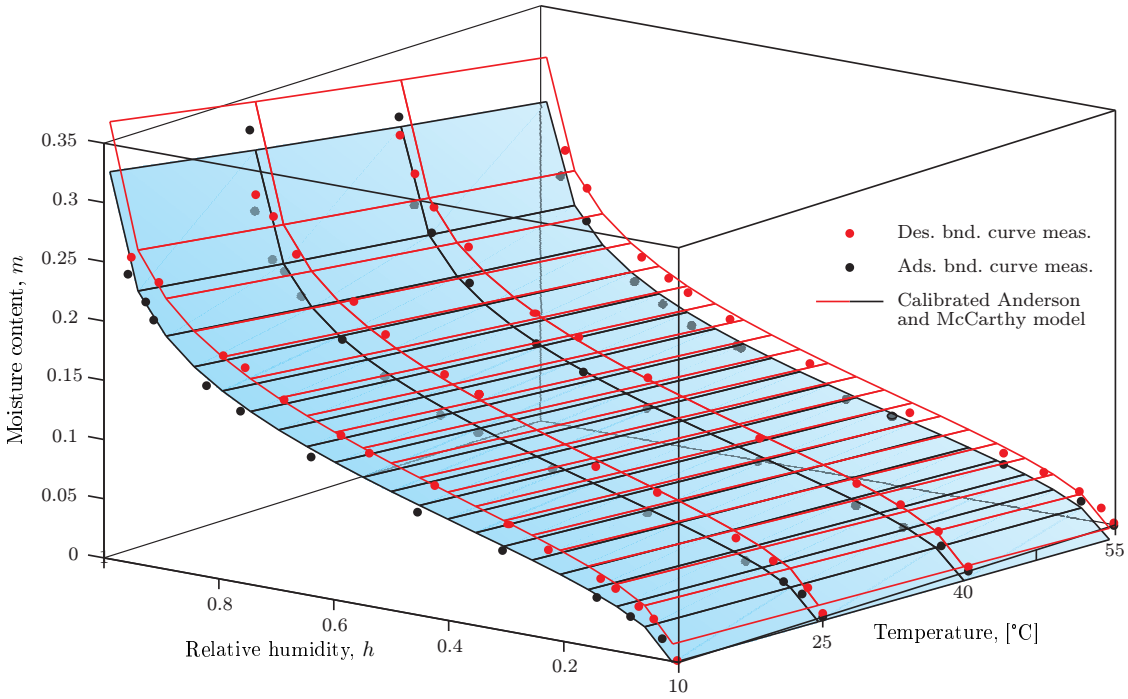

Figure 1 Measurements of the sorption boundary curves at different temperatures by Kelsey (1956) and calibrations of the Anderson-McCarthy model to them.

similar. However, in (Frandsen and Svensson, 2007) the scanning curve for Scots pine at 20°C deviated slightly from the scanning curve of the two other measurements. Since no measurements for the same species at different temperatures are available no conclusions on the temperature dependency of the scanning curves can be made.

In the present paper, a coupled heat and multi-Fickian moisture transport model with hysteresis is derived. The temperature dependency of the coupled heat and multi-Fickian transport model is discussed initially in section 2. Here the heat and mass conservation equations containing coupling sorption terms and constitutive models describing the Soret effect are derived. Next, the temperature dependency of the incorporated hysteresis model is discussed in section 3.

2 Temperature dependency of multi-Fickian moisture transport

In this section the mass and energy conservation equations are initially stated. These are supplemented with material specific constitutive equations for the mass and heat fluxes in wood. The two sets of equations are combined to yield the governing equations for heat and mass transfer containing coupling hysteretic sorption terms.

2.1 Conservation equations

Mass transport is here simplified to include the transport of the bound-water and water-vapor phases. For this system, the following mass bal-

ance equations can be stated:

$$\frac{\partial c_b}{\partial t} + \boldsymbol{\nabla} \cdot \mathbf{J}_b = \dot{c} \tag{1a}$$

$$\frac{\partial c_v}{\partial t} + \boldsymbol{\nabla} \cdot \mathbf{J}_v = -\dot{c} \tag{1b}$$

where c_b and c_v are the concentration of bound water and water vapor (kg/m^3), respectively, $\mathbf{J}_b$ and $\mathbf{J}_v$ are the corresponding fluxes (kg/m^{2}s), and $\dot{c}$ is the sorption rate (kg/m^{3}s). All concentrations are related to the dry volume of wood.

The energy conservation equation are stated as the accumulated energy equalizing the "negative loss" from transport of energy by conduction as well as transport of mass of phase α with a given enthalpy h_α (J/kg):

$$\underbrace{\frac{\partial}{\partial t}\left(h_b c_b + h_v c_v + h_0 \rho_0\right)}_{\text{accumulation}} = - \underbrace{\boldsymbol{\nabla} \cdot \left(h_b \mathbf{J}_b + h_v \mathbf{J}_v\right)}_{\text{diffusion}} - \underbrace{\boldsymbol{\nabla} \cdot \mathbf{J}_H}_{\text{conduction}}, \tag{2}$$

where h_0 and ρ_0 are the enthalpy and density of dry wood (kg/m^3), respectively.

2.2 Constitutive relations

In the following diffusion kinetics are applied to derive a constitutive model, which takes the temperature dependency of bound-water diffusion into consideration. Furthermore, a constitutive model for the temperature dependency of water vapor is proposed.

Bound-water diffusion

The cause for fixation, i.e., bonding of a water molecule to a sorption site is that the molecule experiences a minimum of potential energy, i.e., a stable state. The molecule oscillates about the sorption site with a mean energy of $3k_B T$, where k_B is Boltzmann's constant (1.38×10^{-23} J/atom K). By continually occurring collisions kinetic energy is transferred between the water molecules. If a molecule gains sufficient kinetic energy to exceed the potential energy of the bond, the molecule will diffuse from the site and is said to be activated. Thus, the kinetic energy required to exceed this potential barrier is called the activation energy e_b (J/atom) (Figure 2).

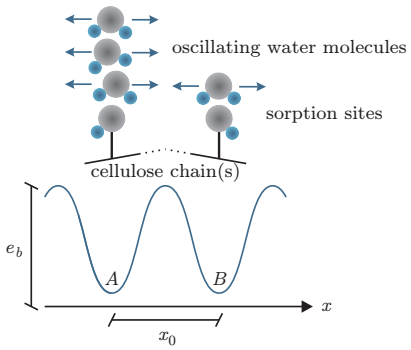

Figure 2 Oscillating water molecules bound at sorption sites A and B.

The probability for this occurrence is determined from Boltzmann's distribution as:

$$P = \exp\left(-\frac{e_b}{k_B T}\right), \tag{3}$$

where T is the temperature (K). The number of average number of bound-water molecules leaving the site A, the so-called activated molecules $\tilde{n}_b^A$, can now be determined from this probability and the total number of water molecules as:

$$\tilde{n}_b^A = n_b^A P, \tag{4}$$

and the number of molecules leaving the site per second is:

$$j_b^A = \tilde{n}_b^A f. \tag{5}$$

where f is frequency of the oscillation. At an adjacent site B, j_b^B water molecules leave per second and the net exchange of molecules between site A and B becomes:

$$j_b^{A \to B} = -(\tilde{n}_b^B - \tilde{n}_b^A) f P_d, \tag{6}$$

where P_d is the probability for the molecule to move in the specified direction. $P_d = 1/6$ for sites organized in a grid in an isotropic material, since the molecules can diffuse in 6 different directions in three dimensions (Ashby and

Jones, 2005). For an orthotropic material, P_d varies with the material direction. However, for simplicity the following derivation is kept one-dimensional.

Before abstracting this to a continuum averaged description, note that the probability for a water molecule to leave a site increases with the temperature. So even if an equal amount of molecules occurs at two adjacent sites, there is a higher probability for water molecules to leave the warmer. Thus, molecules must be expected to shift from warmer to colder sites.

Now, consider a small volume $x_0 A_0$ with an amount of sorption sites with an average number of bound-water molecules bounded at each site n_b (Figure 3). In this volume the concentration of bound-water molecules is:

$$c_b = \frac{n_b N_A M_{\mathrm{H_2O}}}{x_0 A_0}, \tag{7}$$

where N_A is Avogadro's number ($6.0221 \times 10^{23}\,\mathrm{atoms/mol}$) and $M_{\mathrm{H_2O}}$ is the molar mass of water ($18.02 \times 10^{-3}\,\mathrm{kg/mol}$).

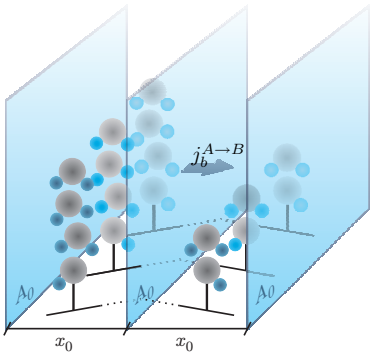

Figure 3 Flux between two small volumes confining an amount of sorption sites.

Likewise, the possibility for exceeding the activation energy is expressed in measurable quantities by:

$$P = \exp\left(-\frac{N_A e_b}{N_A k_B T}\right) = \exp\left(-\frac{E_b}{RT}\right), \tag{8}$$

where $E_b = N_A e_b$ (J/mol) and R is the universal gas constant (8.314 J/mol K).

The concentration of activated bound-water molecules can then be determined by isolating n_b in Eq. (7) and inserting into Eq. (4):

$$\tilde{c}_b = c_b \exp\left(-\frac{E_b}{RT}\right). \tag{9}$$

The mass flux to an adjacent volume J_b through the surface A_0 is $A_0 N_A M_{\mathrm{H_2O}}\, j_b^{A\to B}$. By letting the thickness of the volume in the direction of the flux x_0 converge to zero and by using Eqs. (6) and (7) one gets:

$$\begin{aligned} J_b &= N_A M_{\mathrm{H_2O}} x_0 \lim_{x_0 \to 0^+} \left(\frac{j_b^{A\to B}}{x_0}\right) \\ &= -f\, x_0^2 P_d \frac{d\tilde{c}_b}{dx}. \end{aligned} \tag{10}$$

The term $f\, x_0^2 P_d$ is signified D_b^0 and varies for different material directions in wood ($D_b^0(T)$: $D_b^0(L) \simeq 1 : 2.5$ (Siau, 1995)).

For the non-isothermal case $d\tilde{c}_b/dx$ can be expanded to:

$$\frac{d\tilde{c}_b}{dx} = \frac{\partial \tilde{c}_b}{\partial c_b}\frac{\partial c_b}{\partial x} + \frac{\partial \tilde{c}_b}{\partial T}\frac{\partial T}{\partial x}, \tag{11}$$

where Eq. (9) provides:

$$\frac{\partial \tilde{c}_b}{\partial c_b} = \exp\left(-\frac{E_b}{RT}\right) \tag{12a}$$

$$\frac{\partial \tilde{c}_b}{\partial T} = \frac{c_b E_b}{RT^2} \exp\left(-\frac{E_b}{RT}\right). \tag{12b}$$

Thus, for a one-dimensional case the constitutive equation for bound-water diffusion Eq. (10)-Eq. (12) can be rewritten as:

$$J_b = -D_b \frac{\partial c_b}{\partial x} - D_{bT}\frac{\partial T}{\partial x}, \tag{13}$$

where

$$D_b = D_b^0 \exp\left(-\frac{E_b}{RT}\right) \tag{14a}$$

$$D_{bT} = D_b^0 \frac{c_b E_b}{RT^2} \exp\left(-\frac{E_b}{RT}\right). \tag{14b}$$

where D_{bT} will be referred to as the thermal coupling bound-water diffusion coefficient in the following.

The second term on the right hand side of equation Eq. (13) is the background for the so-called Soret effect, which is the thermal coupling to bound-water diffusion observed by Choong (1963); Siau et al. (1986); Avramidis et al. (1987); Avramidis and Siau (1987) among others.

Note that for the isothermal case ($\partial T/\partial x = 0$) Eqs. (13) and (14) yield Arrhenius' law, with the diffusion coefficient being exponentially dependent on temperature.

Water-vapor diffusion

The temperature dependency in the empirical expression for diffusion of water vapor in bulk air by Schirmer (1938) in Eq. (15) indicates that the kinetic principles for bound-water diffusion might apply for diffusion of water vapor as well .

$$D_{va} = 2.31 \times 10^{-5} \frac{\mathrm{m}^2}{\mathrm{s}} \frac{p_{\mathrm{atm}}}{p_{\mathrm{atm}} + p_v} \left(\frac{T}{273\mathrm{K}} \right)^{1.81}, \tag{15}$$

where p_{atm} is the atmospheric pressure and p_v the partial vapor pressure.

For the isothermal case a modification of this diffusion coefficient to take the resistance from the cellular structure of wood into consideration has provided good results (Frandsen et al., 2007a):

$$D_v = \xi D_{va}, \tag{16}$$

where ξ is the estimated reduction factor due to hindrance of the diffusion in the cellular structure. ξ is different for the different material directions. This is generalized below, but for simplicity in the following derivation, this is maintained as a one-dimensional quantity.

Since the diffusion coefficient is temperature dependent, the following hypothesis for estimating the temperature dependent water-vapor diffusion coefficient is stated. The temperature dependency of water-vapor diffusion in wood could be obtained by assuming an activated vapor pressure:

$$\tilde{p}_v = p_v \left(\frac{T}{273K} \right)^{1.81}. \tag{17}$$

By the approach of expanding $\partial \tilde{p}_v/\partial x$ (see above), this assumption leads to the one-dimensional constitutive relation:

$$J_v = -D_v \frac{\partial p_v}{\partial x} - D_{vT} \frac{\partial T}{\partial x}, \tag{18}$$

where

$$D_v = D_v^0 \left(\frac{T}{273K} \right)^{1.81} \tag{19a}$$

$$D_{vT} = D_v^0 \frac{1.81\, p_v}{T} \left(\frac{T}{273K} \right)^{1.81} \tag{19b}$$

$$D_v^0 = \xi\, 2.31 \times 10^{-5} \frac{m^2}{s} \frac{p_{\mathrm{atm}}}{p_{\mathrm{atm}} + p_v}. \tag{19c}$$

where D_{vT} will be referred to as the thermal coupling water-vapor diffusion coefficient in the following.

It must be stressed that this is a hypothesis that has not been confirmed by measurements, why it should be used with caution. This model is based on the assumption that a higher temperature would increase the mobility of water molecules, and thus the probability of an atom to diffuse from a warmer location is higher than from a colder location.

Diffusion in an orthotropic material

By generalizing Eq. (13) and Eq. (18) the following constitutive equations can be stated for three dimensional orthotropic model:

$$\mathbf{J}_b = -\mathbf{D}_b \boldsymbol{\nabla} c_b - \mathbf{D}_{bT} \boldsymbol{\nabla} T \tag{20a}$$

$$\mathbf{J}_v = -\mathbf{D}_v \boldsymbol{\nabla} c_v - \mathbf{D}_{vT} \boldsymbol{\nabla} T, \tag{20b}$$

where the matrices $\mathbf{D}_\alpha$ and $\mathbf{D}_{\alpha T}$ contain the diffusion coefficient and thermal coupling diffusion coefficients (see Eq. (14) and Eq. (19)) of the various material directions in the diagonal.

For the heat transport equation, Fourier's law is applied:

$$\mathbf{J}_H = -\mathbf{k}_{\mathrm{mix}} \boldsymbol{\nabla} T \tag{21}$$

where the matrix $\mathbf{k}_{\text{mix}}$ contains the thermal conductivities of the various material directions in the diagonal. These can be estimated by considering various components of a cell as parallel and serial connected resistances, see e.g. (Siau, 1995). This will not be discussed further here.

Furthermore, Whitaker (1977) assumed a linear relationship between enthalpy and temperature, which is reasonable for wood (Skaar, 1972), and for vapor the specific heat capacity changes less than one per cent within the range considered. Thus, the enthalpy can be written as:

$$h_\alpha = h_\alpha^0 + C_\alpha (T_\alpha - T_{\text{ref}}) \tag{22}$$

where C_α is the specific heat capacity of the α-component of the mixture.

2.3 Governing equations

Inserting the fluxes in Eq. (20) into the mass conservation Eq. (1) provides:

$$\frac{\partial c_b}{\partial t} = \boldsymbol{\nabla} \cdot (\mathbf{D}_b \boldsymbol{\nabla} c_b + \mathbf{D}_{bT} \boldsymbol{\nabla} T) + \dot{c} \tag{23a}$$

$$\frac{\partial c_v}{\partial t} = \boldsymbol{\nabla} \cdot (\mathbf{D}_v \boldsymbol{\nabla} c_v + \mathbf{D}_{vT} \boldsymbol{\nabla} T) - \dot{c} \tag{23b}$$

It is sometimes more convenient to formulate the mass transport equations of vapor in terms of a partial vapor pressure in preference to concentration by applying the ideal gas law. The principle is illustrated in (Frandsen et al., 2007a):

$$\frac{\partial}{\partial t}\left(p_v \frac{\varphi M_{\text{H}_2\text{O}}}{RT}\right) = \boldsymbol{\nabla} \cdot \left(\mathbf{D}_v \boldsymbol{\nabla}\left(p_v \frac{\varphi M_{\text{H}_2\text{O}}}{RT}\right) + \mathbf{D}_{vT} \boldsymbol{\nabla} T\right) - \dot{c}. \tag{24}$$

Expanding the differentiation of the accumulative and diffusive terms in the energy balance equation (2) leads to:

$$\frac{\partial h_b}{\partial t} c_b + \frac{\partial h_v}{\partial t} c_v + \frac{\partial h_0}{\partial t} \rho_0 + h_b \frac{\partial c_b}{\partial t} + h_v \frac{\partial c_v}{\partial t} + h_b \boldsymbol{\nabla} \cdot \mathbf{J}_b + h_v \boldsymbol{\nabla} \cdot \mathbf{J}_v + \mathbf{J}_b \cdot \boldsymbol{\nabla} h_b + \mathbf{J}_v \cdot \boldsymbol{\nabla} h_v = \boldsymbol{\nabla} \cdot (\mathbf{k}_{\text{mix}} \boldsymbol{\nabla} T), \tag{25}$$

which can be simplified by insertion of the mass conservation equations (1) and (22), and assuming immediate thermal equilibrium between the different components, i.e., $T_\alpha = T$ for $\alpha \in \{b, v, 0\}$:

$$\underbrace{(c_b C_b + c_v C_v + \rho_0 C_0)\frac{\partial T}{\partial t}}_{\text{accumulation}} + \underbrace{(h_b - h_v)\dot{c}}_{\text{sorption}} + \underbrace{(C_b \mathbf{J}_b + C_v \mathbf{J}_v) \cdot \boldsymbol{\nabla} T}_{\text{diffusion}} = \underbrace{\boldsymbol{\nabla} \cdot (\mathbf{k}_{\text{mix}} \boldsymbol{\nabla} T)}_{\text{conduction}}. \tag{26}$$

The third term on the left hand side is the background for the so-called Dufour effect, i.e., transport of heat by mass transport of molecules with a given enthalpy.

In Eq. (26) the accounting of energy content is hereby stated in terms of concentration of the individual component, its specific heat capacity and the common temperature of the components (Figure 4). Furthermore, the energy gained by the phase change from water vapor to bound water is included in the balance.

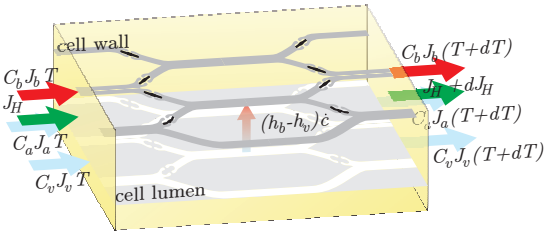

Figure 4 Various paths for transport of heat in the cellular structure of wood.

3 Temperature dependency of sorption

Adsorption is a time-dependent exothermal reaction, i.e., heat is produced during the reaction. Hence, according to Le Chatelier's principle the reaction is promoted by lowering the temperature, i.e., more water can be bound in the cell wall. This is also seen in Figure 1 as a negative slope of the sorption boundary "surfaces" with temperature.

However, according to Arrhenius' rate law the reaction rate will increase with temperature. As seen in (Christensen, 1965; Frandsen et al., 2007a) the reaction rate $\dot{c}$ decreases significantly as equilibrium is approached at higher relative humidities h $(= p_v/p_s)$:

$$\dot{c} = H(c_{bl}, c_b, h, T)\,(c_{bl} - c_b), \qquad (27)$$

where c_b is the bound-water concentration in the cell wall, c_{bl} is a bound-water concentration in equilibrium with the vapor pressure p_v in the lumens, and h is the relative humidity of the vapor in the lumens. As the bound-water concentration approaches the equilibrium concentration c_{bl}, the sorption ceases. The equilibrium bound-water concentration changes hysteretically with the water-vapor pressure p_v.

Alternatively, the sorption rate could be formulated in terms of pressures (Frandsen et al., 2007a), but this will not be further discussed here.

3.1 Temperature dependency of hysteresis

The bound-water concentration in equilibrium with the vapor pressure in the lumens c_{bl} can be determined by:

$$\frac{c_{bl}}{\rho_0} = m = m_a + s(m_d - m_a), \qquad (28)$$

where m_a and m_d are the temperature and relative humidity dependent adsorption and desorption boundary curves (Figure 5) (Frandsen et al., 2007b; Frandsen and Svensson, 2007). s is the fraction of exploited sorption sites ($0 \leq s \leq 1$), which depends on temperature and the preceding relative humidity variations.

By rearranging Eq. (28), s can be expressed as the fraction:

$$s = \frac{m - m_a}{m_d - m_a}, \qquad (29)$$

which is the expression for the normalized scanning curves. Formulating the scanning curves in terms of s, these become independent of the boundary curves, and the temperature dependency of the scanning curves and the boundary curves can be treated separately.

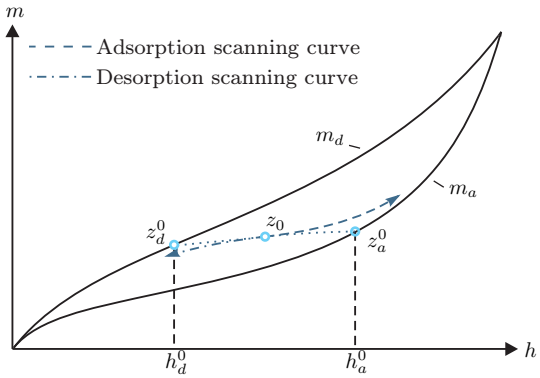

Figure 5 Prediction of the scanning curves from the current state z_0 and the origins of the scanning curves z_a^0 and z_d^0.

As mentioned in the introduction, the temperature dependency of the boundary curves has been experimentally investigated by several researchers. Different more or less empirical expressions to fit these measured curves have been proposed; for a review of the most common models see (Babiak, 1990; Siau, 1995). Here the Anderson-McCarthy model is chosen due to the continuous variation of the shape parameters with temperature (Figure 6). The model has been calibrated to the measurements by Hawley (1931) here cited from (Kollmann and Côté, 1968) and the measurements by Kelsey (1956):

$$m_\alpha = -\frac{\ln(\ln(1/h)/f_1^\alpha)}{f_2^\alpha} \quad , \quad \alpha \in \{a, d\}, \qquad (30)$$

where h is the relative humidity. The continuous variations of the shape parameters f_i^α with temperature have been approximated with the polynomial (Figure 6):

$$f_i^\alpha = \sum_{j=0}^{n} b_{ij}^\alpha T^j \quad , \quad i \in \{1, 2\}, \qquad (31)$$

where b_{ij}^α is given in Table 1, and a and d denotes adsorption and desorption, respectively.

	Species	α	n	b^{α}_{12} [K^{-2}]	b^{α}_{11} [K^{-1}]	b^{α}_{10}	b^{α}_{22} [K^{-2}]	b^{α}_{21} [K^{-1}]	b^{α}_{20}
Babiak	?	?	1	0	−0.0143	7.73	0	0.0567	0.875
Hawley	sitka spruce	d	2	-4.228×10^{-5}	0.0196	1.47	9.53×10^{-4}	−0.518	87.6
Kelsey	klinki pine	a	1	0	−0.0234	11.1	0	0.0657	0.0865
Kelsey	klinki pine	d	1	0	−0.0367	16.3	0	0.0535	2.13

Table 1 The b^{α}_{ij} parameters of Eq. (31). The parameters fitted by Babiak (1990), fit of desorption isotherms measured by Hawley (1931), and fit to adsorption and desorption isotherms measured by Kelsey (1956).

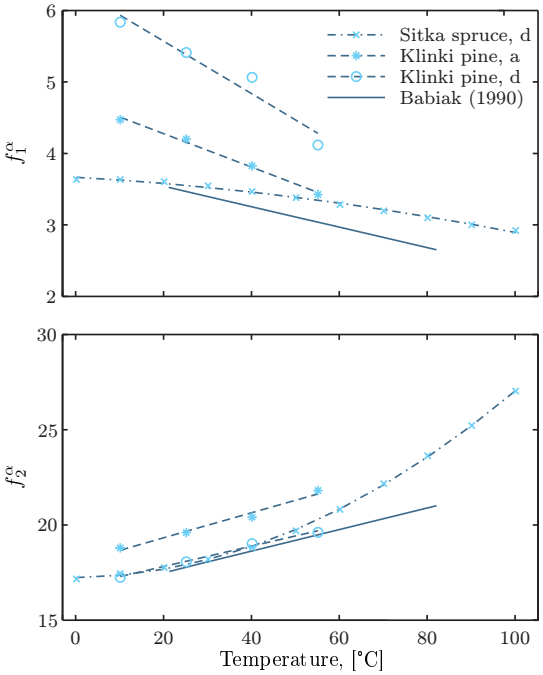

Figure 6 The variation with temperature of the shape parameters in the Anderson-McCarthy sorption model.

Whether the shape of the normalized scanning curves is temperature dependent cannot be concluded on the current experimental work. The scanning curves are here assumed to be independent of the temperature ($s(h) = s(h,T)$).

The hysteresis model applied is developed in (Frandsen et al., 2007b). Here it was argued that the scanning curves are uniquely defined by their origin on one of the boundary curves. Thus, the scanning curves can be explicitly formulated in terms of their origin on the boundary curves h^0_a and h^0_d (Figure 5):

$$s = -1 + 2^{\left(\frac{1-h}{1-h^0_d}\right)^{\left(\frac{d_1}{\ln(d_2(1-h^0_d))}\right)}}, \quad \dot{h} > 0 \wedge s_0 > 0 \tag{32a}$$

$$s = 2 - 2^{\left(\frac{h}{h^0_a}\right)^{\left(\frac{d_1}{\ln(d_2\, h^0_a)}\right)}}, \quad \dot{h} < 0 \wedge s_0 < 1 \tag{32b}$$

$$s = 0, \quad \dot{h} > 0 \wedge s_0 = 0 \tag{32c}$$

$$s = 1, \quad \dot{h} < 0 \wedge s_0 = 1, \tag{32d}$$

where d_1 and d_2 are shape parameters. Eq. (32a) and Eq. (32b) model the scanning curves during adsorption ($\dot{h} > 0$) and during desorption ($\dot{h} < 0$), respectively. (32c) simply expresses that a state with origin on the adsorption boundary curve ($s_0 = 0$) will follow the adsorption boundary curve if adsorption is taking place ($\dot{h} > 0$) and similarly for desorption in Eq. (32d).

Since the scanning curves are known to trail through the current state $z_0 = \{h_0, m_0\}$, expressions for h^0_a and h^0_d can be obtained by solving Eq. (32a) and (32b) for h^0_a and h^0_d, respectively, where $h = h_0$ and $s = s_0$:

$$h^0_a = h_0(d_2 h_0)^{q_1} \tag{33}$$

$$h^0_d = 1 - (1 - h_0)(d_2(1 - h_0))^{q_2}, \tag{34}$$

where

$$q_1 = -\frac{\ln(\ln(2)) - \ln(\ln(2 - s_0))}{\ln(\ln(2)) - \ln(\ln(2 - s_0)) - d_1} \tag{35}$$

$$q_2 = -\frac{\ln(\ln(2)) - \ln(\ln(1+s_0))}{\ln(\ln(2)) - \ln(\ln(1+s_0)) - d_1}. \quad (36)$$

Example

To illustrate the temperature dependency of this hysteresis model, scanning curves of klinki pine at constant and at varying temperatures have been calculated. For the calculation the data for the boundary curves of klinki pine in Table 1 and the shape parameters of the scanning curves in Table 2 have been applied.

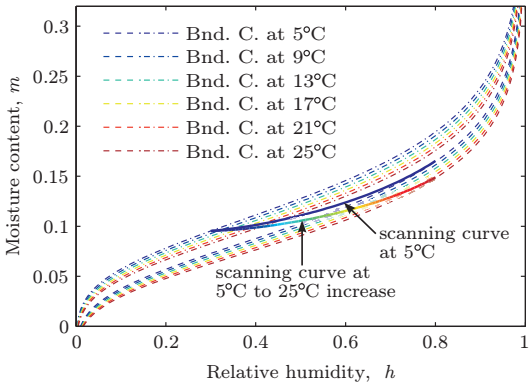

Figure 7 Scanning curves with and without the influence of varying temperature.

d_1	d_2
−1.3	0.88

Table 2 The shape parameters of the scanning curves (Frandsen et al., 2007b).

The relative humidity is increased from 30% to 80% for both scanning curves, i.e., at constant temperature and at increasing temperature. Both curves initiate on the desorption boundary curve ($s = 1$). The temperature for the first curve is kept constant at 5°C and for the second the temperature increase is linear proportional to the relative humidity from 5°C to 25°C. The result is shown in Figure 7.

4 Conclusions

This paper proposes the initial mathematical framework for temperature dependent multi-Fickian moisture transport model with hysteresis. Doing so the following issues were addressed:

- Moisture transport depends on temperature gradients, and conversely, mass transport involves transport of heat as well, i.e., the so-called Soret and Dufour effect, respectively. Therefore, a fully coupled heat and mass transport model is formulated. The model takes the phase changes between water vapor and bound water into consideration in the mass transportation as well as heat transportation.
- A constitutive model for temperature dependent bound-water diffusion based on diffusion kinetics is derived.
- A constitutive model for temperature dependent diffusion of water vapor has been proposed based on the empirical model by Schirmer (1938). This model is based on the assumption that a higher temperature would increase the mobility of water molecules. The model has not been verified and should be used with caution.
- Temperature dependence of the boundary curves has been taken into account in the formulation of the temperature-dependent sorption hysteresis model. This was possible because of the decoupling of scanning curves from the boundary curves in the applied hysteresis model. The temperature dependency of the boundary curves was described by the Anderson and McCarthy model.
- The shape of the normalized scanning curves was here assumed to be independent of temperature, since in the few available measurements the shape does not vary significantly. A designated experimental investigation of the temperature dependency of the normalized scanning curves remains.

References

Absetz, I. and Koponen, S. (1997). Fundamental diffusion behaviour of wood. In Hoffmeyer, P., editor, *Proceedings of the International Conference on Wood-Water Relations, Copenhagen*, volume E8, pages 89–106.

Ashby, M. F. and Jones, D. R. H. (2005). *Engineering Materials 1: An Introduction to Microstructures, Processing and Design*. Butterworth-Heinemann.

Avramidis, S., Kuroda, N., and Siau, J. F. (1987). Experiments in nonisothermal diffusion of moisture in wood, part 2. *Wood and Fiber Science*, 19(4):407–413.

Avramidis, S. and Siau, J. F. (1987). Experiments in nonisothermal diffusion of moisture in wood, part 3. *Wood Science and Technology*, 21(4):329–334.

Avramidis, S. and Wu, H. (2007). Artificial neural network and mathematical modeling comparative analysis of nonisothermal diffusion of moisture in wood. *Holz als Roh- und Werkstoff*, 65(2).

Babiak, M. (1990). Wood-water system. *Vedecké Pedagickeé Aktuality. Technical University In Zvolen*.

Briggs, G. E. (1967). Movement of water in plants. *Botanical Monographs, Davis, Philadelphia*, 7.

Choong, E. T. (1963). Movement of moisture through a softwood in the hygroscopic range. *Forest products journal*, 13(11):489–498.

Christensen, G. N. (1965). The rate of sorption by thin materials. In Wexler, A. and Winn, P. A., editors, *Humidity and Moisture*, volume 4, pages 279–293. Reinhold Publishing Corporation.

Cunningham, M. J. (1994). A model to explain "anomalous" moisture sorption in wood under step function driving forces. *Wood and Fiber Science*, 27(3):265–277.

Eriksson, J., Ormarsson, S., and Petersson, H. (2006). Finite-element analysis of coupled nonlinear heat and moisture transfer in wood. *Numerical Heat Transfer*, 50(9):851–864.

Frandsen, H. L., Damkilde, L., and Svensson, S. (2007a). A revised multi-fickian moisture transport model to describe non-fickian effects in wood. *Holzforschung*, 61(5):563–572.

Frandsen, H. L. and Svensson, S. (2007). Implementation of sorption hysteresis in multi-fickian moisture transport. *Holzforschung*, 61(6):693–701.

Frandsen, H. L., Svensson, S., and Damkilde, L. (2007b). A hysteresis model suitable for numerical simulation of moisture content in wood. *Holzforschung*, 61(2):175–181.

Kelsey, K. E. (1956). The sorption of water vapor by wood. *Australian Journal Of Applied Science*, 8(1):42–54.

Kollmann, F. F. P. and Côté, W. A. (1968). *Principles of wood science and technology*. Springer Verlag.

Krabbenhøft, K. and Damkilde, L. (2004). A model for non-fickian moisture transfer in wood. *Materials and Structures*, 37(273):615–622.

Nelson, R. M. (1986). Diffusion of bound water in wood. *Wood Science and Technology*, 20(4):309–328.

Nelson, R. M. (1991). Heats of transfer and activation energy for bound-water diffusion in wood. *Wood Science and Technology*, 25:193–202.

Perré, P. and Degiovanni, A. (1990). Control-volume formulation of simultaneous transfers in anisotropic porous media: Simulations of softwood drying at low and high temperature. *International Journal of Heat and Mass Transfer*, 33(11):2463–2478.

Perré, P. and Turner, I. W. (1996). *Mathematical Modeling and Numerical Techniques in Drying Technology*, chapter The use of macroscopic equations to simulate heat and mass transfer in porous media. Marcel Dekker, New York,.

Perré, P. and Turner, I. W. (1999). A 3-d version of transpore: a comprehensive heat and mass transfer computational model for simulating the drying of porous media. *International Journal of Heat and Mass Transfer*, 42(24):4501–4521.

Salin, J.-G. (1996). Mass transfer from wooden surfaces and internal moisture non-equilibrium. *Drying Technology*, 14(10):2213–2224.

Schirmer, R. (1938). Die diffusionszahl von wasserdampf-luftgemischen und die verdampfungsgeschwindigkeit. *VDI Beihaft Verfahrestechnik*, 6:170.

Siau, J. F. (1982). Chemical potential as a driving force for nonisothermal moisture movement in wood. *Wood Science and Technology*, 17(2):101–105.

Siau, J. F. (1984). *Transport Processes in Wood*. Springer-Verlag, Heidelberg.

Siau, J. F. (1995). *Wood: Influence of moisture on physical properties*. Department Of Wood Science and Forrest Products, Virginia polytechnic Institute and State University.

Siau, J. F. and Avramidis, S. (1993). Application of a thermodynamic model to nonisothermal diffusion of moisture in wood. *Wood Science and Technology*, 27(2):95–114.

Siau, J. F., Bao, F., and Avramidis, S. (1986). Experiments in nonisothermal diffusion of moisture in wood. *Wood and Fiber Science*, 18(1):84–89.

Skaar, C. (1972). *Water in Wood*. Syracause University.

Skaar, C. and Siau, J. F. (1981). Thermal diffusion of bound water in wood. *Wood Science and Technology*, 15(2):105–112.

Wadsö, L. (1994). Unsteady-state water-vapor adsorption in wood: An experimental-study. *Wood and Fiber Science*, 26(1):36–50.

Whitaker, S. (1977). *Advances in heat transfer*, volume 13, chapter Simultaneous heat, mass, and momentum transfer in porous media: A theory of drying, pages 119–203. Academic Press, New York.

Whitaker, S. (1998). *Advances in heat transfer*, volume 31, chapter Coupled transport in multiphase systems: A theory of drying, pages 1–104. Academic Press, New York.

Paper VII

Couplings in orthotropic creep of wood

A discussion paper

Paper VII

Transverse couplings in orthotropic creep of wood

- A discussion paper -

Henrik Lund Frandsen[1], Lech Muszynski[2] and Staffan Svensson[3]
[1]*Department of Civil Engineering, Aalborg University, Denmark*
[2]*Department of Wood Science and Engineering, Oregon State University, USA*
[3]*Department of Civil Engineering, Technical University of Denmark, Denmark*

Abstract
The Poisson's ratios of the time-dependent mechanical response of wood under sustained load have been observed to vary with time. This is a consequence of directionally distinct response rates of the cellular orthotropic material. The present paper concerns various aspects of this phenomenon of directionally distinct creep response rates. Together with recent theoretical considerations on the topic the experimental observations of time-dependent Poisson ratios provide a new perspective to consider the modeling of orthotropic creep of wood. Different widely applied approaches for modeling orthotropic creep of wood are addressed. It is explained why the plausible approach for modeling the phenomenon by a applying the time-dependent Poisson ratios as material parameters is inapplicable. The requirements for a constitutive model to yield directionally independent creep rates, i.e., time-dependent Poisson ratios, are treated. Based on this, a constitutive model for orthotropic creep, which provides this independency and gives resemblance to distribution of stresses in the cellular structure of wood, is proposed. The object is to establish a correspondence between the material parameters and the structure of wood and thus to contribute with general considerations on the mechanical couplings. Two approaches for implementing the proposed constitutive model into a finite element model are shown. The theoretical considerations will be complemented by ongoing experimental work. In this paper the experimental procedure is presented.

Key words: creep, constitutive modeling, coupling terms, orthotropic, incremental, Poisson's ratio

1 Introduction

Creep is the time-dependent deformation response to sustained load. It has received a considerable amount of attention in order to model strains in drying processes and long-term behavior of structural wood.

The cellular structure, layered composition of the cell wall, and hygroscopy due to various chemical bonds resolves in a number of moisture, time, stress-level and temperature dependent deformations in wood.

When wood is subjected to loads the

stresses distributes in the cellular structure. On the ultrastructure level the cell walls can be regarded as a composite material, see e.g. (Barber, 1968; Yamamoto and Kojima, 2002; Pang, 2002). The microfibrils in the cell wall layers function as reinforcing fibers, and lignin and the hemicelluloses constitute the matrix material. The microfibrils are deformed axially as matrix material adhering the fibrils is molded. The molding of the adhesive matrix material involves breakage and reestablishment of hydrogen bonds. This process commences gradually with time, and the deformation becomes a time-dependent process.

For different directions of load different distribution paths of the stresses in the composite structure occur. For instance, if the cell is tensed in the longitudinal direction, the cell is stretched and due to Poisson's effect in the cell wall, the cell radius will diminish. In the different directions of deformation, the compositions of matrix material and the reinforcing microfibril fibers are different. Thus, the rate of deformation in the different directions will be correspondingly distinct.

The creep response in the direction of load for different directions has been well studied. Creep is classically assumed to be composed of two independent types of creep, i.e., time-dependent creep and mechano-sorptive creep. The time-dependent creep rate is increased at higher temperatures and moisture contents see e.g. (Hanhijärvi, 1995; Wu and Milota, 1995; Svensson, 1996; Mårtensson and Svensson, 1997; Hanhijärvi, 1999; Passard and Perré, 2005a,b).

When exposed to moisture changes, the mechano-sorptive creep of wood is activated and relatively large strains compared to the pure time-dependent creep are formed, see e.g. (Toratti and Svensson, 2000). The constitutive models applied are similar to those describing the time-dependent creep with the difference that, roughly speaking, changes over time are replaced by changes of moisture content (Takemura, 1967; Ranta-Maunus, 1975; Salin, 1992).

Some experiments question the assumption of the independency of the two types of creep (Hanhijärvi and Hunt, 1998; Hunt, 1999), and much interesting research on the connection between the two types of creep remains.

In this paper, however, focus will be on the transverse deformation and multidimensional modeling of creep; and creep will here be considered as one phenomenon. Hereby the complexity of the couplings to temperature and moisture and the even more sophisticated couplings to changes of the latter is temporarily disregarded. The considerations in the following will, however, be general, and the above-mentioned complexities can be accounted for within this framework.

First, the attention is directed towards some interesting experimental observations on the transverse deformations in creep experiments. Together with recent theoretical considerations on the time-dependency of Poisson's ratios, these provide a new perspective to consider different widely applied orthotropic constitutive models.

The time-dependent behavior of Poisson's ratios provides useful information about the transverse deformations. However, as shown in the following the measured time-dependent Poisson ratios cannot be applied as a material parameter in an orthotropic constitutive model itself.

Next, a constitutive model for orthotropic creep, which avoids the concept of time-dependent Poisson ratios, is derived. The model provides independent responses for different orthotropic material directions as expected by the distribution of stresses in the cellular structure of wood.

The objective of this research is to establish a correspondence between the material parameters and the structure of wood and contribute with general considerations on the mechanical couplings. To draw such conclusions, the correspondence between the assumed couplings between the rheological systems of the constitutive model presented, a supplement of an ex-

perimental study of the phenomenon is greatly needed. In this ongoing work experiments are being carried out at Oregon State University. The experimental procedure and setup of this study are described at the end of this paper.

1.1 Experimental observations of time-dependent Poisson ratios

Poisson's ratio (PR) was defined as the ratio of the transverse contraction to the elongation in the direction of the load applied, i.e.: $\nu_{12} = -\varepsilon_2/\varepsilon_1$ by Poisson (1829). This parameter can be applied in elastic constitutive models to obtain instantaneous response of both isotropic and orthotropic materials.

As many other materials, wood is showing creep behavior and over time it changes size and shape under sustained load. If the PRs of this time-dependent deformation should remain constant over time, the ratio between the longitudinal and transverse rate of strain should be identical to the ratio of the instantaneous PRs in a uniaxial load case. Measurements of PRs in other materials prone to creep (e.g. concrete, poly(methyl methacrylate) and silicon nitride (Gopalakrishnan et al., 1969; Lu et al., 1997; Mazzotti and Savoia, 2002; Ernst et al., 2003; Lofaj et al., 2003)) show that this is not the case.

To the authors' knowledge the amount of research on the time-dependent PRs in wood limits to one publication by Schniewind and Barrett (1972). They observed a PR (ν_{LT}) varying over time due to contractions in the tangential direction of a specimen loaded in the longitudinal direction (Figure 1).

The strain variations leading to the varying PR in Figure 1 are, however, questionable, since they indicate that creep recovery occurs in the transverse direction simultaneously with creep in the longitudinal direction. However, in some of the experiments by Schniewind and Barrett (1972) the opposite trend was observed, i.e., creep occurred in the transverse direction. The details on these experiments are, however, limited. With regard to the pioneering work by

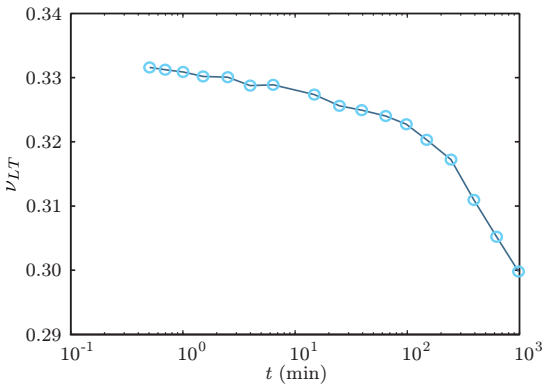

Figure 1 Varying PR from contractions tangentially to the fiber loaded in the longitudinal direction in the experiment by Schniewind and Barrett (1972).

Schniewind and Barrett (1972) it must be concluded that the uncertainty arising from this deviating behavior calls for a further investigation of the phenomenon.

1.2 Theoretical background for time-dependent Poisson's ratios

Tschoegl et al. (2002) have shown mathematically that for an isotropic viscoelastic material, PR will be a monotonously increasing function of the time, t.

For an isotropic viscoelastic material it is possible to define a time-dependent PR, which can be applied in the elastic-viscoelastic correspondence principle (Hilton, 2001; Tschoegl et al., 2002):

$$\nu(t) = -\frac{\varepsilon_j(t)}{\varepsilon_i}, \tag{1}$$

where the strain in the loaded direction ε_i is kept constant over time, i.e., in a relaxation experiment, where the strain transverse to the direction of load $\varepsilon_j(t)$ decreases over time due to relaxation of the stresses. Hereby it is also implied that the general definition of PR:

$$\nu(t) = -\frac{\varepsilon_j(t)}{\varepsilon_i(t)} \tag{2}$$

cannot be used as material parameter in the elastic-viscoelastic correspondence principle.

For anisotropic materials the mathematical consequences of PRs being constant are treated in (Hilton, 2001). Hilton concluded that the assumption of time-*in*dependent PRs lays severe mathematical restrictions on the solutions, and in general, PRs can be concluded to be time dependent.

In view of the experimental observations and these mathematical restrictions, it must be concluded that the orthotropic constitutive models should reflect the behavior of time-dependent PRs.

2 Modeling of orthotropic creep

A creep model can be represented by a higher-order differential equation, the hereditary approach or a set of first-order differential equations. The two latter representations are more suitable for implementation into a numerical method, why the focus in this paper will be directed towards those.

2.1 The hereditary approach

The classical approach for modeling the time-dependent orthotropic response of wood is the hereditary approach also known as the convolution integral approach, see e.g. (Schniewind and Barrett, 1972; Mårtensson, 1992; Ormarsson, 1999) and for a large displacement formulation (Mauget and Perré, 1999). The increments in stresses $\partial\sigma_j/\partial\tau$ are multiplied by the creep compliance or so-called master creep curves $J_{ij}(t-\tau)$ shifted to the time of action τ and summed over time:

$$\boldsymbol{\varepsilon}(t) = \int_{-\infty}^{t} \mathbf{J}(t-\tau)\frac{\partial\boldsymbol{\sigma}(\tau)}{\partial\tau}d\tau, \qquad (3)$$

where $\boldsymbol{\varepsilon}$ and $\boldsymbol{\sigma}$ are the strain and stress vectors containing the components ε_i and σ_j, respectively. $\mathbf{J}$ is the creep compliance matrix containing the components J_{ij}.

The diagonal components of the creep compliance matrix have been estimated for different species at different temperatures and moisture contents in various experiments. The magnitude and rates of creep in the different directions vary.

For example, the creep strains in the tangential direction are larger than those in the longitudinal direction, whereas the rate by which the final strain is approached is faster for the longitudinal strains in (Schniewind and Barrett, 1972).

Thus, the diagonal components of the creep compliance matrix differ not only in magnitude but they are also proportionally different over time:

$$J_{\underline{ii}}(t) \neq kJ_{\underline{jj}}(t) \quad , \quad i \neq j \qquad (4)$$

where k is a constant.

In the following different approaches for obtaining the off-diagonal compliances (J_{ij}, $i \neq j$) are addressed.

For an incremental finite element formulation of the hereditary approach addressed in this section, see e.g. (Ormarsson, 1999; Mauget and Perré, 1999).

Assumption of constant Poisson's ratios

In this section the different consequences of the choice of constant PRs in an orthotropic creep model is treated. Mårtensson (1992) proposed a constitutive model, in which the off-diagonal creep compliances ($J_{ji}(t)$) were assumed to be proportional to the to the diagonal ones ($J_{\underline{ii}}(t)$), where the factors of proportionality were the elastic PRs ($\nu_{\underline{ij}}$):

$$J_{ji}(t) = -\nu_{\underline{ij}}J_{\underline{ii}}(t) \quad , \quad i \neq j, \qquad (5)$$

where the underlined subscripts indicate exceptions from Einstein's summation convention, which otherwise applies.

By considering the creep compliances symmetrically located to these:

$$J_{ij}(t) = -\nu_{\underline{ji}}J_{\underline{jj}}(t) \quad , \quad i \neq j, \qquad (6)$$

it is seen that these equal one another when $t = 0$, i.e., at the initial elastic response at the

time of loading. However, for $t > 0$ it can be seen from Eq. (4) that:

$$J_{ji}(t) = -\nu_{\underline{i}j} J_{\underline{i}i}(t) \neq -\nu_{\underline{j}i} J_{\underline{j}j}(t) = J_{ij}(t). \quad (7)$$

Thus, the assumption of constant PRs leads to asymmetric compliance matrices, which according to Onsager's reciprocal principle should be symmetric (Biot, 1954; Halpin and Pagano, 1968).

Time-dependent Poisson ratios as material parameters

A hypothetic method for obtaining a creep response yielding time-dependent PRs, is to apply the measured time-dependent PRs as material parameters. This can be done by imitating the elastic orthotropic formulation by:

$$J_{ji}(t) \stackrel{?}{=} -\nu_{\underline{i}j}(t) J_{\underline{i}i}(t) \quad , \quad i \neq j. \quad (8)$$

The PRs $\nu_{ji}(t)$ are measured as the ratio between the transverse strains $\varepsilon_j(t)$ and the strain $\varepsilon_i(t)$ parallel to the direction of a uniaxial load $\sigma_i(t)$:

$$\nu_{ij}(t) = -\frac{\varepsilon_j(t)}{\varepsilon_i(t)}. \quad (9)$$

The strains $\varepsilon_j(t)$ and $\varepsilon_i(t)$ in Eq. (9) can be evaluated by Eq. (3) and by inserting the assumed constitutive model Eq. (8):

$$\begin{aligned} \nu_{ij}(t) &= -\frac{\int_{-\infty}^{t} J_{j\underline{i}}(t-\tau)\frac{\partial \sigma_{\underline{i}}(\tau)}{\partial \tau} d\tau}{\int_{-\infty}^{t} J_{i\underline{i}}(t-\tau)\frac{\partial \sigma_{\underline{i}}(\tau)}{\partial \tau} d\tau} \\ &\stackrel{?}{=} \frac{\int_{-\infty}^{t} \nu_{\underline{i}j}(t-\tau) J_{\underline{i}i}(t-\tau)\frac{\partial \sigma_{i}(\tau)}{\partial \tau} d\tau}{\int_{-\infty}^{t} J_{i\underline{i}}(t-\tau)\frac{\partial \sigma_{\underline{i}}(\tau)}{\partial \tau} d\tau}. \end{aligned} \quad (10)$$

Hence, recalculating the PRs by applying the assumed constitutive model Eq. (8) does not yield the measured PRs. Thus, the measured time-dependent PRs cannot be applied as material parameters in an orthotropic creep model as defined in Eq. (8).

Requirements for directionally independent creep rates

In the following a widely applied viscoelastic constitutive model based on a generalized Kelvin series are investigated.

The creep compliance in a one-dimensional model is often obtained by solving the differential equations for a generalized Kelvin model yielding the Dirichlet series:

$$J(t) = \sum_{n=1}^{N} \frac{1}{Q^{(n)}} \left(1 - e^{\left(-\frac{Q^{(n)}}{\eta^{(n)}} t\right)}\right) \quad (11)$$

or

$$J(t) = \sum_{n=1}^{N} C^{(n)} \left(1 - e^{\left(-\frac{t}{T^{(n)}}\right)}\right), \quad (12)$$

where $Q^{(n)}$ and $C^{(n)}$ and are the stiffness and compliance of the spring in the nth Kelvin element, and $\eta^{(n)}$ is the viscosity of the dashpot in the nth Kelvin element. $T^{(n)} = \eta^{(n)}/Q^{(n)}$ is the so-called retardation time of the nth Kelvin element.

This one-dimensional creep compliance is often generalized to a three-dimensional orthotropic formulation, see e.g. (Schniewind and Barrett, 1972; Mauget and Perré, 1999; Hanhijärvi, 1999; Ormarsson, 1999):

$$\mathbf{J}(t) = \sum_{n=1}^{N} \mathbf{C}^{(n)} \left(1 - e^{\left(-\frac{t}{T^{(n)}}\right)}\right). \quad (13)$$

For this formulation the PRs can be obtained by inserting Eq. (12) into Eq. (9):

$$\nu_{ji}(t) = \frac{\int_{-\infty}^{t} \sum_{n=1}^{N} C_{j\underline{i}}^{(n)} \left(1 - e^{\left(-\frac{t}{T^{(n)}}\right)}\right) \frac{\partial \sigma_{\underline{i}}(\tau)}{\partial \tau} d\tau}{\int_{-\infty}^{t} \sum_{n=1}^{N} C_{i\underline{i}}^{(n)} \left(1 - e^{\left(-\frac{t}{T^{(n)}}\right)}\right) \frac{\partial \sigma_{\underline{i}}(\tau)}{\partial \tau} d\tau}. \quad (14)$$

From Eq. (14) it is seen that the requirement to avoid time independent PRs is that the off-diagonal compliances $C_{j\underline{i}}^{(n)}$ scale differently to

the diagonal $C_{\underline{ii}}^{(n)}$ for the different Kelvin elements, i.e.:

$$\frac{C_{\underline{ji}}^{(n)}}{C_{\underline{ji}}^{(m)}} \neq \frac{C_{\underline{ii}}^{(n)}}{C_{\underline{ii}}^{(m)}} \quad , \quad n \neq m \quad , \quad i \neq j \ . \tag{15}$$

where $m = 1, 2, \ldots N$. If this restriction is not obeyed, the rate of the (i,i)th and (j,i)th strain components will be identical yielding constant PRs. For example, let the components of the compliances scale proportionally to those of the elastic compliance matrix: $C_{ij}^{(0)} = k_1^- 1 C_{ij}^{(1)} \ldots = k_n^- 1 C_{ij}^{(n)}$, and Eq. (14) yields:

$$\frac{C_{j\underline{i}}^{(0)} \int_{-\infty}^{t} \sum_{n=1}^{N} k_n \left(1 - e^{\left(-\frac{t}{T^{(n)}}\right)}\right) \frac{\partial \sigma_i(\tau)}{\partial \tau} d\tau}{C_{i\underline{i}}^{(0)} \int_{-\infty}^{t} \sum_{n=1}^{N} k_n \left(1 - e^{\left(-\frac{t}{T^{(n)}}\right)}\right) \frac{\partial \sigma_i(\tau)}{\partial \tau} d\tau} = \frac{C_{j\underline{i}}^{(0)}}{C_{i\underline{i}}^{(0)}} = \nu_{ji}. \tag{16}$$

Thus, the PRs become constant in this case.

Hence, the requirement in Eq. (14) can also be formulated as:

$$\mathbf{C}^{(n)} \neq k\mathbf{C}^{(m)} \quad , \quad n \neq m, \tag{17}$$

where k is a constant. Thus, the off-diagonal components must scale differently from the diagonal components of the compliance matrices.

Typically, the elastic compliance matrix $\mathbf{C}^{(0)}$, the compliances $C_{\underline{ii}}^{(n)}$ and retardation times $T^{(n)}$ from one-dimensional experiments are available. An appealing approach for estimating the unknown off-diagonal components $C_{\underline{ij}}^{(n)}$ would be to assume that these scale to the corresponding elastic components $C_{\underline{ij}}^{(0)}$ similar to the scaling of the known diagonal components $C_{\underline{ii}}^{(n)} = kC_{\underline{ii}}^{(0)}$ (see e.g. (Hanhijärvi and Mackenzie-Helnwein, 2003)). However, according to the requirement stated in Eq. (17), this approach would lead to constant PRs.

2.2 The differential equation approach

Another approach for obtaining an orthotropic creep model suitable for implementation into a numerical method is to formulate a set of first order differential equations. Hanhijärvi and Mackenzie-Helnwein (2003) applied the following generalized three-dimensional Kelvin series with N Kelvin elements:

$$T^{(n)}\dot{\boldsymbol{\varepsilon}}^{(n)} + \boldsymbol{\varepsilon}^{(n)} = \mathbf{C}^{(n)}\boldsymbol{\sigma}, \tag{18}$$

where $\mathbf{C}^{(n)}$ is the generalized compliance matrix and $T^{(n)}$ is the retardation time for the nth Kelvin element, where $n = 1, 2, \ldots N$. This formulation by Hanhijärvi and Mackenzie-Helnwein (2003) can be be shown to be the same as Eq. (13) (Appendix 1). Thus, the requirements for time-dependent PRs are identical to those in Eq. (15).

In the following a model of this type, which allows independent creep rates in the different material directions, will be derived.

3 An orthotropic creep model

In Figure 2 a schematic diagram of the proposed orthotropic creep model with three coupled rheological systems is shown. The center system models the deformation in the direction of the load. The deformation in the two outer rheological systems are connected to the direction of load by lattices, which gives resemblance to the distribution of stress in the cellular structure of wood. In the cellular structure the stress is hereby transferred to deformations orthogonal to its direction. For simplicity, only one spring modeling the elastic response and one Kelvin element modeling the creep are illustrated.

In the following derivation, a two-dimensional simplified version of the model is presented. The equations are consequentially generalized. The model can be generalized to three dimensions and with a base of a more complex creep model or for that matter a mechano-sorptive model.

In Figure 3 the two-dimensional constitutive model for an orthotropic material stressed

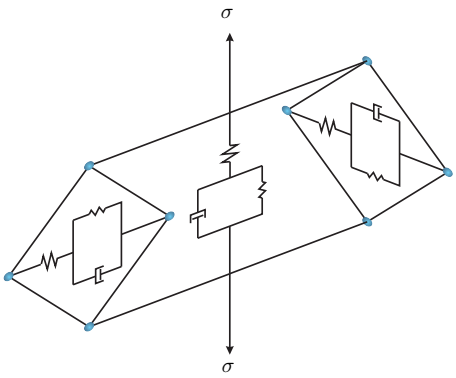

Figure 2 Parallel coupled rheological systems modeling strain and strain rate in various direction due to a longitudinal stress.

in the longitudinal direction is shown. In the model Q designates spring-stiffnesses and η viscosities. The model consists of two rheological systems. The upper set models the time-dependent longitudinal strain and the lower one models the transverse strains caused by the Poisson effect.

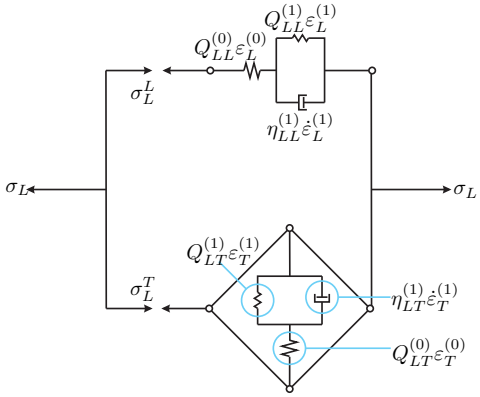

Figure 3 Two parallel coupled rheological systems modeling transverse and longitudinal strain and strain rate due to a longitudinal stress.

The shear stresses and strains decouple from the other strain and stress components, and the simple constitutive model for these shown in Figure 4 is chosen.

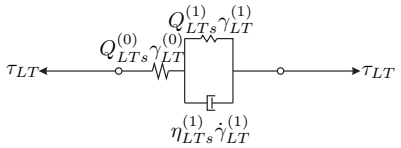

Figure 4 A rheological system modeling the dependence of the shear strain on the shear stress.

For the basic rheological system chosen, the total strain in the longitudinal direction ε_L consists of the elastic strain $\varepsilon_L^{(0)}$ from the spring and viscoelastic strain $\varepsilon_L^{(1)}$ in the Kelvin element and similarly for the transverse strain ε_T. The total strains are given by:

$$\varepsilon_L = \varepsilon_L^{(0)} + \varepsilon_L^{(1)} \tag{19a}$$

$$\varepsilon_T = \varepsilon_T^{(0)} + \varepsilon_T^{(1)}. \tag{19b}$$

The total stress in the longitudinal direction equilibrates the sum of the stresses on each of the set of the two parallel rheological systems, σ_L^L and σ_L^T (Figure 3):

$$\sigma_L = \sigma_L^L + \sigma_L^T. \tag{20}$$

Furthermore, the stress σ_L^L equilibrates the stress in the spring $Q_{LL}^{(0)}\varepsilon_L^{(0)}$ and the stress on the Kelvin element $Q_{LL}^{(1)}\varepsilon_L^{(1)} + \eta_{LL}^{(1)}\dot{\varepsilon}_L^{(1)}$. Similar considerations can be made for the rheological system modeling the transverse strains:

$$\sigma_L^L = Q_{LL}^{(0)}\varepsilon_L^{(0)} \tag{21a}$$

$$\sigma_L^L = Q_{LL}^{(1)}\varepsilon_L^{(1)} + \eta_{LL}^{(1)}\dot{\varepsilon}_L^{(1)} \tag{21b}$$

$$\sigma_L^T = Q_{LT}^{(0)}\varepsilon_T^{(0)} \tag{21c}$$

$$\sigma_L^T = Q_{LT}^{(1)}\varepsilon_T^{(1)} + \eta_{LT}^{(1)}\dot{\varepsilon}_T^{(1)}. \tag{21d}$$

Assembling the stresses on the elastic elements in Eq. (21a) and Eq. (21c) by Eq. (20) yields:

$$\sigma_L = Q_{LL}^{(0)}\varepsilon_L^{(0)} + Q_{LT}^{(0)}\varepsilon_T^{(0)}. \tag{22}$$

The stresses on the Kelvin elements in Eq. (21b) and Eq. (21d) are assembled in Eq. (20)

as well, providing:

$$\sigma_L = Q_{LL}^{(1)}\varepsilon_L^{(1)} + \eta_{LL}^{(1)}\dot{\varepsilon}_L^{(1)} + Q_{LT}^{(1)}\varepsilon_T^{(1)} + \eta_{LT}^{(1)}\dot{\varepsilon}_T^{(1)}. \tag{23}$$

Considering a constitutive model for the stress in the transverse direction σ_T, similar constitutive equations can be derived. With the constitutive model for the shear stress, the complete constitutive model for the two-dimensional orthotropic viscoelastic material can be formulated in matrix notation, yielding:

$$\begin{bmatrix} \sigma_L \\ \sigma_T \\ \tau_{LT} \end{bmatrix} = \begin{bmatrix} Q_{LL}^{(0)} & Q_{LT}^{(0)} & 0 \\ Q_{TL}^{(0)} & Q_{TT}^{(0)} & 0 \\ 0 & 0 & G_{LT}^{(0)} \end{bmatrix} \begin{bmatrix} \varepsilon_L^{(0)} \\ \varepsilon_T^{(0)} \\ \gamma_{LT}^{(0)} \end{bmatrix} \tag{24}$$

$$\begin{bmatrix} \sigma_L \\ \sigma_T \\ \tau_{LT} \end{bmatrix} = \begin{bmatrix} Q_{LL}^{(1)} & Q_{LT}^{(1)} & 0 \\ Q_{TL}^{(1)} & Q_{TT}^{(1)} & 0 \\ 0 & 0 & G_{LT}^{(1)} \end{bmatrix} \begin{bmatrix} \varepsilon_L^{(1)} \\ \varepsilon_T^{(1)} \\ \gamma_{LT}^{(1)} \end{bmatrix} + \begin{bmatrix} \eta_{LL}^{(1)} & \eta_{LT}^{(1)} & 0 \\ \eta_{TL}^{(1)} & \eta_{TT}^{(1)} & 0 \\ 0 & 0 & \eta_{LTS}^{(1)} \end{bmatrix} \begin{bmatrix} \dot{\varepsilon}_L^{(1)} \\ \dot{\varepsilon}_T^{(1)} \\ \dot{\gamma}_{LT}^{(1)} \end{bmatrix}. \tag{25}$$

Or in contracted notation:

$$\boldsymbol{\sigma} = \mathbf{Q}^{(0)}\boldsymbol{\varepsilon}^{(0)} \tag{26}$$

$$\boldsymbol{\sigma} = \mathbf{Q}^{(1)}\boldsymbol{\varepsilon}^{(1)} + \boldsymbol{\eta}^{(1)}\dot{\boldsymbol{\varepsilon}}^{(1)}. \tag{27}$$

The sum of $\boldsymbol{\varepsilon}^{(0)}$ and $\boldsymbol{\varepsilon}^{(1)}$ yields the total strain as stated in Eq. (19).

The rheological systems can be expanded by a number of N Kelvin elements and to three dimensions:

$$\boldsymbol{\sigma} = \boldsymbol{\eta}^{(n)}\dot{\boldsymbol{\varepsilon}}^{(n)} + \mathbf{Q}^{(n)}\boldsymbol{\varepsilon}^{(n)}, \tag{28}$$

where the total strains are obtained by:

$$\boldsymbol{\varepsilon} = \sum_{n=0}^{N} \boldsymbol{\varepsilon}^{(n)}. \tag{29}$$

Mathematically the model by Hanhijärvi and Mackenzie-Helnwein (2003) is a special case of Eq. (28). This is realized by reformulating Eq. (13) to:

$$\mathbf{Q}^{(n)}\boldsymbol{\varepsilon}^{(n)} + T^{(n)}\mathbf{Q}^{(n)}\dot{\boldsymbol{\varepsilon}}^{(n)} = \boldsymbol{\sigma}, \tag{30}$$

where $\mathbf{Q}^{(n)} = (\mathbf{C}^{(n)})^{-1}$. By comparison with Eq. (28) it is seen that the simplification in the model by Hanhijärvi and Mackenzie-Helnwein (2003) involves the assumption of $\boldsymbol{\eta}^{(n)} = T^{(n)}\mathbf{Q}^{(n)}$. If this assumption is applied the components of the compliance matrices cannot scale identically as stated in Eq. (17).

The general formulation in Eq. (28) can be stated as a hereditary approach as well. The solution is slightly more mathematically complicated. The solution has a structure similar to Eq. (3) and Eq. (12):

$$\boldsymbol{\varepsilon}(t) = \int_{-\infty}^{t} \mathbf{J}^{(n)}(t-\tau)\frac{\partial \boldsymbol{\sigma}(\tau)}{\partial \tau}d\tau, \tag{31}$$

where

$$\mathbf{J}^{(n)}(t) = \left(\mathbf{I} - e^{\mathbf{A}^{(n)}t}\right)\mathbf{C}^{(n)}, \tag{32}$$

where $\mathbf{C}^{(n)} = (\mathbf{Q}^{(n)})^{-1}$ and $\mathbf{A}^{(n)} = (\boldsymbol{\eta}^{(n)})^{-1}\mathbf{Q}^{(n)}$ and $\mathbf{I}$ is the identity matrix. The matrix exponential function $e^{\mathbf{A}^{(n)}t}$ is defined in Appendix 2, and a procedure to calculate this matrix is presented as well. Furthermore, a proof of the solution is given in Appendix 2. This solution allows application of this model together with the usual incremental approach, see e.g. (Hanhijärvi, 1999).

The equation system is composed by $2I$ equations coupled with $2I \times N$ first-order differential equations, where I is the dimension of the problem considered. As shown in Appendix 3, these can be stated in an alternative finite-element formulation. The equations and differential equations can be stacked in a single matrix equation:

$$\mathbf{C}\dot{\tilde{\mathbf{a}}} + \mathbf{K}\tilde{\mathbf{a}} = \tilde{\mathbf{F}}, \tag{33}$$

where $\tilde{\mathbf{a}} = [\mathbf{a}^T \quad \mathbf{a}^{(n)T}]^T$. $\mathbf{a}$ and $\mathbf{a}^{(n)}$ are the discretized displacements and viscoelastic strains,

respectively. The symmetric damping matrix $\mathbf{C}$ and stiffness matrix $\mathbf{K}$ are given in Appendix 3. Note that the damping matrix $\mathbf{C}$ do not relate to the compliance matrices $\mathbf{C}^{(n)}$, and the notations are maintained from their respective area of application. The time discretization and integration can be performed by various methods, see e.g. (Bathe, 1995).

4 Experimental study of deformations orthogonal to the direction of load

The initial study is performed on the deformations in the tangential-longitudinal plane. To provide clear and easy interpretable results a well defined and relatively simple loading of the specimens is chosen.

The experiments will be conducted by subjecting plane clear straight-grained wood specimens to uniaxial loading in the two material directions studied. This yields plane states of stress, where the transverse displacement is only induced by a single stress component.

High accuracy is required to study the deformations orthogonal to the direction of load, especially for the stiff longitudinal direction. This requires a constant mechanical stress field plus a very stable level of relative humidity and temperature in the ambient air. Therefore, a test bench as shown in Figure 5 has been designed for the purpose. The design is described in section 4.1.

By the DIC technique deformations on the specimen are traced through a series of pictures taken by one or two digital cameras (Figure 5). The technique has the advantage of measuring the deformations in a dense grid allowing evaluation of the strain field on the surface. Hence, much more information is available about the distribution of strains compared to application of strain gauges, for example. The technique is further described in section 4.2. An additional advantage of the technique is that physical and chemical disturbances from a e.g. a strain gauge on the region of interest on the specimens is avoided.

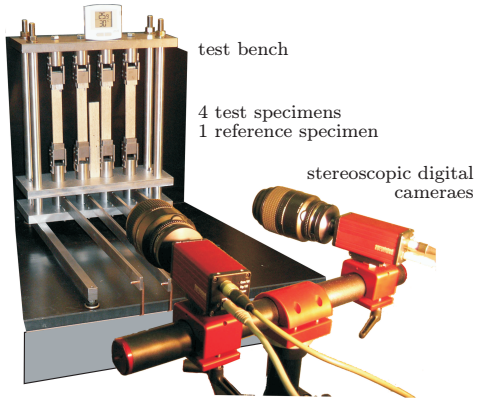

Figure 5 The experimental setup with two digital cameras and a test bench.

4.1 Design of test bench

The test bench has been designed to meet a number of critiria to obtain the required accuracy.

To obtain a controlled loading and unloading, a rigidly framed cantilever system with an explicit direction of forces is used. The force from the lever arm is directed through a cylindrical shaft and grip. Apart from easy manufacturing, the cylindrical design was chosen to avoid wedging from oblique edges. The force is transferred through the lever onto the cylinder and the rigid frame by a dowel and a high-grade steel ball bearing (Figure 6).

The design of the cantilever system allows compressive as well as tensile loading of the specimens. Also, the frame is designed to be adaptable with regard to specimen sizes by letting the plate supporting the upper grips be bolted to the vertical threaded bars.

The specimens are mounted close together letting the cameras frame as many specimens as possible without compromising manageability around the fixtures. The fixtures have a traditionally wedged construction, where the inclination ensures sufficiently low steel-to-steel friction during clenching. The wedges can be

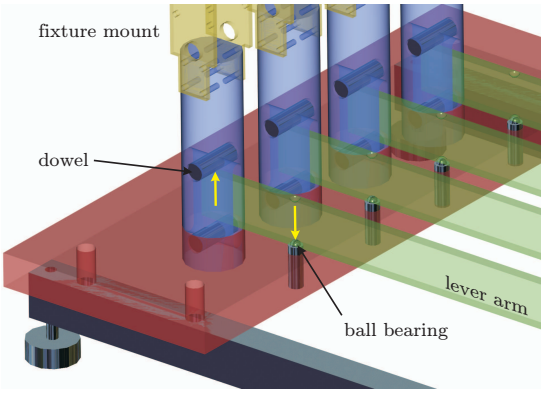

Figure 6 Transfer of forces from the cantilever system to the frame and shaft through a high-grade steel ball bearing and a dowel.

attached to grip in both of the two opposite loading modes (Figure 7).

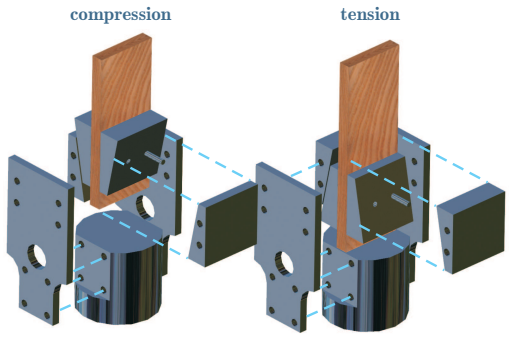

Figure 7 Setup of the fixtures in compression and tension mode.

4.2 Digital image correlation technique

The digital image correlation is facilitated by one or two cameras, which are continuously taking pictures during the experiment. On these pictures, one or more regions of interest for acquiring displacements and strains are specified.

In each region an array of reference square pixel subsets are defined. Relative changes in position of the reference subsets on the consecutive images of the same area of interest are then reported as displacements of subset centroids

Each region is covered by an array with fixed step size of so-called subsets that are squares of pixels (Figure 8).

The center of the reference subsets in the first image specifies discrete points at which the displacement will be determined in the subsequent series of pictures. Thus, a discrete field of displacements in the entire region of interest is obtained.

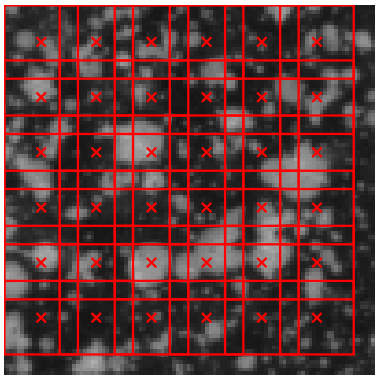

Figure 8 Distribution of subsets in the region of interest.

Each subset can be represented by a square matrix $\mathbf{\Omega}$, where each component corresponds to the matching pixels' shade of gray. In the following the subsets on the specimen in the undisturbed reference image, the so-called reference subset, is denoted $\mathbf{\Omega}^R$.

The displacement of the reference subset $\mathbf{\Omega}^R$ is determined by finding the maximum cross-correlation coefficient $\rho(\eta, \xi)$ in a region around the last displacement known. The coordinate (η, ξ) of the maximum cross-correlation coefficient yields the displacement of the subset in that image.

The cross-correlation coefficient can either be determined in the physical space (Chiang, 1982; Sutton et al., 1983; Chu et al., 1985) or in a Fourier space (Chen et al., 1993; Chiang et al., 1997). To illustrate the procedure, a simple approach in the physical space is presented here.

In this simple approach, the cross-correlation coefficient for matching two

subsets is determined by:

$$\rho(\eta,\xi) = \frac{\mathbf{\Omega}^R_{ij}(x,y)\mathbf{\Omega}^*_{ij}(x+\eta,y+\xi)}{\left(\mathbf{\Omega}^R_{kl}(x,y)\right)^2\left(\mathbf{\Omega}^*_{mn}(x+\eta,y+\xi)\right)^2} \tag{34}$$

where $\mathbf{\Omega}^*(x+\eta,y+\xi)$ is a trial subset at the coordinate $(x+\eta,y+\xi)$.

In Figure 9 two subsequent images of a wood-plastic composite specimen in a tensile experiment are shown. The first image is used as a reference, and the displacement of the subset marked is requested in the subsequent image.

The computed cross-correlation coefficient in a region around the last displacement known is shown for both images in Figure 10. Not surprisingly the displacements are equal to zero for both directions in the first image, whereas the displacement in the latter equals (-2,11) pixels. The displacement is shown in Figure 11.

As indicated above, this is a crude approach and it allows detection of displacements on the pixel level only. Interpolation or application of fast Fourier transforms, as mentioned above, provides sub-pixel accuracy. The latter technique has been implemented into the commercial software by Correlated Solutions applied in the experiments.

Furthermore, a stereoscopic camera setup that provides out-of-plane displacements has been used in the experiments.

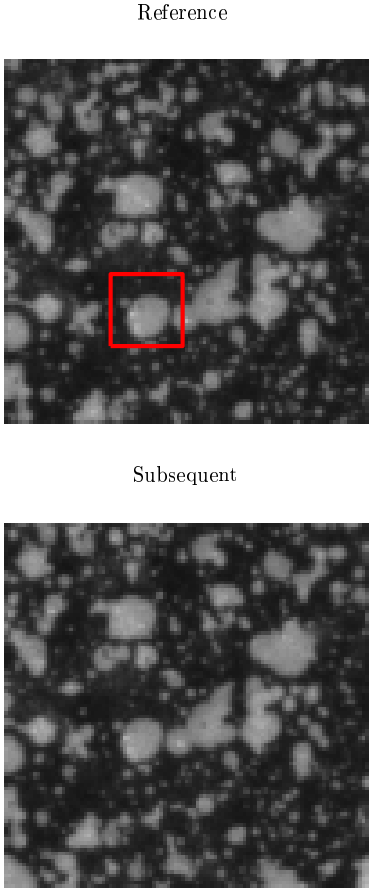

Figure 9 Two subsequent images of a wood-plastic composite specimen in a tensile experiment.

5 Conclusions

Creep transverse to the direction of load in wood caused by the Poisson effect has so far received very little attention. In order to obtain accurate modeling of creep in multi-axial states of stress, these are needed. Therefore, the coupling terms have been estimated in various multi-dimensional models. In these estimations the Poisson ratios are typically assumed to be a constant. However, in experiments Poisson's ratios have been observed to be time dependent, and this observation is well supported by theoretical considerations. This calls for theoretical as well as experimental investigations of the transverse couplings in creep of wood.

The appealing approach of introducing time-dependent Poisson's ratios as material parameter was shown to be inapplicable. Thus, a constitutive model must be expressed in moduli only.

In this perspective the requirements for widely applied orthotropic constitutive models based on a generalized Kelvin series were investigated. It was found that the components of the creep compliance matrices must scale differ-

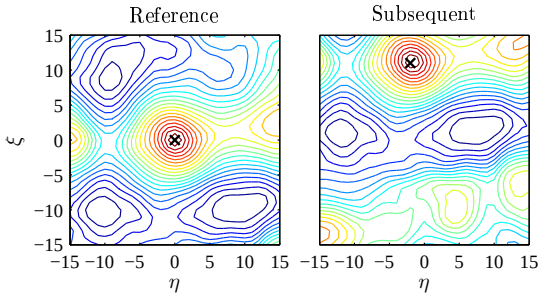

Figure 10 The cross-correlation coefficient in a region around the last known displacement for the subset in Figure 9.

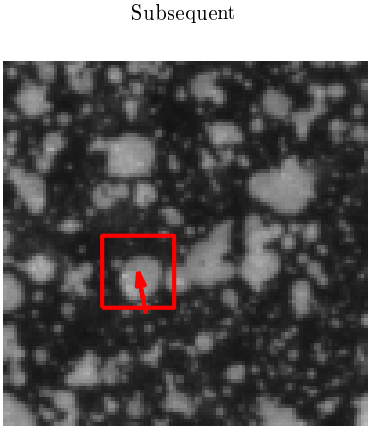

Figure 11 The displacement of the subset in the subsequent image.

ently to those of the elastic compliance matrix.

Furthermore, a new general orthotropic formulation, which resembles the distribution of stresses in the cellular structure of wood, is proposed. Two approaches for implementing the constitutive model into a finite element model are addressed.

To qualitatively draw conclusions on the correspondence between the proposed orthotropic constitutive model and the cellular structure of wood, an experimental study is currently being carried out at Oregon State University. Here the experimental procedure and setup of this study are described.

For accuracy and to avoid physical contact with the specimens, the measurements are conducted with cameras and by use of the digital image correlation technique. To frame as many specimens as possible with the cameras, the specimens are mounted close together in a test bench designed for the purpose.

As this is a paper on ongoing work, the final conclusions on correspondence between the coupled rheological systems in the proposed constitutive model and the cellular structure of wood strived for, remains. To draw these conclusions the theoretical considerations of this paper will be complemented with the experimental study described.

Acknowledgements

Thanks to Milo Clauson for providing skilful guidance with design of the test bench, accuracies in fabrication of technical drawings, and other mechanical issues. This work has been funded in part by the Danish Forest and Nature Agency and in part by the Center for Wood Utilization Research, USDA WUR Grant no.: 2005-34158-16380. Their financial support is gratefully acknowledged.

Appendix 1

In this appendix Eq. (18) will be shown to be an identical representation of Eq. (3) and Eq. (13).

Eq. (18) consists of $2I$ differential equations, which for a constant stress state $\boldsymbol{\sigma} = \boldsymbol{\sigma}^0$ can be expressed as 6 one-dimensional differential equations:

$$T^{(n)}\dot{\varepsilon}_i^{(n)} + \varepsilon_i^{(n)} = C_{ij}{}^{(n)}\sigma_j^0. \tag{35}$$

The solutions to these equations are:

$$\varepsilon_i^{(n)}(t) = C_{ij}^{(n)}\left(1 - e^{\left(-\frac{t}{T^{(n)}}\right)}\right)\sigma_j^0. \tag{36}$$

The viscoelastic responses to different loads can be superimposed. Superimposing the responses $d\varepsilon_i^{(n)}(t)$ for stepwise constant stress increments $d\sigma_{ij}$ acting at the time τ, and letting

both be infinitesimal yields:

$$\int_{-\infty}^{t} d\varepsilon_i^{(n)}(t) = \int_{-\infty}^{t} C_{ij}^{(n)} \left(1 - e^{\left(-\frac{t-\tau}{T^{(n)}}\right)}\right) d\sigma_j, \tag{37}$$

which by summing the N viscoelastic strain components provides Eq. (3) and Eq. (13).

Appendix 2

In this appendix a hereditary integral solution for the differential Eq. (28) is proven to exist. For convenience, is the following proof and representation of the solution in Eq. (28) rearranged to:

$$\dot{\boldsymbol{\varepsilon}}^{(n)} = \mathbf{A}^{(n)}\boldsymbol{\varepsilon}^{(n)} + \mathbf{A}^{(n)}\mathbf{C}^{(n)}\boldsymbol{\sigma}, \tag{38}$$

where $\mathbf{C}^{(n)} = (\mathbf{Q}^{(n)})^{-1}$ is the compliance of the spring in the nth Kelvin element, and $\mathbf{A}^{(n)} = -(\boldsymbol{\eta}^{(n)})^{-1}\mathbf{Q}^{(n)}$.

The solution corresponds to that of the one-dimensional case given in Eq. (3) and Eq. (12):

$$\boldsymbol{\varepsilon}(t) = \int_{-\infty}^{t} \mathbf{J}^{(n)}(t-\tau)\frac{\partial \boldsymbol{\sigma}(\tau)}{\partial \tau} d\tau, \tag{39}$$

where

$$\mathbf{J}^{(n)}(t) = \left(\mathbf{I} - e^{\mathbf{A}^{(n)}t}\right)\mathbf{C}^{(n)}. \tag{40}$$

The matrix exponential function $e^{\mathbf{A}^{(n)}t}$ is defined by:

$$e^{\mathbf{A}^{(n)}t} \equiv I + t\mathbf{A}^{(n)} + t^2\frac{(\mathbf{A}^{(n)})^2}{2!} + t^3\frac{(\mathbf{A}^{(n)})^3}{3!}..., \tag{41}$$

where $(\mathbf{A}^{(n)})^2 = \mathbf{A}^{(n)}\mathbf{A}^{(n)}$ and $(\mathbf{A}^{(n)})^3 = \mathbf{A}^{(n)}\mathbf{A}^{(n)}\mathbf{A}^{(n)}$ etc. Notice that for $t = 0$, $e^{\mathbf{A}^{(n)}0} = I$. And notice that $e^{\mathbf{A}^{(n)}t}$ and $\mathbf{A}^{(n)}$ have the same eigenvectors, why they commute:

$$e^{\mathbf{A}^{(n)}t}\mathbf{A}^{(n)} = \mathbf{A}^{(n)}e^{\mathbf{A}^{(n)}t}. \tag{42}$$

Differentiating Eq. (41) with respect to time, it appears that:

$$\frac{\partial}{\partial t}e^{\mathbf{A}^{(n)}t} = \mathbf{A}^{(n)}e^{\mathbf{A}^{(n)}t}. \tag{43}$$

To avoid truncation of the series in Eq. (41) and the inherent uncertainties, following decomposition of $\mathbf{A}^{(n)}$ can be applied to obtain an exact expression for $e^{\mathbf{A}^{(n)}t}$:

$$\mathbf{A}^{(n)} = \boldsymbol{\Phi}^{(n)}\boldsymbol{\Lambda}^{(n)}(\boldsymbol{\Phi}^{(n)})^{-1}, \tag{44}$$

where the columns of the matrix $\boldsymbol{\Phi}^{(n)}$ are the eigenvectors of $\mathbf{A}^{(n)}$, and the eigenvalues $\lambda_m^{(n)}$ are organized in the diagonal of the matrix $\boldsymbol{\Lambda}^{(n)}$:

$$\boldsymbol{\Lambda}^{(n)} = \begin{bmatrix} \lambda_1^{(n)} & \mathbf{0} & \dots & \mathbf{0} \\ \mathbf{0} & \lambda_2^{(n)} & \dots & \mathbf{0} \\ \vdots & \vdots & \ddots & \vdots \\ \mathbf{0} & \mathbf{0} & \dots & \lambda_M^{(n)} \end{bmatrix}. \tag{45}$$

Thus, the matrix exponential function $e^{\mathbf{A}^{(n)}t}$ can be expressed as:

$$\begin{aligned} e^{\mathbf{A}^{(n)}t} =& I + t\boldsymbol{\Phi}^{(n)}\boldsymbol{\Lambda}^{(n)}(\boldsymbol{\Phi}^{(n)})^{-1} \\ &+ t^2\frac{\boldsymbol{\Phi}^{(n)}\boldsymbol{\Lambda}^{(n)}\boldsymbol{\Lambda}^{(n)}(\boldsymbol{\Phi}^{(n)})^{-1}}{2!}... \\ =& \boldsymbol{\Phi}^{(n)}e^{\boldsymbol{\Lambda}^{(n)}t}(\boldsymbol{\Phi}^{(n)})^{-1}, \end{aligned} \tag{46}$$

where the diagonal matrix $e^{\boldsymbol{\Lambda}^{(n)}t}$ can be evaluated as:

$$e^{\boldsymbol{\Lambda}^{(n)}t} = \begin{bmatrix} e^{\lambda_1^{(n)}} & \mathbf{0} & \dots & \mathbf{0} \\ \mathbf{0} & e^{\lambda_2^{(n)}} & \dots & \mathbf{0} \\ \vdots & \vdots & \ddots & \vdots \\ \mathbf{0} & \mathbf{0} & \dots & e^{\lambda_M^{(n)}} \end{bmatrix}. \tag{47}$$

From this formulation it is also seen that:

$$e^{\mathbf{A}^{(n)}(t-\tau)} = e^{\mathbf{A}^{(n)}t}e^{-\mathbf{A}^{(n)}\tau}, \tag{48}$$

which will be applied in the following derivation.

To prove that Eq. (39) and Eq. (40) presents a solution to Eq. (38), Eq. (39) is reformulated by use of partial integration:

$$\begin{aligned} \boldsymbol{\varepsilon}^{(n)}(t) =& [\mathbf{J}^{(n)}(t-\tau)\boldsymbol{\sigma}(\tau)]_{-\infty}^{t} \\ &- \int_{-\infty}^{t} \frac{\partial \mathbf{J}^{(n)}(t-\tau)}{\partial \tau}\boldsymbol{\sigma}(\tau)d\tau. \end{aligned} \tag{49}$$

Evaluating the square bracket:

$$\begin{aligned}&\left[\left(\mathbf{I}-e^{\mathbf{A}^{(n)}0}\right)\mathbf{C}^{(n)}\boldsymbol{\sigma}(t)\right.\\&\left.-\left(\mathbf{I}-e^{\mathbf{A}^{(n)}(t+\infty)}\right)\mathbf{C}^{(n)}0\right]=0,\end{aligned}\tag{50}$$

since $\boldsymbol{\sigma}(t)=\mathbf{0}$ for $t<0$ and $e^{\mathbf{A}^{(n)}0}=\mathbf{I}$. Inserting Eq. (40) into Eq. (49), letting $e^{\mathbf{A}^{(n)}t}$ and $\mathbf{A}^{(n)}$ commute and applying Eq. (42) and Eq. (48) yield:

$$\begin{aligned}\boldsymbol{\varepsilon}^{(n)}(t)&=-\int_{-\infty}^{t}\frac{\partial\left(\mathbf{I}-e^{\mathbf{A}^{(n)}t}\right)\mathbf{C}^{(n)}}{\partial\tau}\boldsymbol{\sigma}(\tau)d\tau\\&=-\int_{-\infty}^{t}\mathbf{A}^{(n)}e^{\mathbf{A}^{(n)}(t-\tau)}\mathbf{C}^{(n)}\boldsymbol{\sigma}(\tau)d\tau\\&=-e^{\mathbf{A}^{(n)}t}\int_{-\infty}^{t}e^{-\mathbf{A}^{(n)}\tau}\mathbf{A}^{(n)}\mathbf{C}^{(n)}\boldsymbol{\sigma}(\tau)d\tau.\end{aligned}\tag{51}$$

Then differentiating Eq. (51) with respect to time and by use of Eq. (42) and insertion of Eq. (51) provides:

$$\begin{aligned}&\dot{\boldsymbol{\varepsilon}}^{(n)}(t)=\\&-\mathbf{A}^{(n)}e^{\mathbf{A}^{(n)}t}\int_{-\infty}^{t}e^{-\mathbf{A}^{(n)}\tau}\mathbf{A}^{(n)}\mathbf{C}^{(n)}\boldsymbol{\sigma}(\tau)d\tau\\&-e^{\mathbf{A}^{(n)}t}\left(0-e^{-\mathbf{A}^{(n)}t}\mathbf{A}^{(n)}\mathbf{C}^{(n)}\boldsymbol{\sigma}(t)\right)\\&=\mathbf{A}^{(n)}\boldsymbol{\varepsilon}^{(n)}(t)+\mathbf{A}^{(n)}\mathbf{C}^{(n)}\boldsymbol{\sigma}(t),\end{aligned}\tag{52}$$

which proves the solution to Eq. (38) stated in Eq. (39) and Eq. (40) or the alternative formulation in Eq. (51). These equations can be implemented into an iterative finite element procedure, see e.g. (Ormarsson, 1999).

Appendix 3

In this appendix a possible finite element formulation of the constitutive model derived in section 3 is presented.

In the first section, the set of equations to be solved is stated on the strong form. In the following two sections the equations are stated in the weak form and a finite element formulation, respectively.

Strong form

The equilibrium equations in the strong form are:

$$\tilde{\boldsymbol{\nabla}}^{T}\boldsymbol{\sigma}+\mathbf{f}_b=0,\tag{53}$$

where $\boldsymbol{\sigma}$ is the stress vector, $\mathbf{f}_b$ the body forces and $\tilde{\boldsymbol{\nabla}}^{T}$ is the transpose of the gradient operator. For the three-dimensional case the gradient operator is defined as:

$$\tilde{\boldsymbol{\nabla}}^{T}=\begin{bmatrix}\frac{\partial}{\partial x}&0&0&\frac{\partial}{\partial y}&\frac{\partial}{\partial z}&0\\0&\frac{\partial}{\partial y}&0&\frac{\partial}{\partial x}&0&\frac{\partial}{\partial z}\\0&0&\frac{\partial}{\partial z}&0&\frac{\partial}{\partial x}&\frac{\partial}{\partial y}\end{bmatrix}.\tag{54}$$

The kinematic relations between the strain vector and small displacements $\mathbf{u}$ are:

$$\tilde{\boldsymbol{\nabla}}\mathbf{u}=\boldsymbol{\varepsilon}.\tag{55}$$

For the boundaries on which a traction force $\mathbf{t}$ acts, the boundary condition is:

$$\mathbf{t}=\tilde{\mathbf{n}}\boldsymbol{\sigma},\tag{56}$$

where $\tilde{\mathbf{n}}$ contains the components of the normal vector to the surface of the three dimensional body n_x, n_y and n_z ordered as:

$$\tilde{\mathbf{n}}=\begin{bmatrix}n_x&0&0&n_y&n_z&0\\0&n_y&0&n_x&0&n_z\\0&0&n_z&0&n_x&n_y\end{bmatrix}.\tag{57}$$

Together with the constitutive equations Eq. (26), Eq. (28) and Eq. (29), these equations constitute the strong form of the problem. The independent variables of the problem are the displacements $\mathbf{u}$ and the viscoelastic strains $\boldsymbol{\varepsilon}^{(n)}$.

To obtain symmetric system matrices with the independent variables chosen, the constitutive equations are reformulated by inserting Eq. (29) into Eq. (26) and Eq. (28):

$$\boldsymbol{\sigma}=\mathbf{Q}^{(0)}\boldsymbol{\varepsilon}^{(0)}=\mathbf{Q}^{(0)}\left(\boldsymbol{\varepsilon}-\sum_{m=1}^{M}\boldsymbol{\varepsilon}^{(m)}\right)\tag{58a}$$

$$\mathbf{Q}^{(0)}\left(\boldsymbol{\varepsilon}-\sum_{m=1}^{M}\boldsymbol{\varepsilon}^{(m)}\right)=\mathbf{Q}^{(n)}\boldsymbol{\varepsilon}^{(n)}+\boldsymbol{\eta}^{(n)}\dot{\boldsymbol{\varepsilon}}^{(n)}.\tag{58b}$$

Weak form

The weak form of the equilibrium Eq. (53) is obtained by initially integrating over the volume Ω and pre-multiplying by the transpose of the weighting functions $\mathbf{v}^T$:

$$\int_\Omega \mathbf{v}^T \tilde{\boldsymbol{\nabla}}^T \boldsymbol{\sigma} dV + \int_\Omega \mathbf{v}^T \mathbf{f}_b dV = 0. \tag{59}$$

Next, the Green - Gauss divergence theorem is applied, and the boundary condition Eq. (56) is imposed:

$$\int_\Omega (\tilde{\boldsymbol{\nabla}}\mathbf{v})^T \boldsymbol{\sigma} dV = \int_{\partial\Omega} \mathbf{v}^T \mathbf{t} dS + \int_\Omega \mathbf{v}^T \mathbf{f}_b dV, \tag{60}$$

where $\mathbf{t}$ is the traction force on the boundary of the body $\partial\Omega$, and dS indicates integration over a surface.

Finally, insertion of the constitutive equation Eq. (58a) and the kinematic conditions Eq. (55) yield the form:

$$\int_\Omega (\tilde{\boldsymbol{\nabla}}\mathbf{v})^T \mathbf{Q}^{(0)} \left(\tilde{\boldsymbol{\nabla}}\mathbf{u} - \sum_{m=1}^{M} \boldsymbol{\varepsilon}^{(m)} \right) dV = \int_{\partial\Omega} \mathbf{v}^T \mathbf{t} dS + \int_\Omega \mathbf{v}^T \mathbf{f}_b dV. \tag{61}$$

The dependent variable, $\boldsymbol{\varepsilon}$, in Eq. (58b) is eliminated by inserting the kinematic condition in Eq. (55). Furthermore, integrating over the domain Ω and pre-multiplying by the transpose of the weighting functions $\mathbf{v}^T$ provide:

$$\int_\Omega \Big(- \mathbf{v}^T \mathbf{Q}^{(0)} \tilde{\boldsymbol{\nabla}}\mathbf{u} + \mathbf{v}^T \mathbf{Q}^{(0)} \sum_{m=1}^{M} \boldsymbol{\varepsilon}^{(m)} + \mathbf{v}^T \mathbf{Q}^{(n)} \boldsymbol{\varepsilon}^{(n)} + \mathbf{v}^T \boldsymbol{\eta}^{(n)} \dot{\boldsymbol{\varepsilon}}^{(n)} \Big) dV = 0. \tag{62}$$

Finite element formulation

The spatial variation of the displacements $\mathbf{u}$ are discretized to the nodal displacements $\mathbf{a}$ and by interpolation between these with the shape function $\mathbf{N}$:

$$\mathbf{u} = \mathbf{N}\mathbf{a}. \tag{63}$$

The same discretization is chosen for the creep strains:

$$\boldsymbol{\varepsilon}^{(n)} = \mathbf{N}\mathbf{a}^{(n)}, \tag{64}$$

where $\mathbf{a}^{(n)}$ is the nodal strain of the nth Kelvin element.

Galerkin variation is chosen, i.e., $\mathbf{v} = \mathbf{N}$. Inserting the spatial discretizations in Eq. (63) and Eq. (64) into Eq. (61) and Eq. (62) yields:

$$\int_\Omega \left(\mathbf{B}^T \mathbf{Q}^{(0)} \mathbf{B}\mathbf{a} - \sum_{m=1}^{M} \mathbf{B}^T \mathbf{Q}^{(0)} \mathbf{N}\mathbf{a}^{(m)} \right) dV = \int_{\partial\Omega} \mathbf{N}^T \mathbf{t} dS + \int_\Omega \mathbf{N}^T \mathbf{f}_b dV, \tag{65a}$$

$$\int_\Omega \Big(- \mathbf{N}^T \mathbf{Q}^{(0)} \mathbf{B}\mathbf{a} - \sum_{m=1}^{M} \mathbf{N}^T \mathbf{Q}^{(0)} \mathbf{N}\mathbf{a}^{(m)} - \mathbf{N}^T \mathbf{Q}^{(n)} \mathbf{N}\mathbf{a}^{(n)} - \mathbf{N}^T \boldsymbol{\eta}^{(n)} \mathbf{N}\dot{\mathbf{a}}^{(n)} \Big) dV = 0, \tag{65b}$$

where $\mathbf{B} = \tilde{\boldsymbol{\nabla}}\mathbf{N}$.

The equations can be rearranged by moving $\mathbf{a}$ and $\mathbf{a}^{(n)}$ outside the spatial integrations leading to:

$$\mathbf{K}_e \mathbf{a} - \sum_{m=1}^{M} \mathbf{K}_{ev}^{(0)} \mathbf{a}^{(m)} = \mathbf{F} \tag{66a}$$

$$- \mathbf{K}_{ve}^{(0)} \mathbf{a} + \sum_{m=1}^{M} \mathbf{K}_v^{(0)} \mathbf{a}^{(m)} + \mathbf{K}_v^{(n)} \mathbf{a}^{(n)} + \mathbf{C}_v^{(n)} \dot{\mathbf{a}}^{(n)} = 0, \tag{66b}$$

where

$$\mathbf{K}_e = \int_\Omega \mathbf{B}^T \mathbf{Q}^{(0)} \mathbf{B} dV \tag{67a}$$

$$\mathbf{K}_{ev}^{(0)} = \int_\Omega \mathbf{B}^T \mathbf{Q}^{(0)} \mathbf{N} dV \tag{67b}$$

$$\mathbf{K}_{ve}^{(0)} = \int_\Omega \mathbf{N}^T \mathbf{Q}^{(0)} \mathbf{B} dV \tag{67c}$$

$$\mathbf{K}_{v}^{(0)} = \int_\Omega \mathbf{N}^T \mathbf{Q}^{(0)} \mathbf{N} dV \tag{67d}$$

$$\mathbf{K}_{v}^{(n)} = \int_\Omega \mathbf{N}^T \mathbf{Q}^{(n)} \mathbf{N} dV \tag{67e}$$

$$\mathbf{C}_{v}^{(n)} = \int_\Omega \mathbf{N}^T \boldsymbol{\eta}^{(n)} \mathbf{N} dV \tag{67f}$$

$$\mathbf{F} = \int_{\partial\Omega} \mathbf{N}^T \mathbf{t} dS + \int_\Omega \mathbf{N}^T \mathbf{f}_b dV. \tag{67g}$$

Eq. (66a) and Eq. (66b) can be solved in an iterative manner by assuming the solution in the previous time step as initial condition. However, it is here chosen to stack Eq. (66a) and Eq. (66b) providing following spatially discretized equation:

$$\mathbf{C}\dot{\tilde{\mathbf{a}}} + \mathbf{K}\tilde{\mathbf{a}} = \tilde{\mathbf{F}}, \tag{68}$$

where

$$\tilde{\mathbf{a}} = \begin{bmatrix} \mathbf{a} \\ \mathbf{a}^{(1)} \\ \vdots \\ \mathbf{a}^{(M)} \end{bmatrix} \quad , \quad \tilde{\mathbf{F}} = \begin{bmatrix} \mathbf{F} \\ \mathbf{0} \\ \vdots \\ \mathbf{0} \end{bmatrix} \tag{69a}$$

$$\mathbf{K} = \begin{bmatrix} \mathbf{K}_e & -\mathbf{K}_{ev}^{(0)} & \dots & -\mathbf{K}_{ev}^{(0)} \\ -\mathbf{K}_{ve}^{(0)} & \mathbf{K}_v^{(0)} + \mathbf{K}_v^{(1)} & \dots & \mathbf{K}_v^{(0)} \\ \vdots & \vdots & \ddots & \vdots \\ -\mathbf{K}_{ve}^{(0)} & \mathbf{K}_v^{(0)} & \dots & \mathbf{K}_v^{(0)} + \mathbf{K}_v^{(M)} \end{bmatrix} \tag{69b}$$

$$\mathbf{C} = \begin{bmatrix} \mathbf{0} & \mathbf{0} & \dots & \mathbf{0} \\ \mathbf{0} & \mathbf{C}_v^{(1)} & \dots & \mathbf{0} \\ \vdots & \vdots & \ddots & \vdots \\ \mathbf{0} & \mathbf{0} & \dots & \mathbf{C}_v^{(M)} \end{bmatrix}. \tag{69c}$$

The time discretization and integration can be performed by various methods, see e.g. (Bathe, 1995).

References

Barber, N. (1968). Theoretical model of shrinking wood. *Holzforschung*, 22(4):97–103.

Bathe, K.-J. (1995). *Finite Element Analysis in Engineering Analysis*. Prentice Hall.

Biot, M. A. (1954). Theory of stress-strain relations in anisotropic viscoelasticity and relaxation phenomena. *Journal of Applied Physics*, 25(11):1385–1391.

Chen, D., Chiang, F., Tan, Y., and Don, H. (1993). Digital speckle-displacement measurement using a complex spectrum method. *Appl. Opt*, 32:1839–1849.

Chiang, F. (1982). Coherent optical technique and experimental mechanics. *Optical Engineering*, 21(3).

Chiang, F., Wang, Q., and Lehman, F. (1997). New developments in full-field strain measurements using speckles. Technical report, ASTM STP 1318, 156.

Chu, T., Ranson, W., Sutton, M., , and Petters, W. (1985). Applications of digital-image-correlation techniques to experimental mechanics. *Experimental Mechanics*, 3:232–244.

Ernst, L. J., Zhang, G. Q., and Jansen, K. M. B. (2003). Time- and temperature-dependent thermo-mechanical modeling of a packaging molding compound and its effect on packaging process stresses. *Journal of Electronic Packaging*, 125(4):539–548.

Gopalakrishnan, K. S., Neville, A. M., and Ghali, A. (1969). Creep poisson's ratio of concrete under multiaxial compression. *American Concrete Institute Journal*, 66(12):1008–1020.

Halpin, J. and Pagano, N. (1968). Observations on linear anisotropic viscoelasticity. *Journal of Composite Materials*, 2(1):68–80.

Hanhijärvi, A. (1995). *Modelling of creep deformation mechanisms in wood*. PhD thesis, Technical Research Centre of Finland, Espoo.

Hanhijärvi, A. (1999). Deformation properties of finnish spruce and pine wood in tangential and radial directions in association to high temperature drying - part ii. experimental results under constant conditions (viscoelastic creep). *Holz als Roh- und Werkstoff*, 57(5):365–372.

Hanhijärvi, A. and Hunt, D. G. (1998). Experimental indication of interaction between viscoelastic and mechano-sorptive creep. *Wood Science and Technology*, 32(1):57–70.

Hanhijärvi, A. and Mackenzie-Helnwein, P. (2003). Computational analysis of quality reduction during drying of lumber due to irrecoverable deformation - part i: Orthotropic viscoelastic-mechanosorptive-plastic material model for the transverse plane of wood. *ASCE Journal of Engineering Mechanics*, 129:996–1005.

Hilton, H. H. (2001). Implications and constraints of time-independent poisson ratios in linear isotropic and anisotropic viscoelasticity. *Journal of Elasticity*, 63(3):221–251.

Hunt, D. G. (1999). A unified approach to creep of wood. *Royal Society of London Proceedings Series A*, 455(1991):4077–4095.

Lofaj, F., Smith, D. T., and Blessing, G. V. (2003). Instrumented indentation and ultrasonic velocity techniques for the evaluation of creep cavitation in silicon nitride. *Journal of Materials Science*, 38(7):1403–1412.

Lu, H., Zhang, X., and Knauss, W. G. (1997). Uniaxial, shear, and poisson relaxation and their conversion to bulk relaxation: studies on poly(methyl methacrylate). *Polymer Engineering and Science*, 37(6):1053–1064.

Mårtensson, A. (1992). *Mechanical behavior of wood exposed to humidity variations*. Ph.d. thesis, Lund Institute of Technology.

Mårtensson, A. and Svensson, S. (1997). Stress-strain relationship of drying wood .1. development of a constitutive model. *Holzforschung*, 51(5):472–478.

Mauget, B. and Perré, P. (1999). A large displacement formulation for anisotropic constitutive laws. *European Journal of Mechanics a-Solids*, 18(5):859–877.

Mazzotti, C. and Savoia, M. (2002). Nonlinear creep, poisson s ratio, and creep-damage interaction of concrete in compression. *ACI Materials Journal*, 99(5).

Ormarsson, S. (1999). *Numerical Analalysis of Moisture-Related Distortions in Sawn Timber*. PhD thesis, Department of Structural Mechanics, Chalmers University of Technology.

Pang, S. (2002). Predicting anisotropic shrinkage of softwood. part 1: Theories. *Wood Science and Technology*, 36:75–91.

Passard, J. and Perré, P. (2005a). Viscoelastic behaviour of green wood across the grain. part i. thermally activated creep tests up to 120 degrees c. *Annals of Forest Science*, 62(7):707–716.

Passard, J. and Perré, P. (2005b). Viscoelastic behaviour of green wood across the grain. part ii. a temperature dependent constitutive model defined by inverse method. *Annals of Forest Science*, 62(8):823–830.

Poisson, S. D. (1829). Mémoire sur l'équilibre et le mouvement des corps Élastiques. *Mémoires de l'Académie Royal des Sciences de l'Institut de France*, 8:357–570.

Ranta-Maunus, A. (1975). The viscoelasticity of wood at varying moisture content. *Wood Science and Technology*, 9:189–205.

Salin, J.-G. (1992). Numerical prediction of checking during timber drying and new mechano-sorptive creep model. *Holz als Roh- und Werkstoff*, 50:195–200.

Schniewind, A. P. and Barrett, J. D. (1972). Wood as a linear orthotropic viscoelastic material. *Wood Science and Technology*, 6(1):43–57.

Sutton, M., Wolters, W., Peters, W., Ranson, W., and McNeill, S. (1983). Determination of displacements using an improved digital correlation method. *Im. Vis. Comp*, 1(3):133Ű139.

Svensson, S. (1996). Strain and shrinkage force in wood under kiln drying conditions. ii: Strain, shrinkage and stress measurements under controlled climate conditions. *Holzforschung*, 50:463–469.

Takemura, T. (1967). Plastic properties of wood in relation to the non-equilibrium states of moisture content. *Mokuzai Gakkaishi*, 6:77–81.

Toratti, T. and Svensson, S. (2000). Mechano - sorptive experiments perpendicular to grain under tensile and compressive loads. *Wood Science and Technology*, 34(4):317–326.

Tschoegl, N. W., Knauss, W. G., and Emri, I. (2002). Poisson's ratio in linear viscoelasticity - a critical review. *Mechanics of Time-Dependent Materials*, 6(1):3–51.

Wu, Q. and Milota, M. (1995). Rheological behavior of douglas-fir perpendicular to grain at elevated temperatures. *Wood and Fiber Science*, 27(3):285–295.

Yamamoto, H. and Kojima, Y. (2002). Properties of cell wall constituents in relation to longitudinal elasticity of wood. part 1. formulation of the longitudinal elasticity of an isolated wood fiber. *Wood Science and Technology*, 36:55–74.

Other publications by the author

During the phD-study the author has contributed to other publications, in which the knowledge are beyond the scope of this thesis or are covered by this thesis:

Frandsen, H. L. (2005). Modeling of moisture transport in wood. In *Wood Science and Timber Engineering*. Department of Structural Engineering and Building Technology, Aalborg University, Aalborg.

Frandsen, H. L., Svensson, S., and Damkilde, L. (2006). A new model applicable for finite element simulations of moisture transport in wood. In *International Conference on Integrated Approach To Wood Structures, Behaviour And Application : Joint meeting of ESWM and COST Action E35*, pages 195–200, Florence, Italy.

Frandsen, H. L. and Muszynski, L. (2006). Modeling of the time and strain dependent poisson effect in wood and wood-based composites. In *International Conference on Integrated Approach To Wood Structures, Behaviour And Application : Joint meeting of ESWM and COST Action E35*, pages 143–148, Florence, Italy.

Muszynski, L. and Frandsen, H. L. (2006). Experimental characterization of the variability of poisson effect in wood and wood-based composites. In *International Conference on Integrated Approach To Wood Structures, Behaviour And Application : Joint meeting of ESWM and COST Action E35*, pages 143–148, Florence, Italy.

Thoft-Christensen, P., Svensson, S., and Frandsen, H. L. (2006). 3d-modelling of corrosion crack opening. In *Advances in Reliability and Optimization of Structural Systems : Proceedings of the 12th IFIP WG 7.5 Working Conference on Reliability and Optimization of Structural Systems*, pages 163–170, Aalborg, Denmark.

Thoft-Christensen, P., Frandsen, H. L., and Svensson, S. (2007). Numerical study of corrosion crack opening. *Accepted for publication in: Structure and Infrastructure Engineering.*

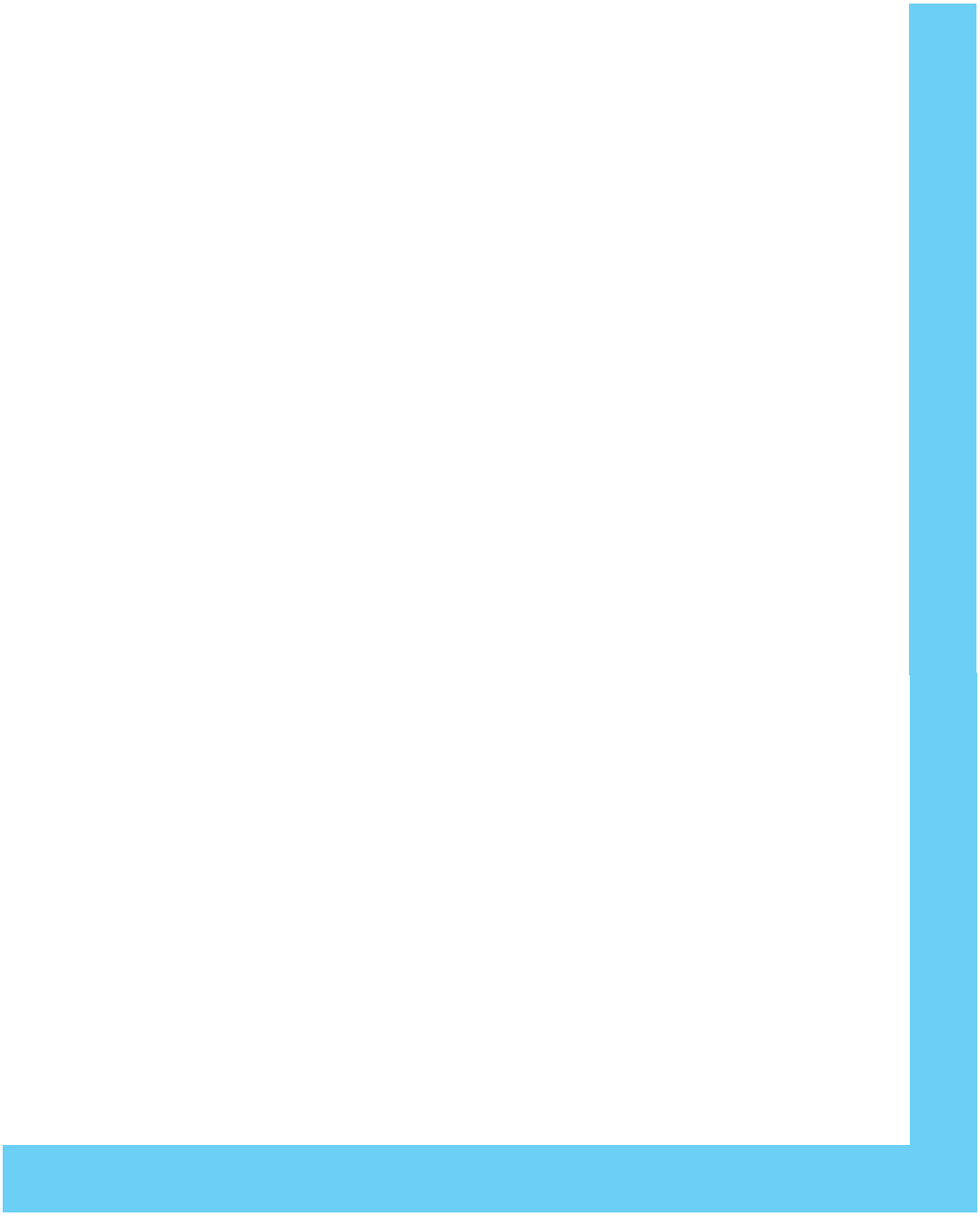

ISSN 1901-7294 DCE Thesis no. 10